# Spatially resolved studies of lensed galaxies

Johan Richard (CRAL)

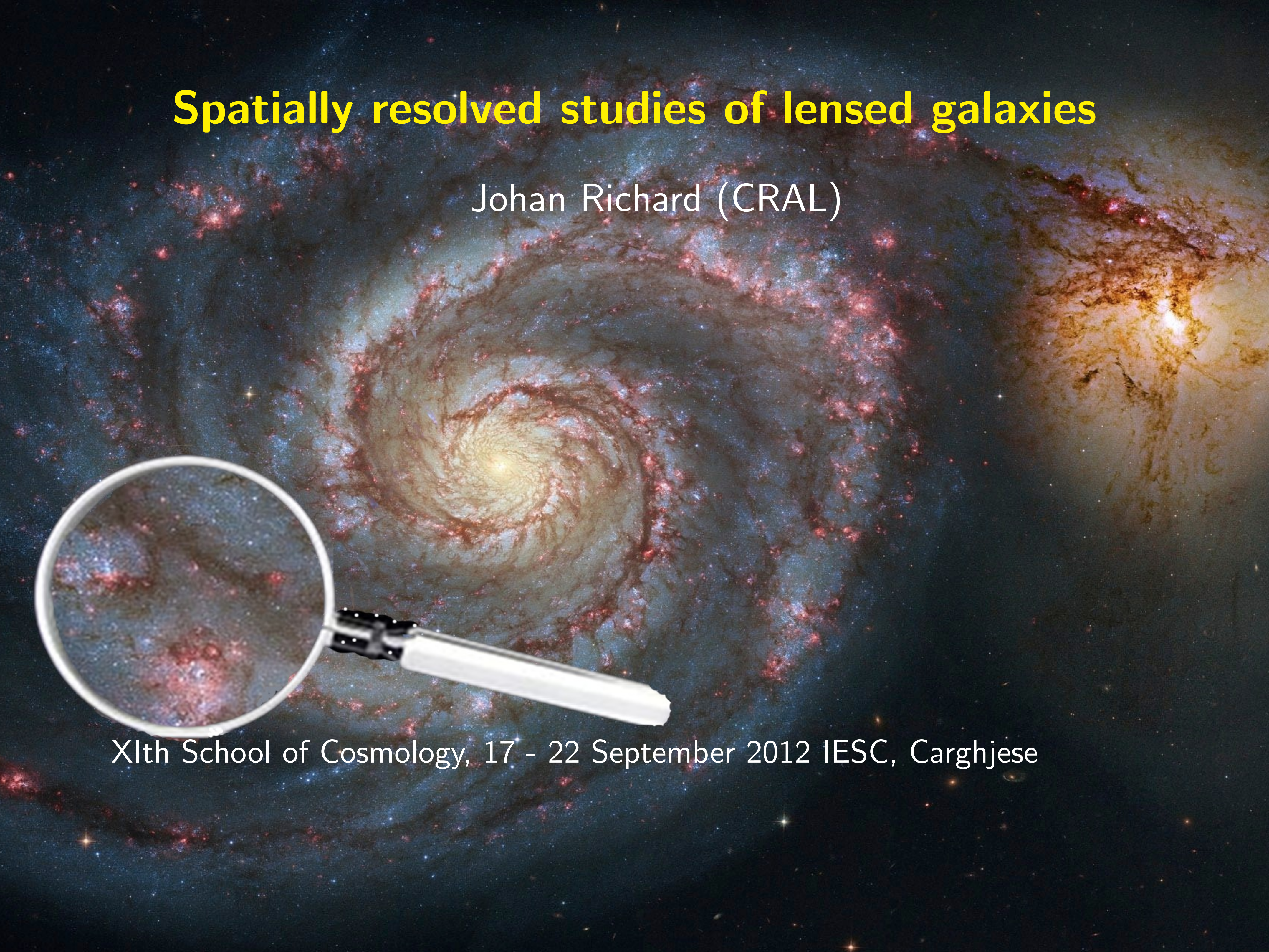

XIth School of Cosmology, 17 - 22 September 2012 IESC, Carghjese

# Outline

- Introduction
  - ⋆ Lensing magnification and source reconstruction
  - ⋆ Reconstruction techniques
- Applications:
  - ⋆ Morphology of lensed galaxies at high redshift
  - ⋆ Source reconstructions at longer wavelengths
- Conclusions

- Spatially resolved kinematics
- Resolved abundances and metallicity gradients
- Conclusions and Perspectives

# Advantages of magnification

$$\mu = \frac{1}{\det A} = \frac{1}{[(1-\kappa)^2 - \gamma^2]}$$

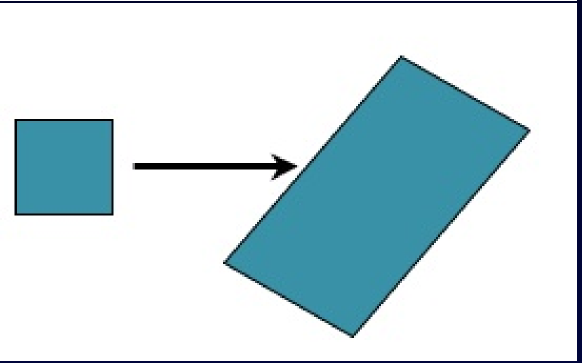

Magnification

- increase of the observed angular size: better spatial resolution in the intrinsic source.

- increase of total flux: better sensitivity.

The gain in resolution is anisotropic: along the shear direction it varies between $\sqrt{\mu}$ and $\mu$.

# Strong lensing and magnification effect

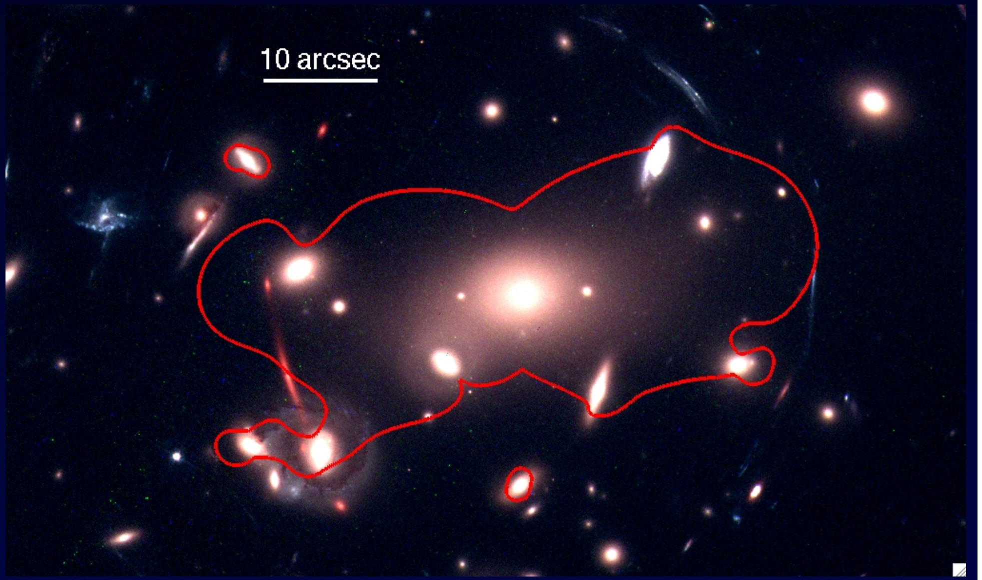


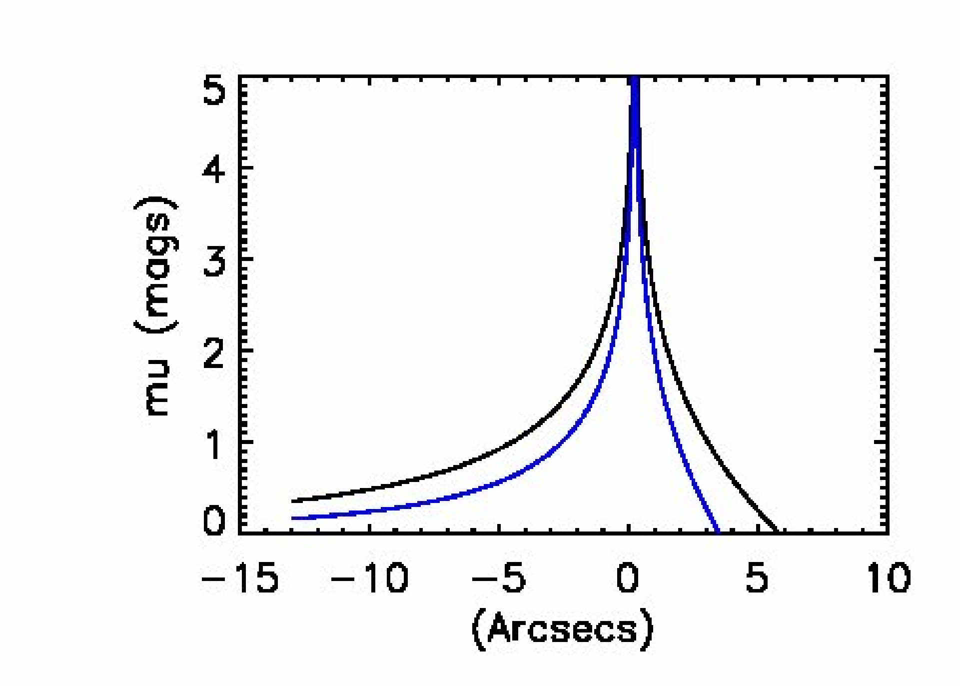


- Maximal magnification effect in the vicinity of the **critical lines**
- $\mu$ drops more quickly away from the critical line for more massive lenses / largest Einstein radii
- Cluster lenses provide the largest image plane area with a large magnification

# Strong lensing and magnification effect

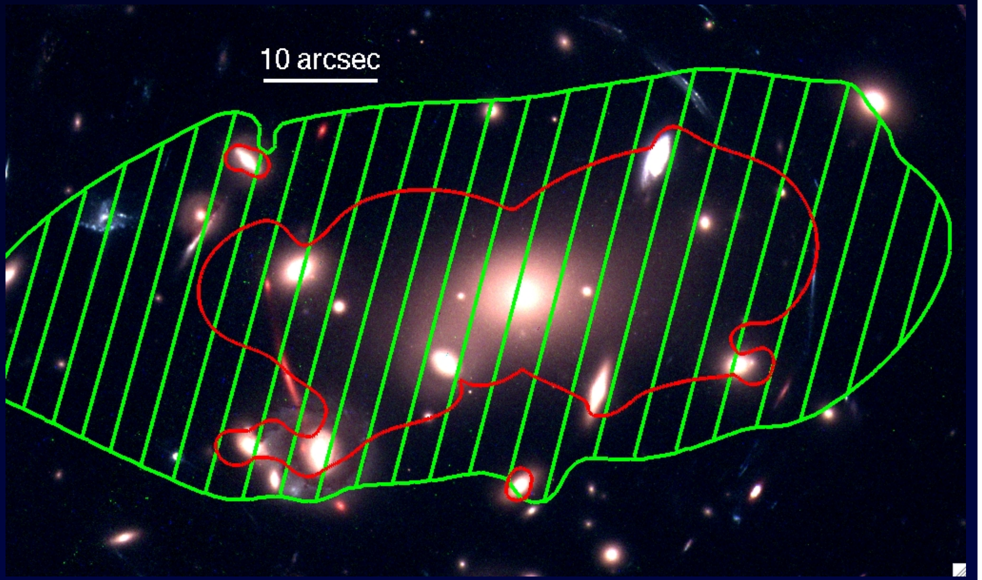


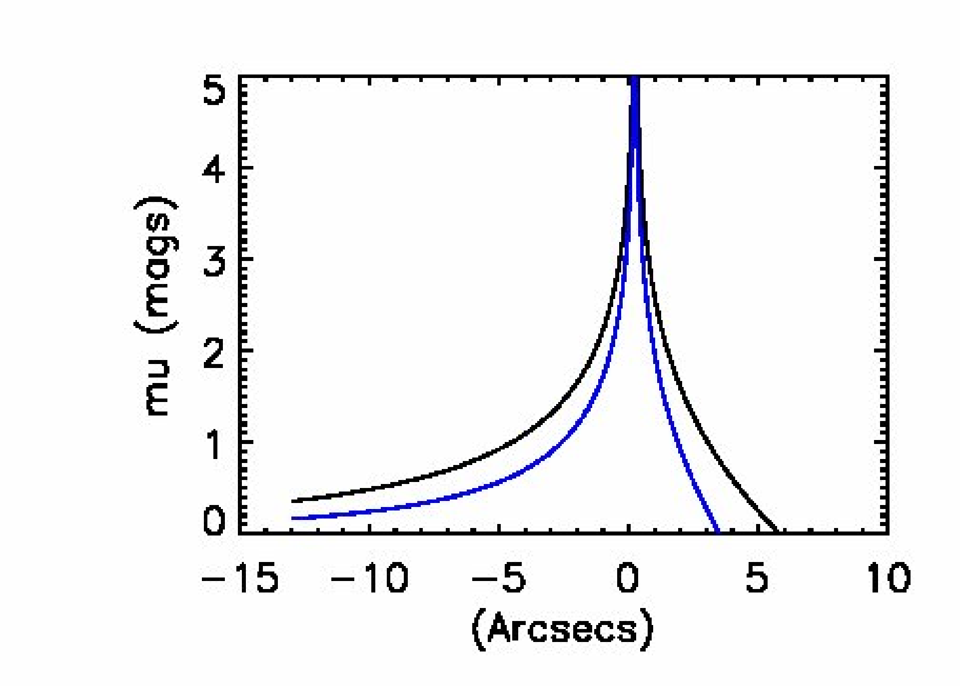


- Maximal magnification effect in the vicinity of the **critical lines**

- $\mu$ drops more quickly away from the critical line for more massive lenses / largest Einstein radii

- Cluster lenses provide the largest image plane area with a large magnification

# Example of resolutions achieved

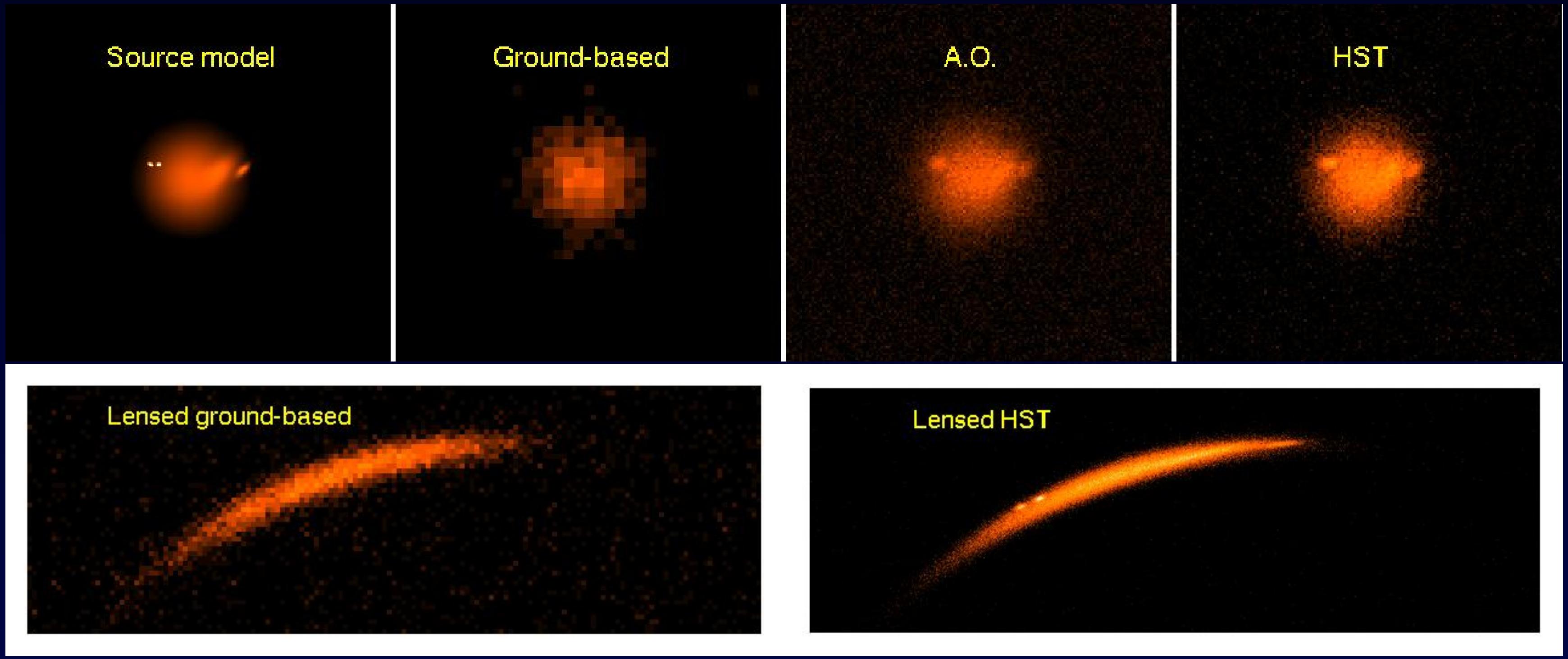


- Model of distant galaxy with multiple components and 2 star-forming regions separated by 500 pc.
- Only with the combination of lensing and high resolution imaging can we reach spatial resolutions $< 1kpc$ in distant galaxies.

# Historically: first source interpretation of a giant arc

CL2244

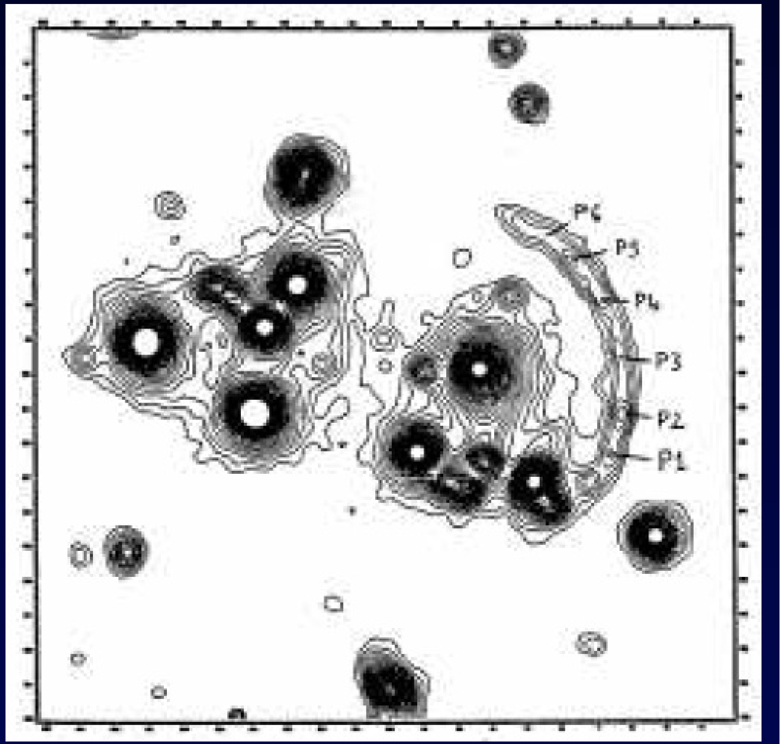


First spatially resolved source interpretation from the identification of bright clumps in a giant gravitational arc *Hammer et al. 1989*

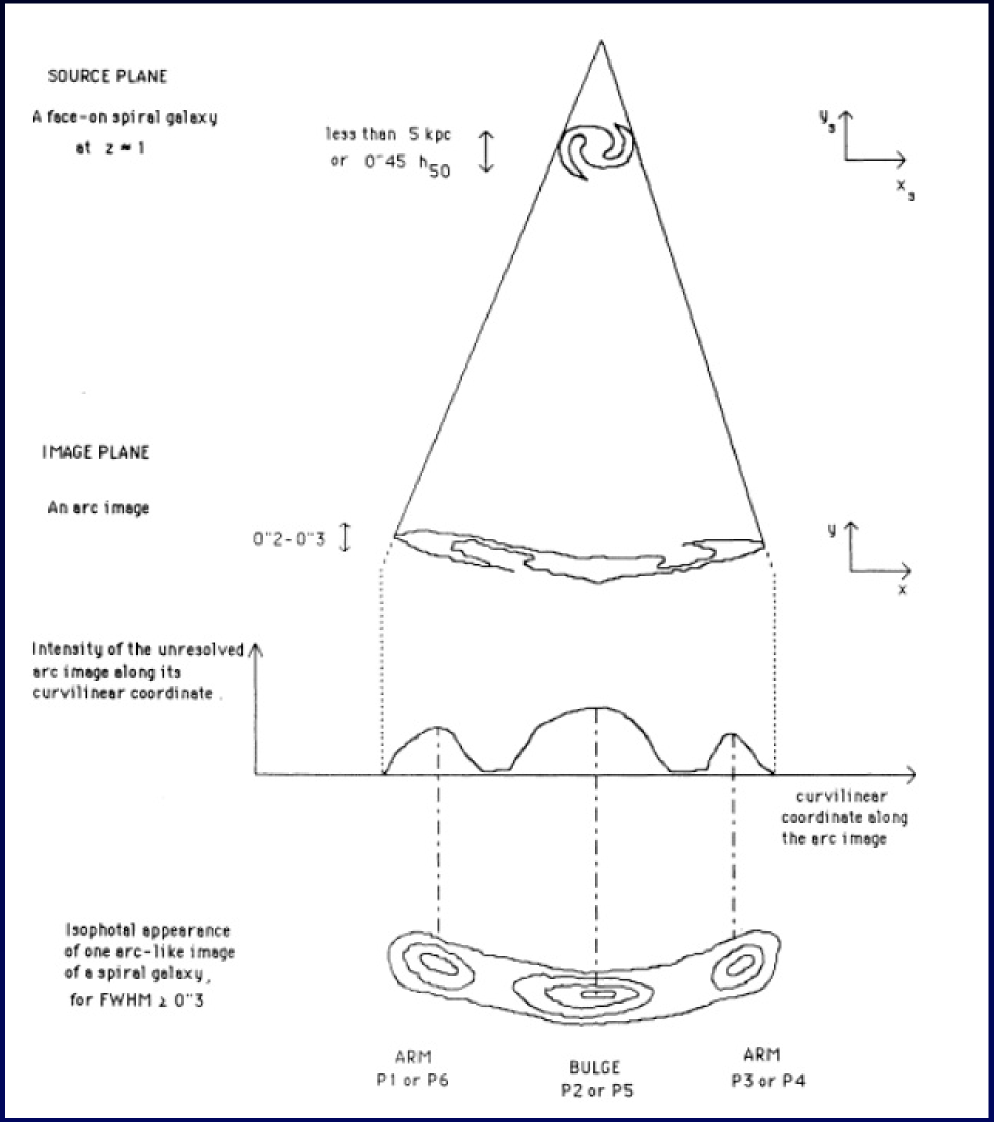


*Hammer & Rigaut 1989*

# Strong Lensing models: constraints from multiple images

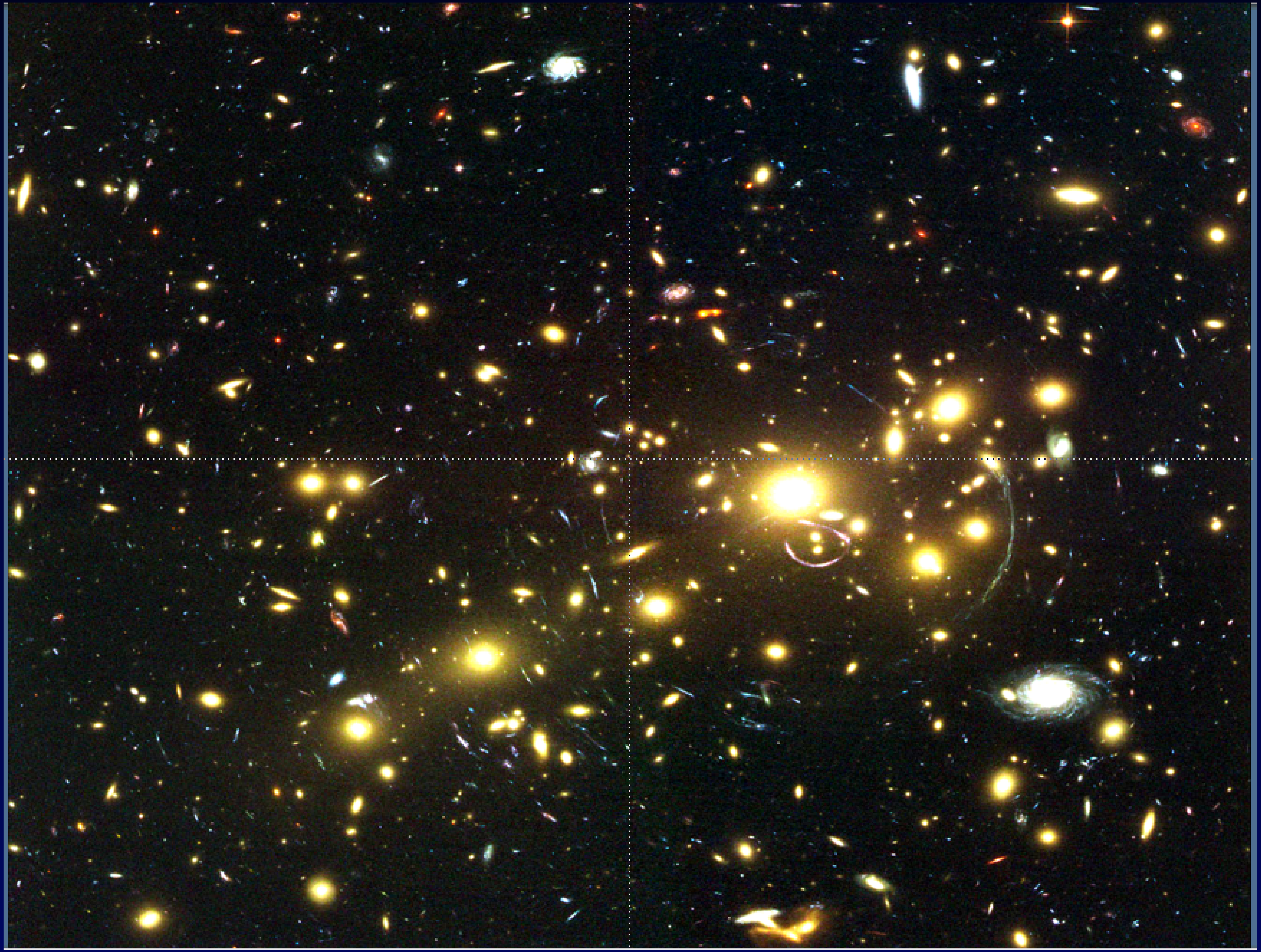

# Strong Lensing models: constraints from multiple images

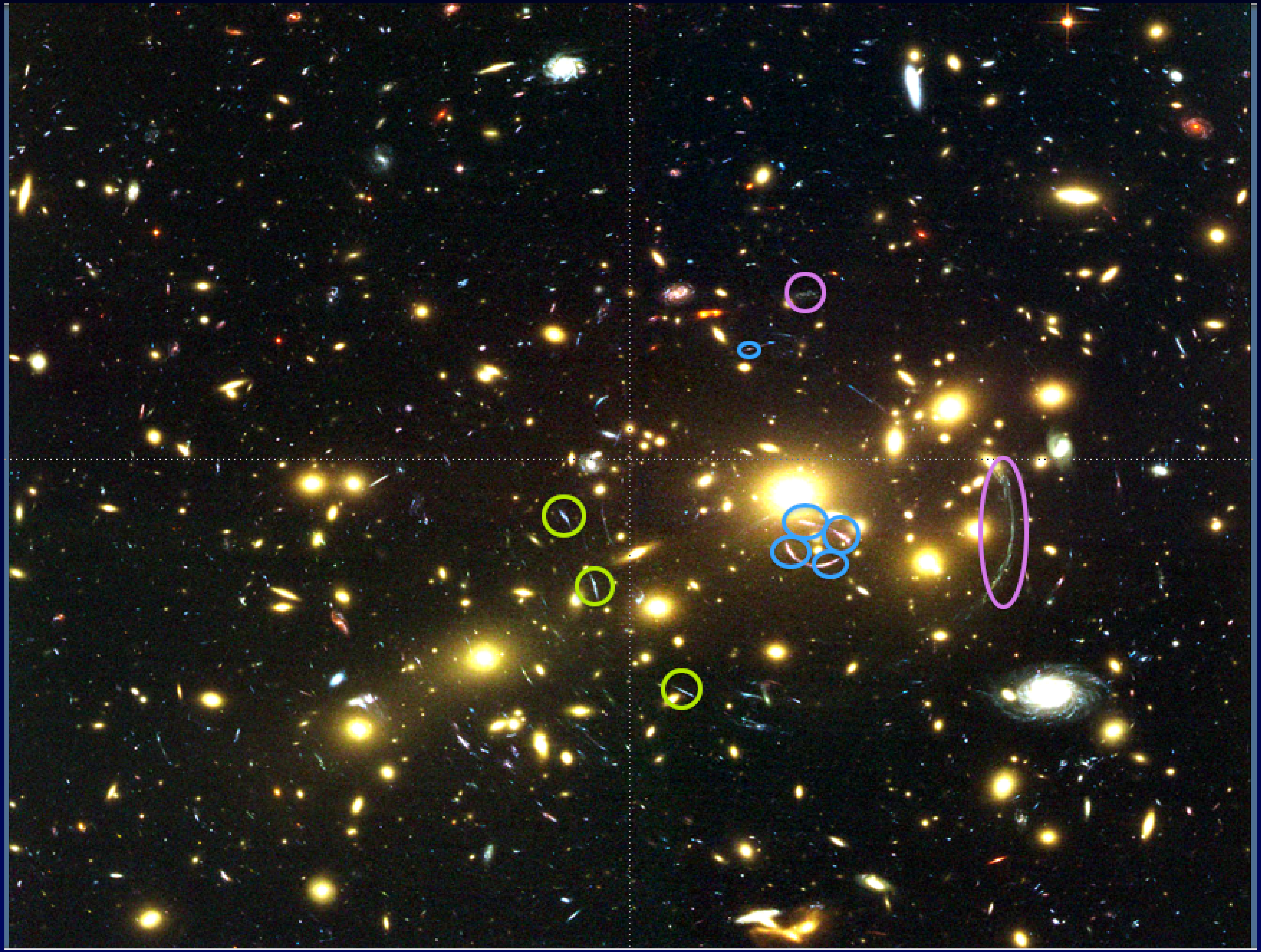

# Strong Lensing models: constraints from multiple images

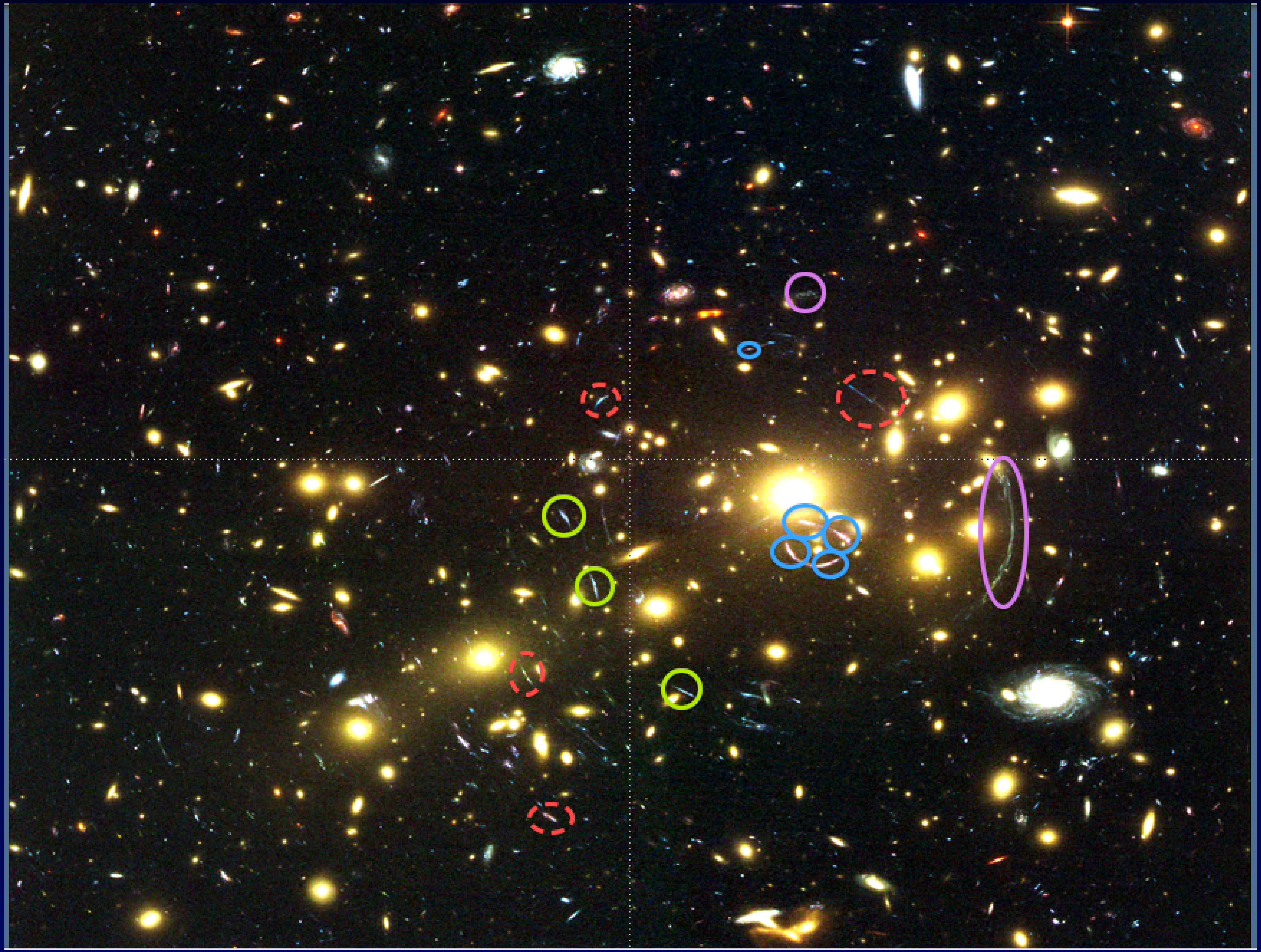

# Multiple images and resolution

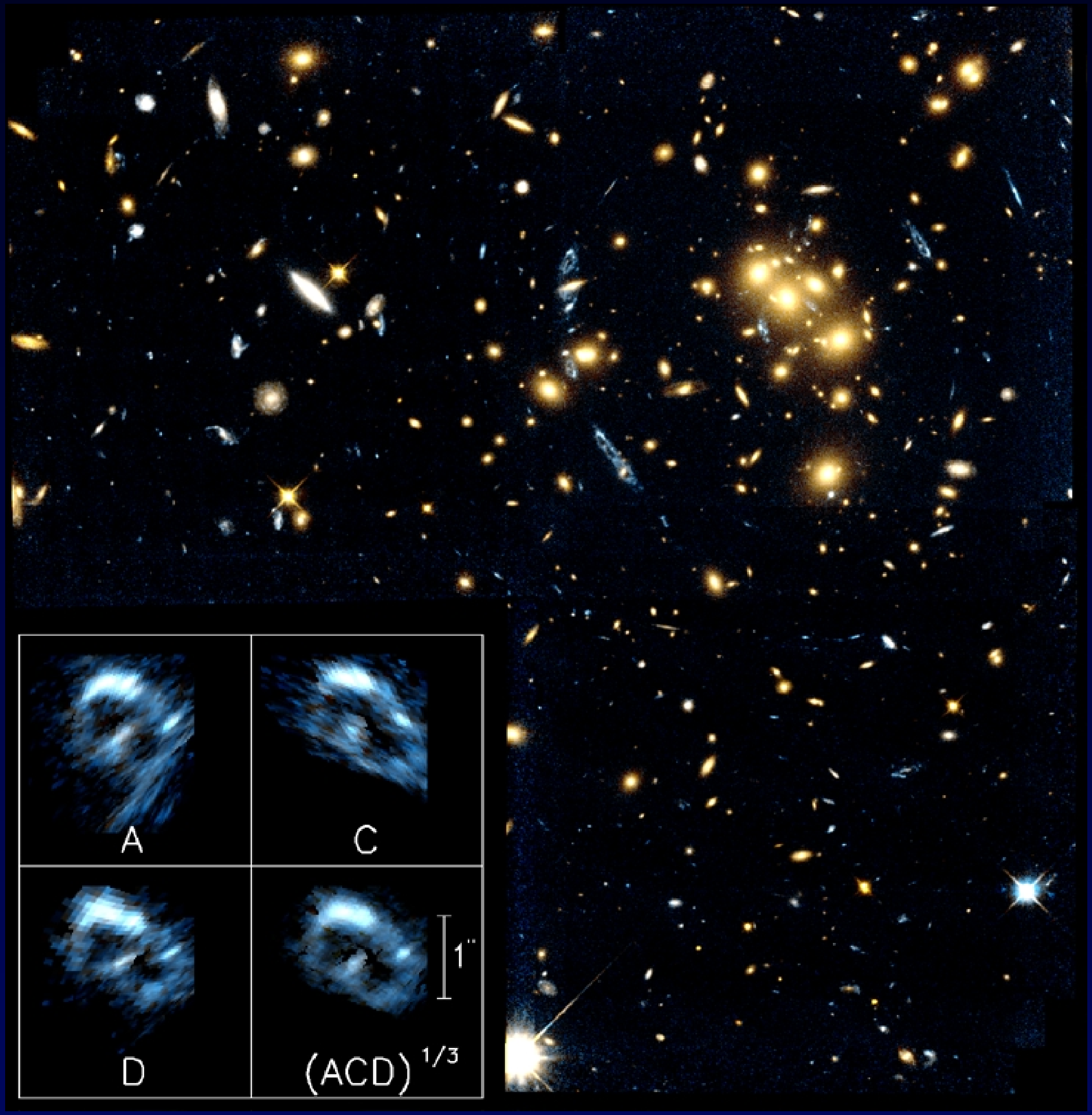


*Colley, Tyson & Turner 1996*

- Magnification differences between multiple images give different source-plane resolution

- Increase signal to noise by averaging the reconstructions of the 3 brightest images

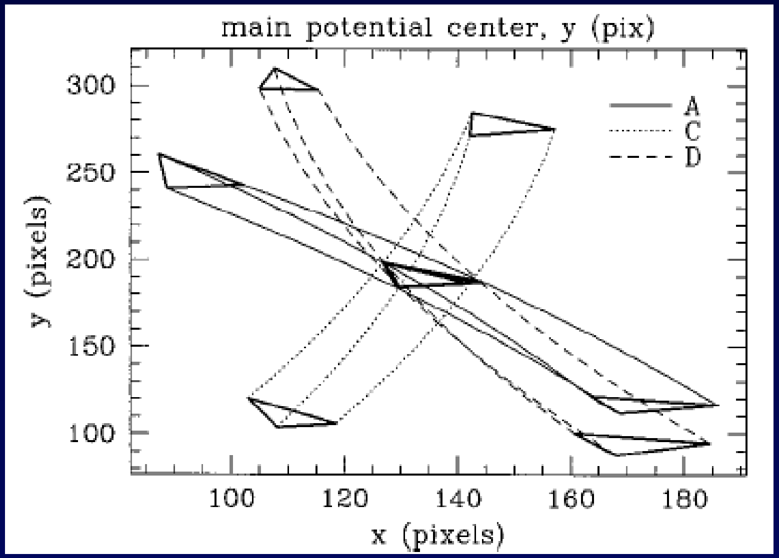

# Multiple images and caustic crossing

For sources crossing the caustic line, the multiple images probe different parts of the source.

$z = 2.07$ lensed source crossing the cluster caustics in Abell 1835

Image plane (*Richard et al. 2010*)

# Multiple images and caustic crossing

For sources crossing the caustic line, the multiple images probe different parts of the source.

$z = 2.07$ lensed source crossing the cluster caustics in Abell 1835

Image plane (*Richard et al. 2010*)

Source plane reconstructions:

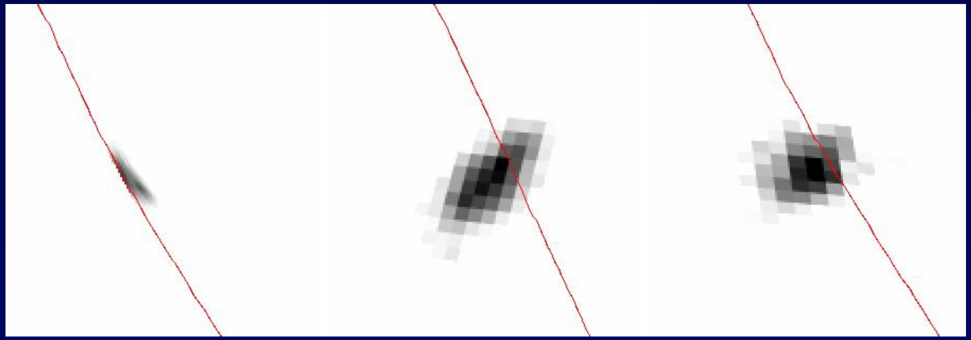

# Direct reconstruction

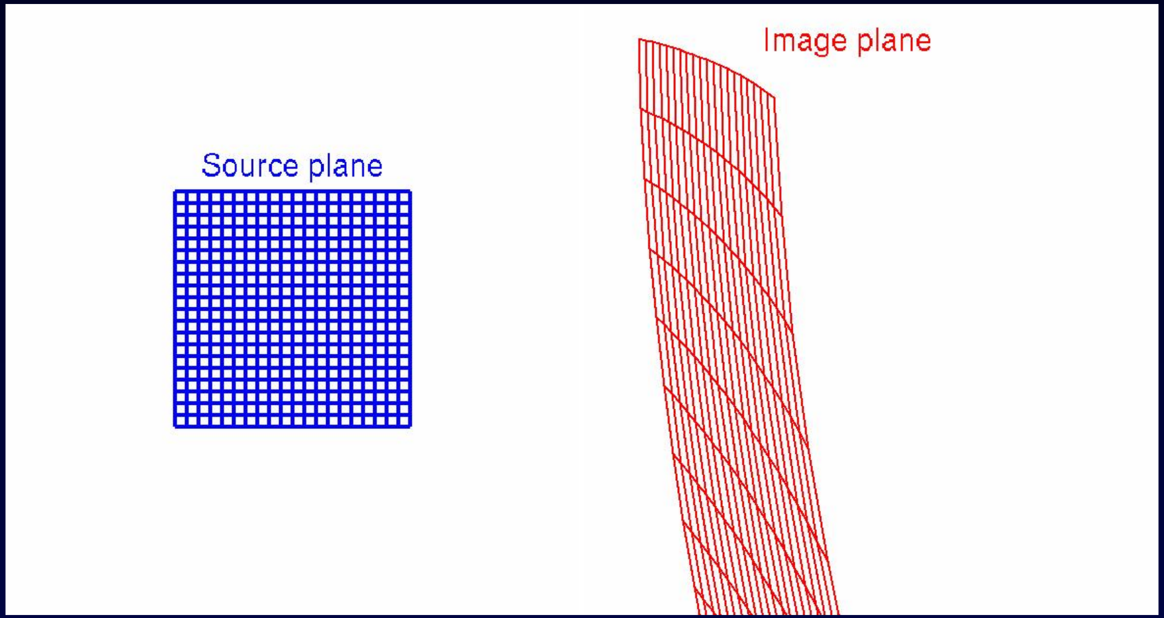


For a given source redshift, the mass model of the lens potential(s) provide the geometrical transformation between the source and image plane positions $(x_i, y_i) = F(x_s, y_s)$.

This transformation can be used for a direct reconstruction on a regular source plane grid, using the surface brightness conservation.

# Direct reconstruction

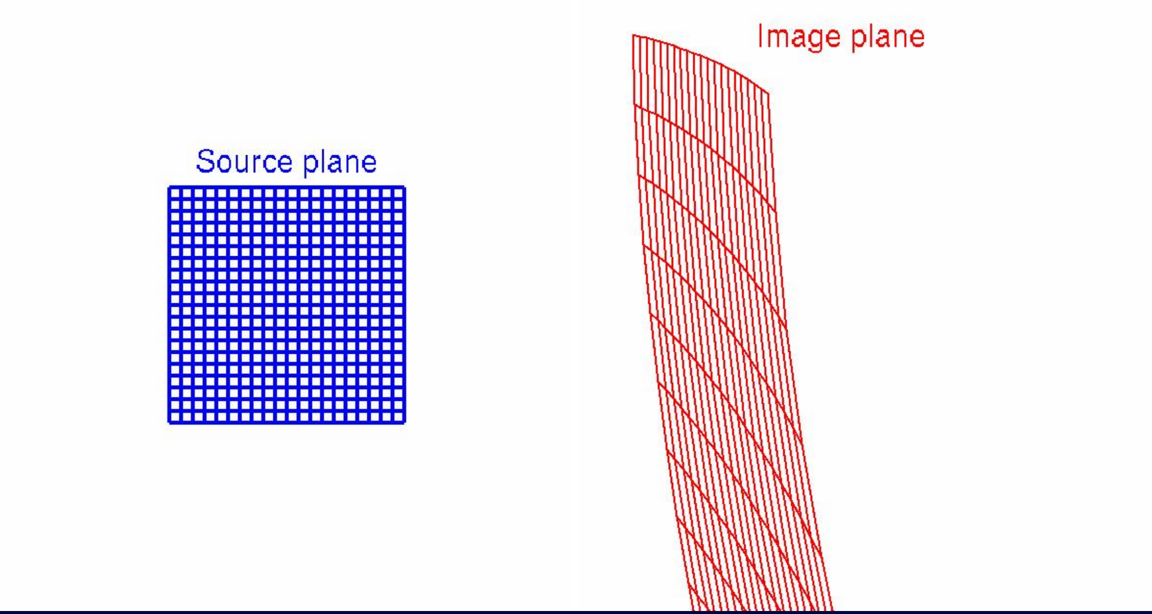


+ Straightforward calculation
+ No assumption on the source morphology

- Correlated source plane pixels at the highest resolution pixel grid
- Point Spread Function remains in the source plane

This technique gives useful results when the PSF is small (Adaptive Optics, Hubble images, good seeing) and when the image to reconstruct is isolated.

# Parametric source reconstructions

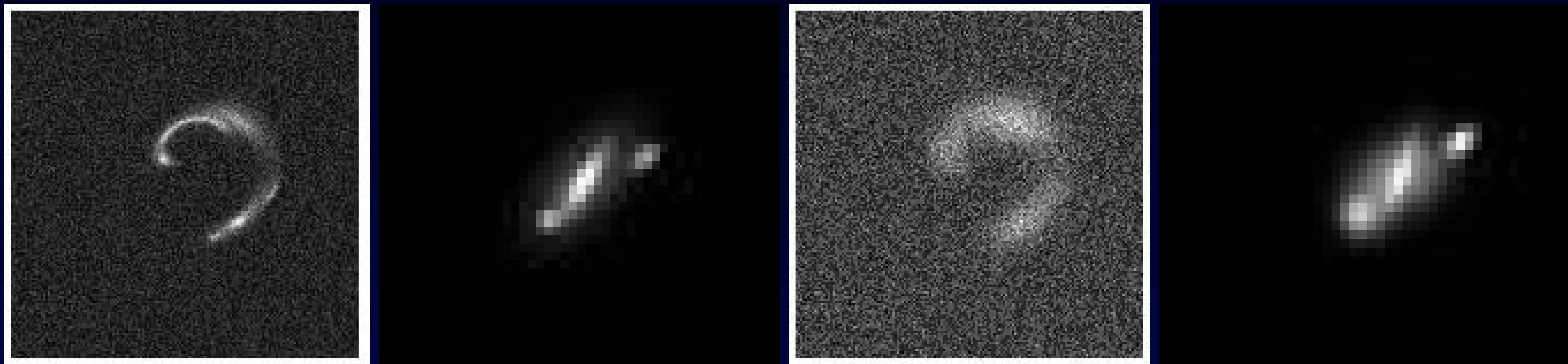

- Based on empirical galaxy morphology, small number of parameters
- The source is a linear combination of elliptical Gaussian or Sérsic profiles
- Similar idea as the Galfit fitting software (*Peng et al. 2010*), but including the lensing effect.

$$\Sigma(r) = \Sigma_0 \exp\left\{-b_n\left[(r/r_e)^{1/n}\right]\right\}$$

# Non-Parametric reconstructions: Adaptive grid

Semi-linear inversion technique (Dye & Warren 2005)

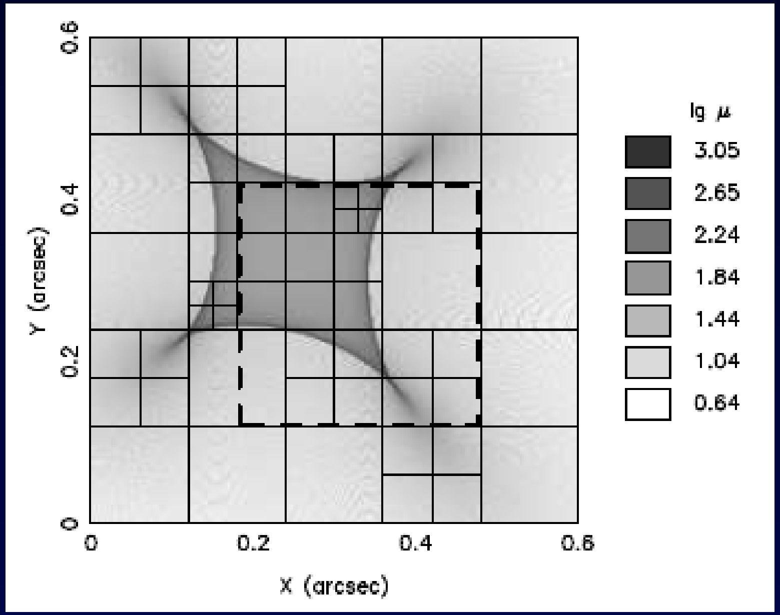


$$\mathbf{S} = \mathbf{F}^{-1}\,\mathbf{D}.$$

$$\mathbf{F}_{ik} = \sum_{j=1}^{J} f_{ij} f_{kj}/\sigma_j^2 \,, \quad \mathbf{D}_i = \sum_{j=1}^{J} f_{ij} d_j/\sigma_j^2 .$$

- Advantage: PSF taken into account, full minimization of lens and source properties
- Unregularised source: adaptive grid depending on magnification factor
- Regularised source: better resolution using best-fit model

# Adaptive grid: application

*Dye et al. 2008*: results on the 'Cosmic Eye'

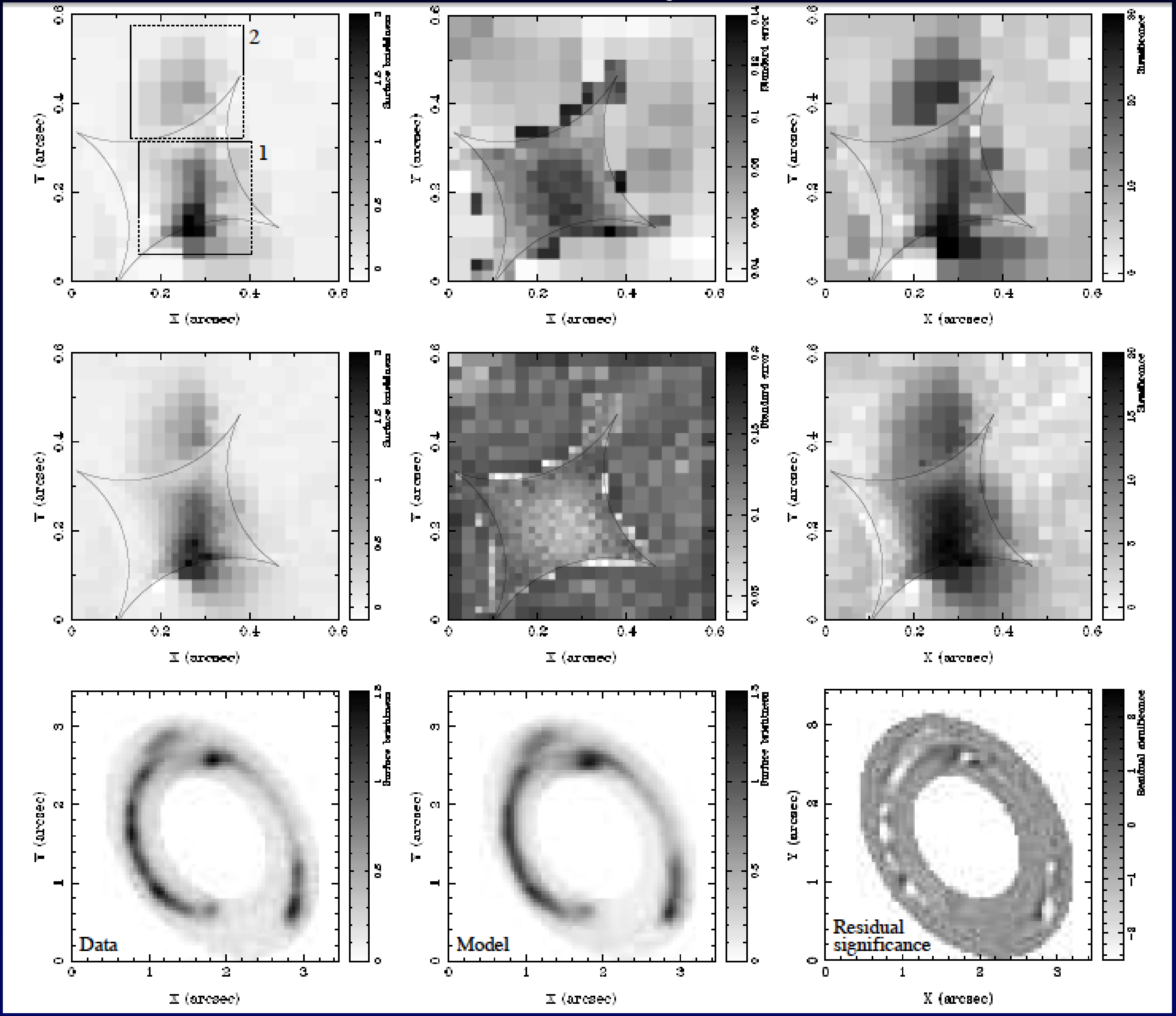

# Resolved morphology

# Resolved morphology

Current galaxy formation models assume that disk galaxies form by gas accretion (quiescent star formation), and then transform into spheroidal stellar systems mostly by major mergers (intense starbursts).

Predictions from numerical simulations: isolated (non-interacting) massive star-forming galaxies show a thick disk extending up to ∼10 kpc with large clumps of $\sim 10^9$ $M_\odot$ each, and sizes $< 1kpc$.

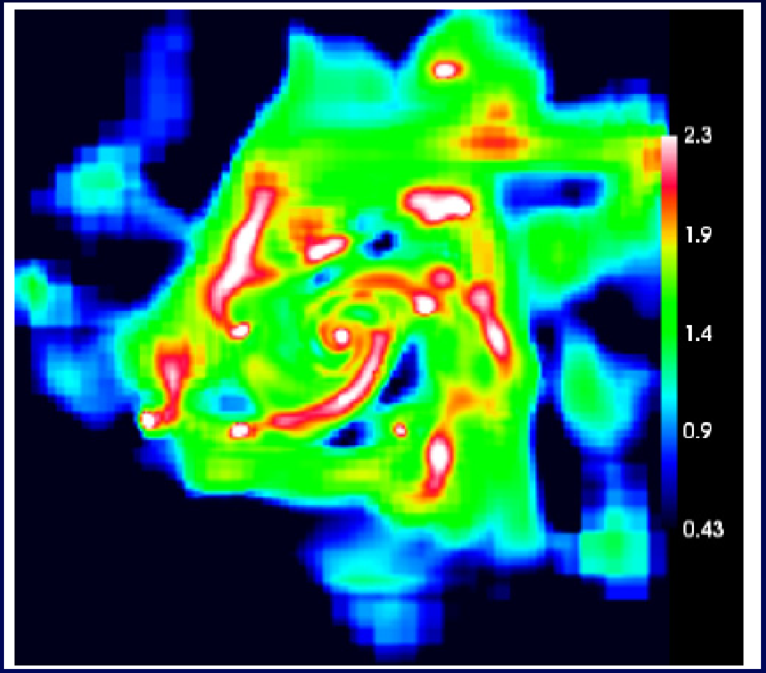


*Dekel et al. 2009*

# Non-lensed examples: observations

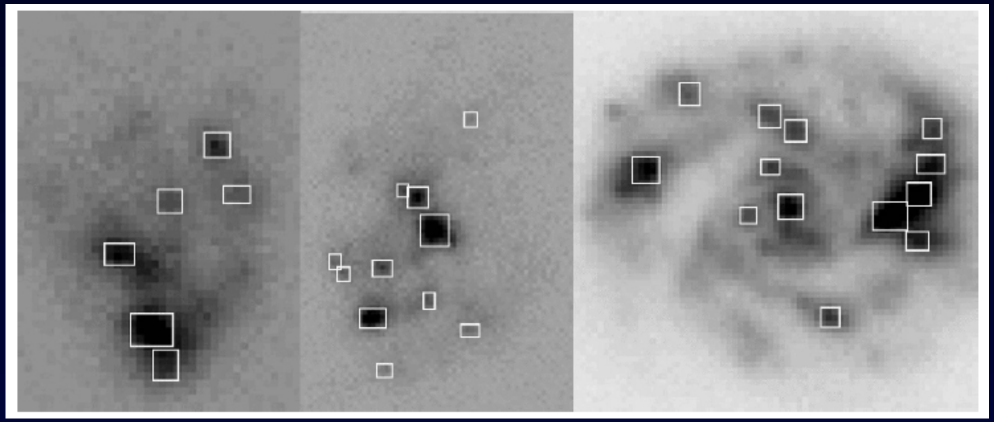

*Elmegreen et al. 2009*

Luminosity and colors of all compact regions (bulges, bulge-like regions and star-forming regions) of extended sources in UDF ($r_e > 0.3$").

Typical clumps have masses of $10^8$ $M_\odot$ at $z > 0.5$.

So-called ‘Chain galaxies’ and ’clump clusters’ which are spiral galaxies in formation.

# Non-lensed examples:SINS

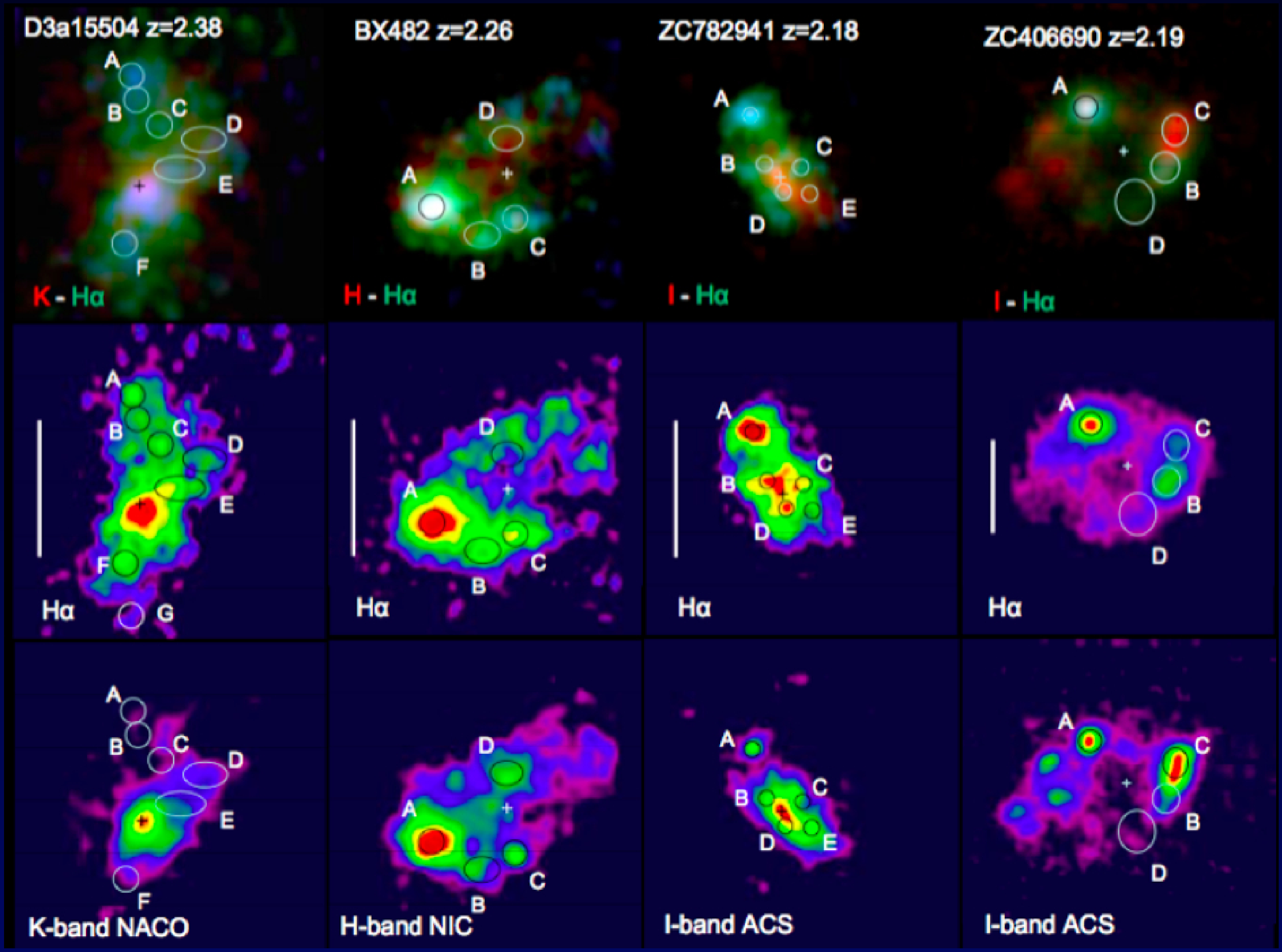

# Non-lensed examples: observations

*Law et al. (2011)*:
morphological measurements
of LBGs with HST/WFC3.

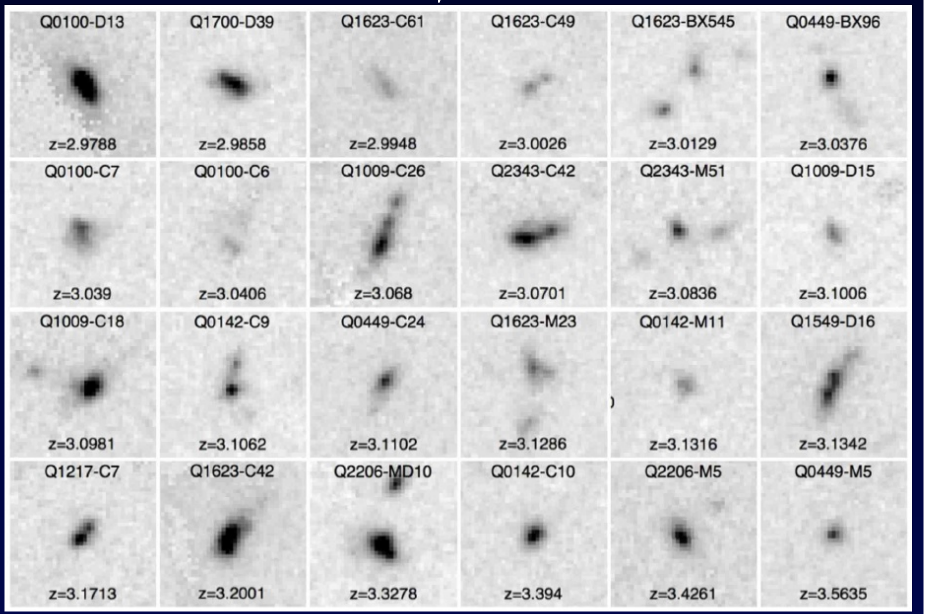


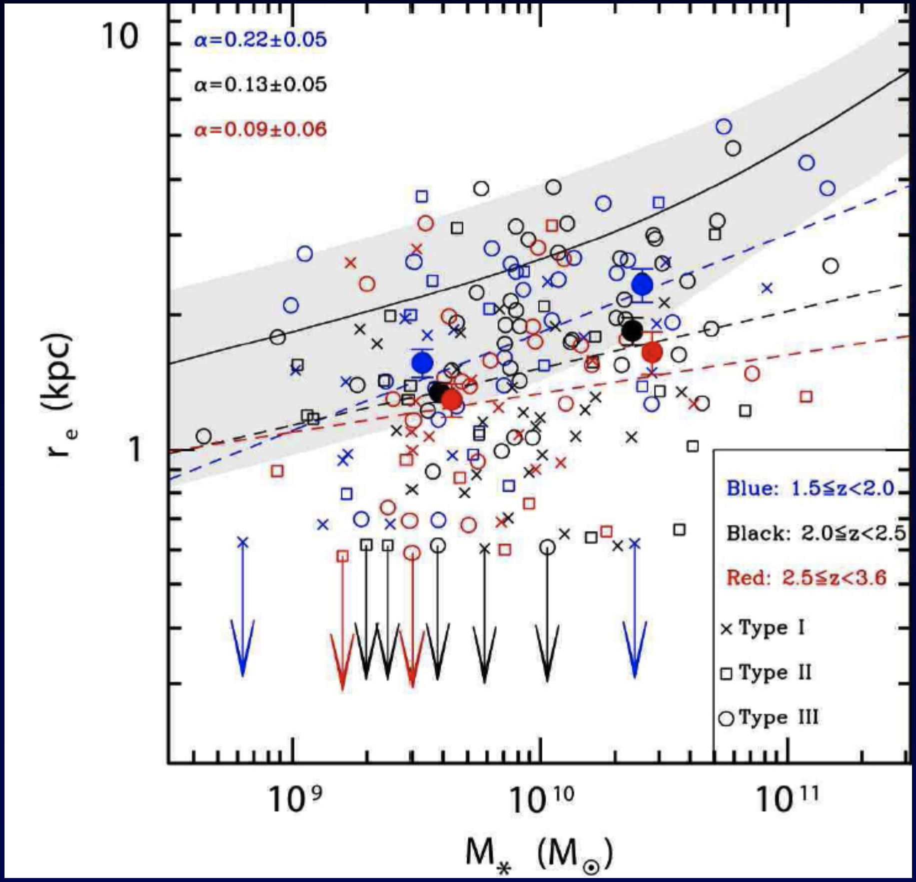


- Typical sizes of massive galaxies at $z = 1.5 - 3.6$ range within re$\sim 0.7 - 3$ kpc
- The stellar mass-radius relation is observed at $z \sim 3$ with an evolution as $\sim (1 + z)^{-1}$

# Non-lensed examples: size evolution

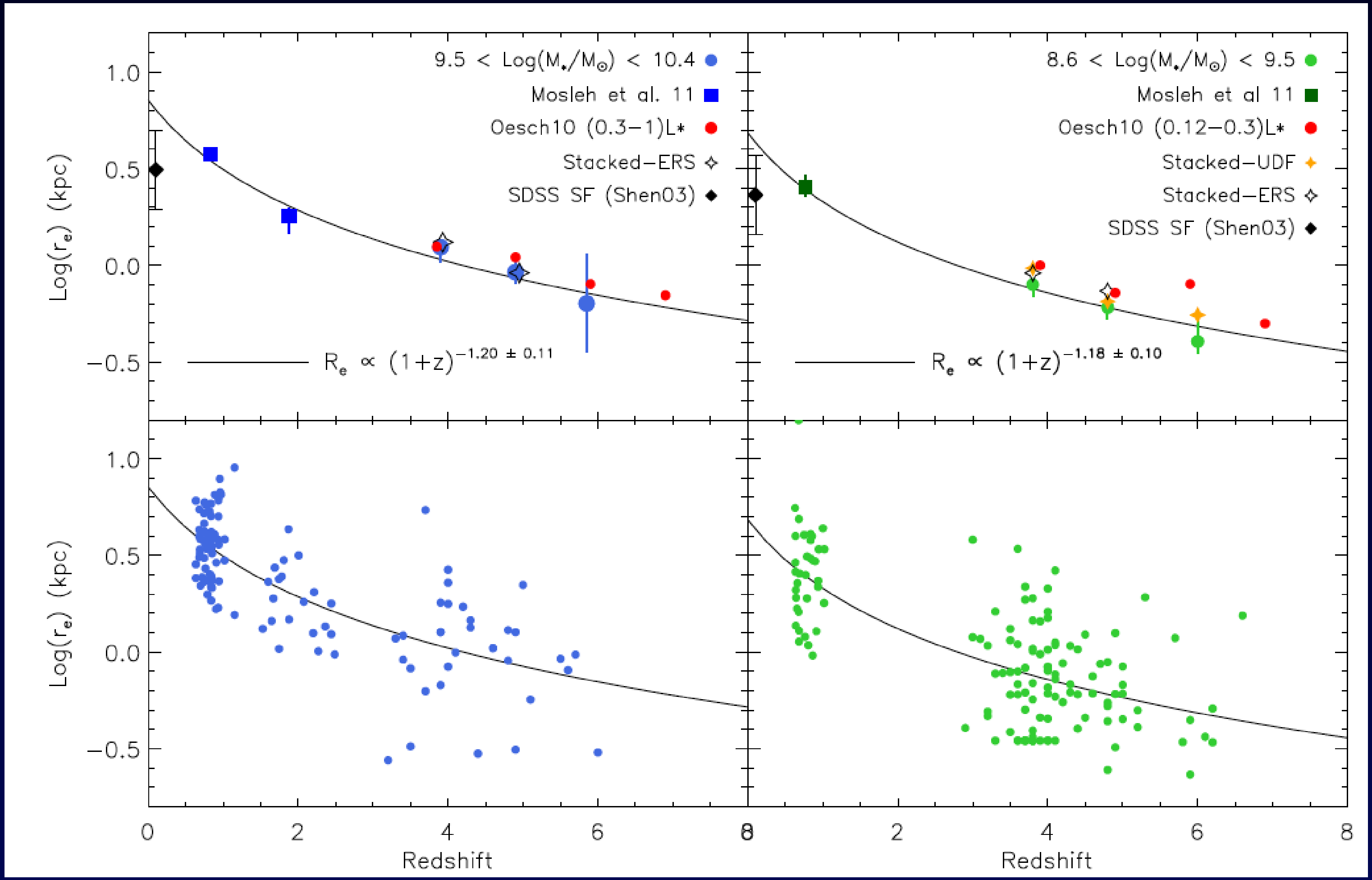


*Mosleh et al. 2012*

Extrapolation: $r_e < 1$ kpc at $z > 3$ (high mass) or $z > 2$ (low mass)

# Resolution limit

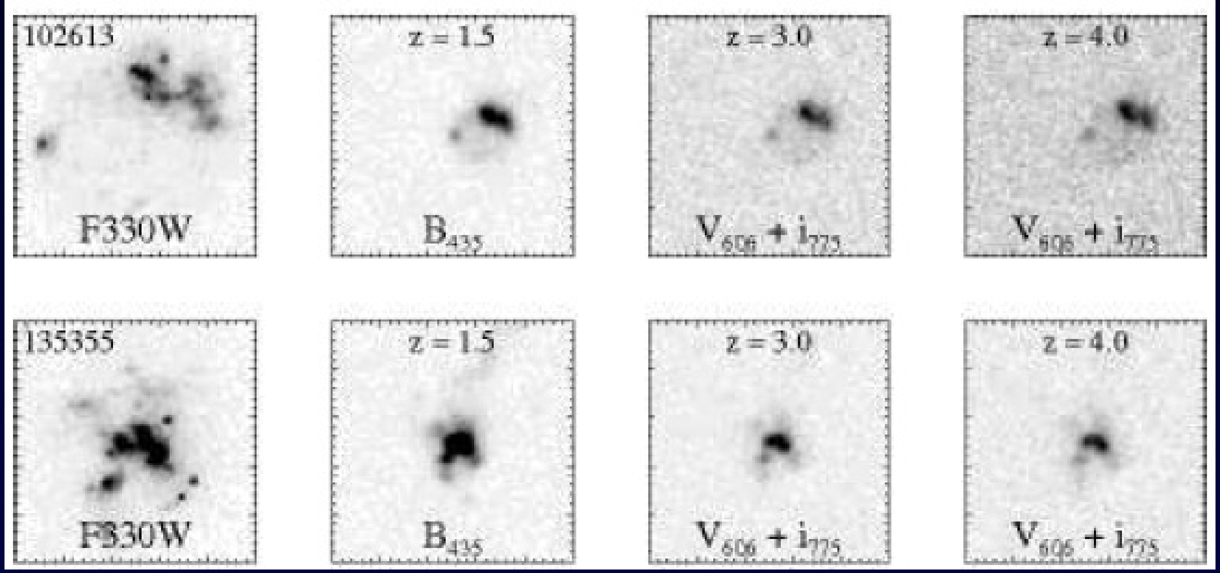


*Overzier et al. 2007*: predictions using local LBG analogs.

At $z > 1.5$ only the brighter clumps are resolved (0.15"=1 kpc)

Gravitational lensing is the only way to resolve multiple star-forming clumps in distant galaxies.

# Spectacular source reconstructions: RCSGA032727-132609

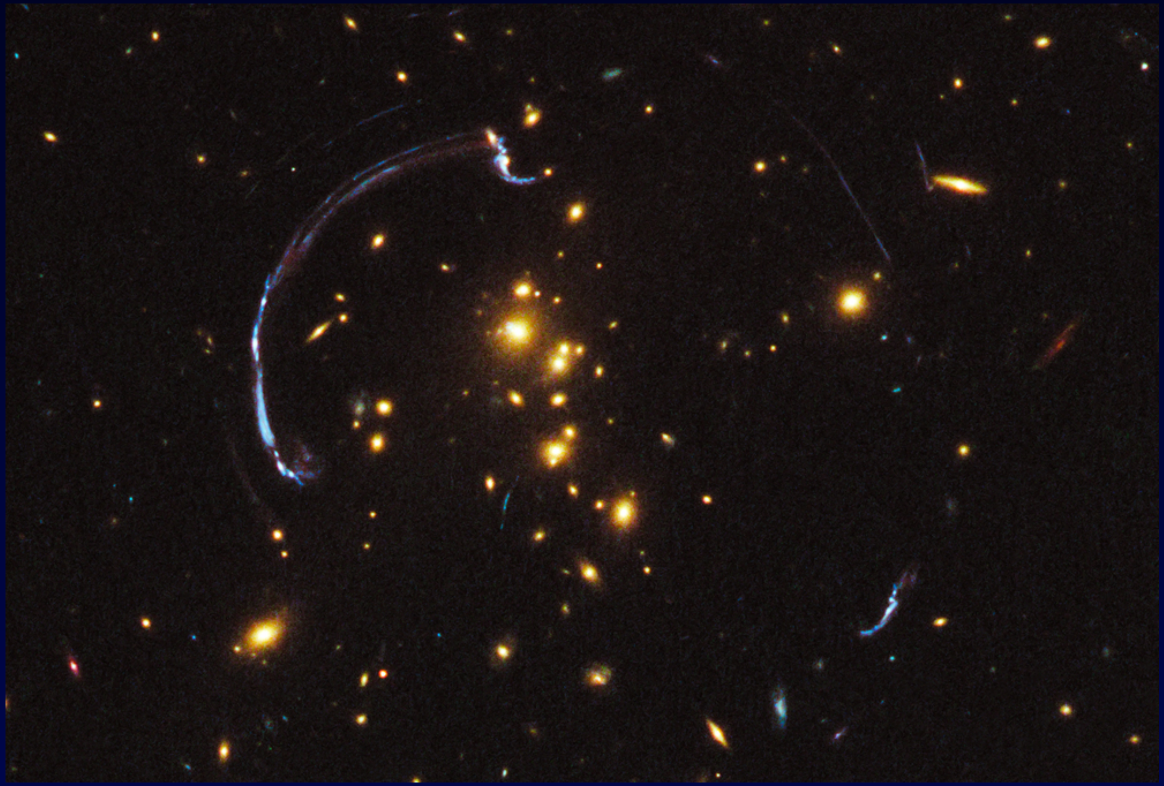

38 arcsec long
Less-magnified counter-image

- Identified in the RCS2 cluster survey (*Gilbank et al. 2011*)
- Spectroscopic redshift $z = 1.7$ (*Wuyts et al. 2010*)
- High resolution HST imaging (*Sharon et al. 2012*) in 6 filters from F390W to F160W

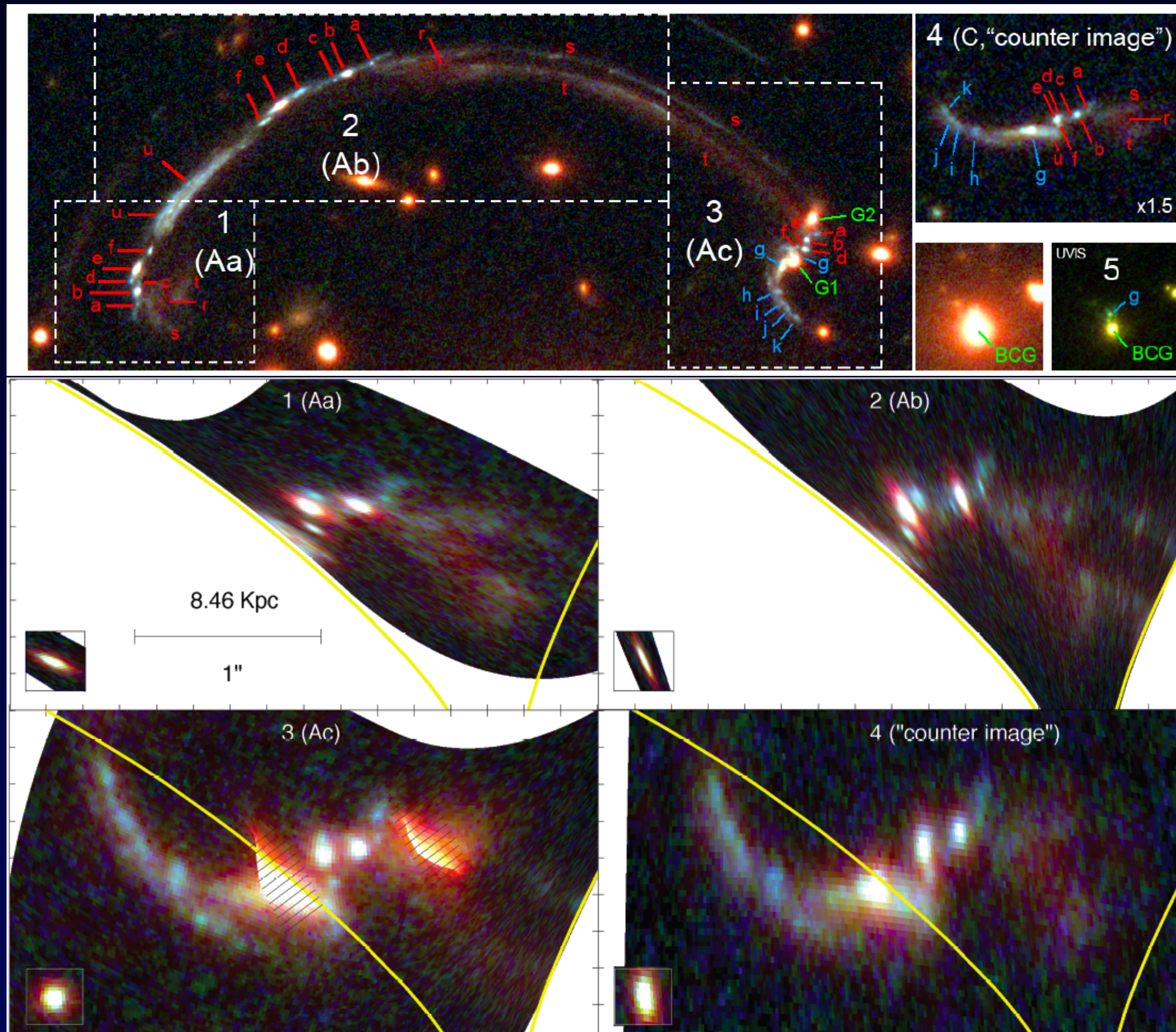
1 (Aa)
2 (Ab)
3 (Ac)
4 (C,“counter image”)
x1.5
BCG
UVIS
5
BCG
G1
G2
1 (Aa)
8.46 Kpc
1"
2 (Ab)
3 (Ac)
4 ("counter image")

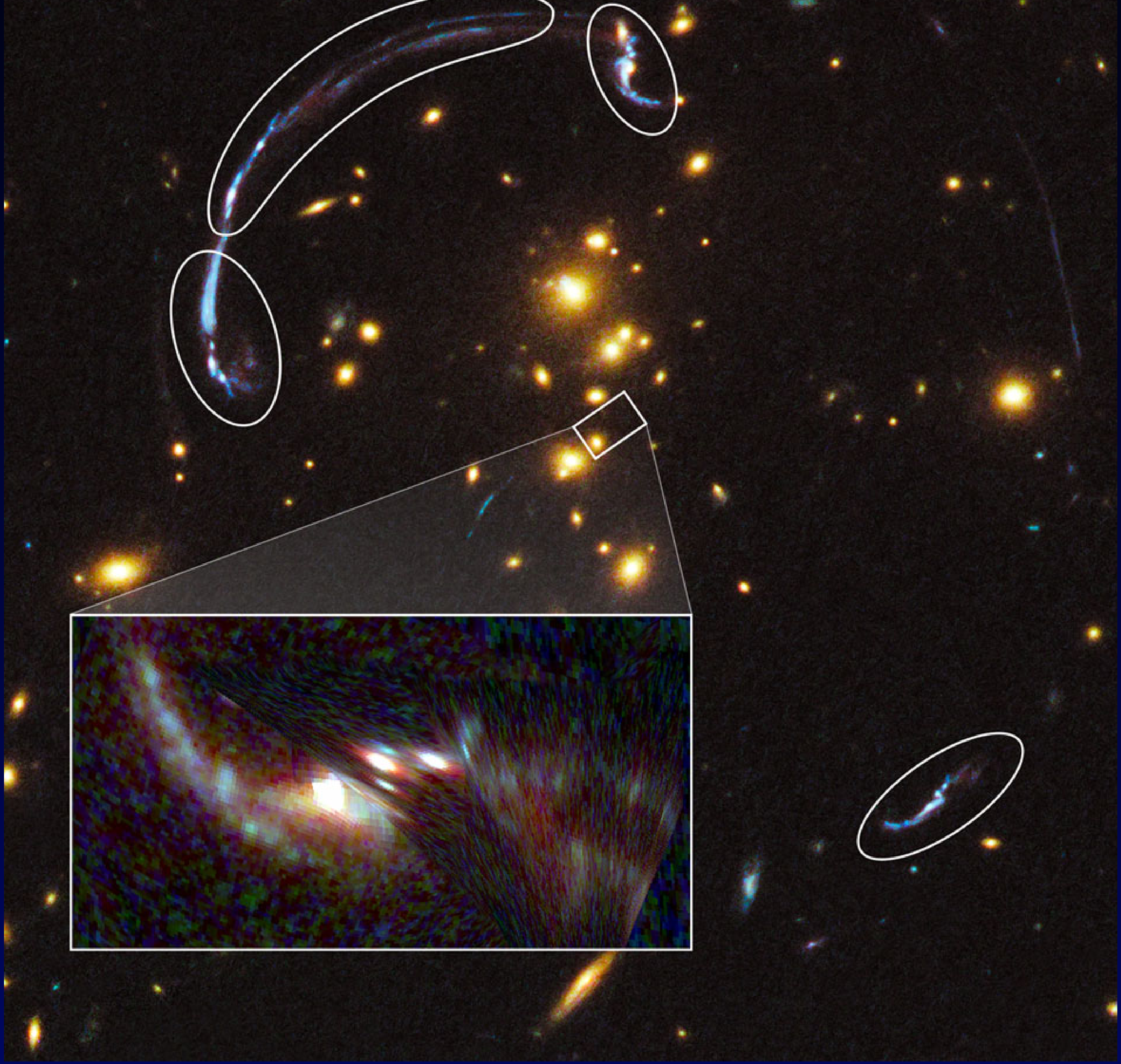

## Spectacular source reconstructions:RCSGA032727-132609

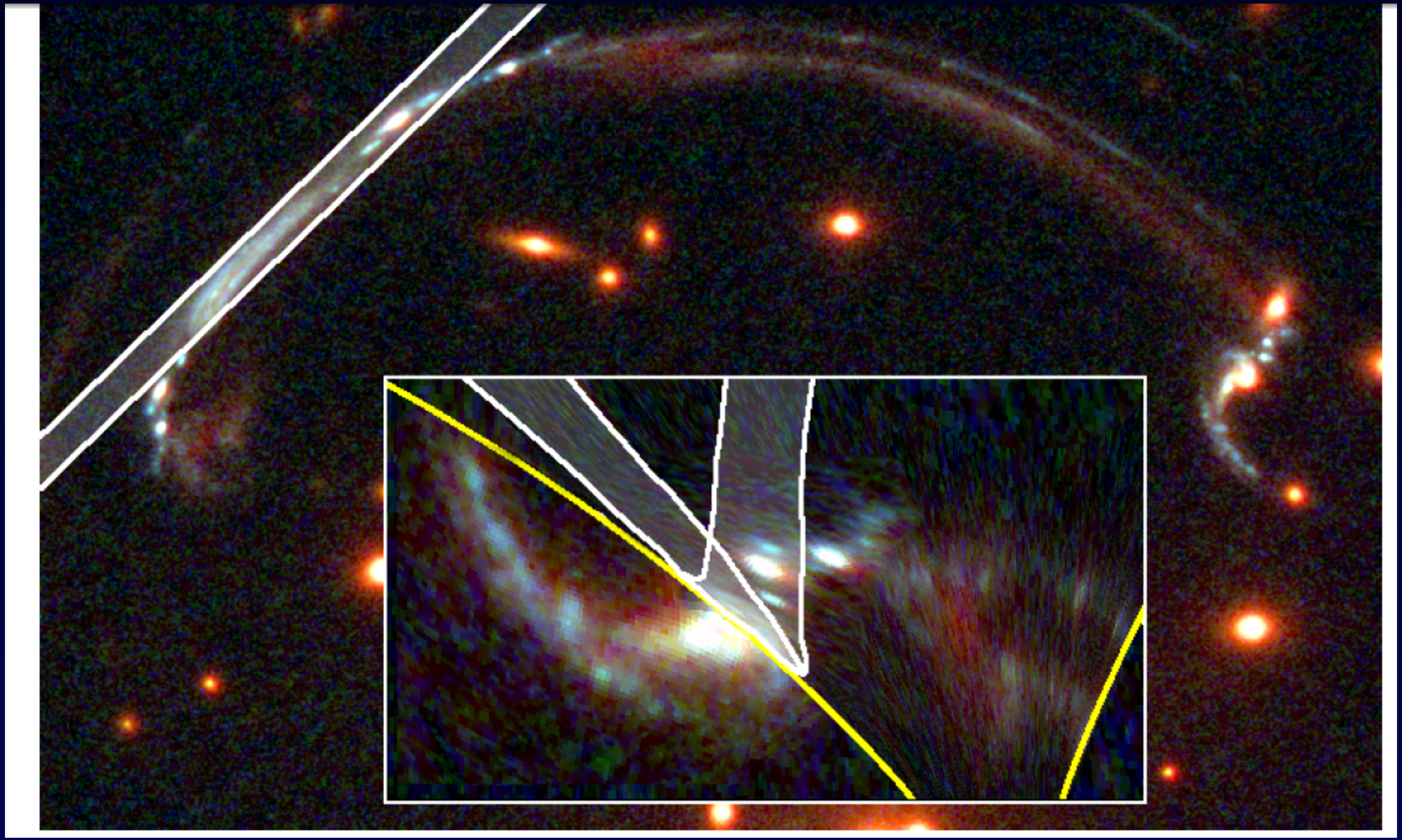

- NIRSPEC long slit observations of the highest resolution part (*Rigby et al. 2011*)
- H$\alpha$ measured only on a small region of the source

# A370 giant arc

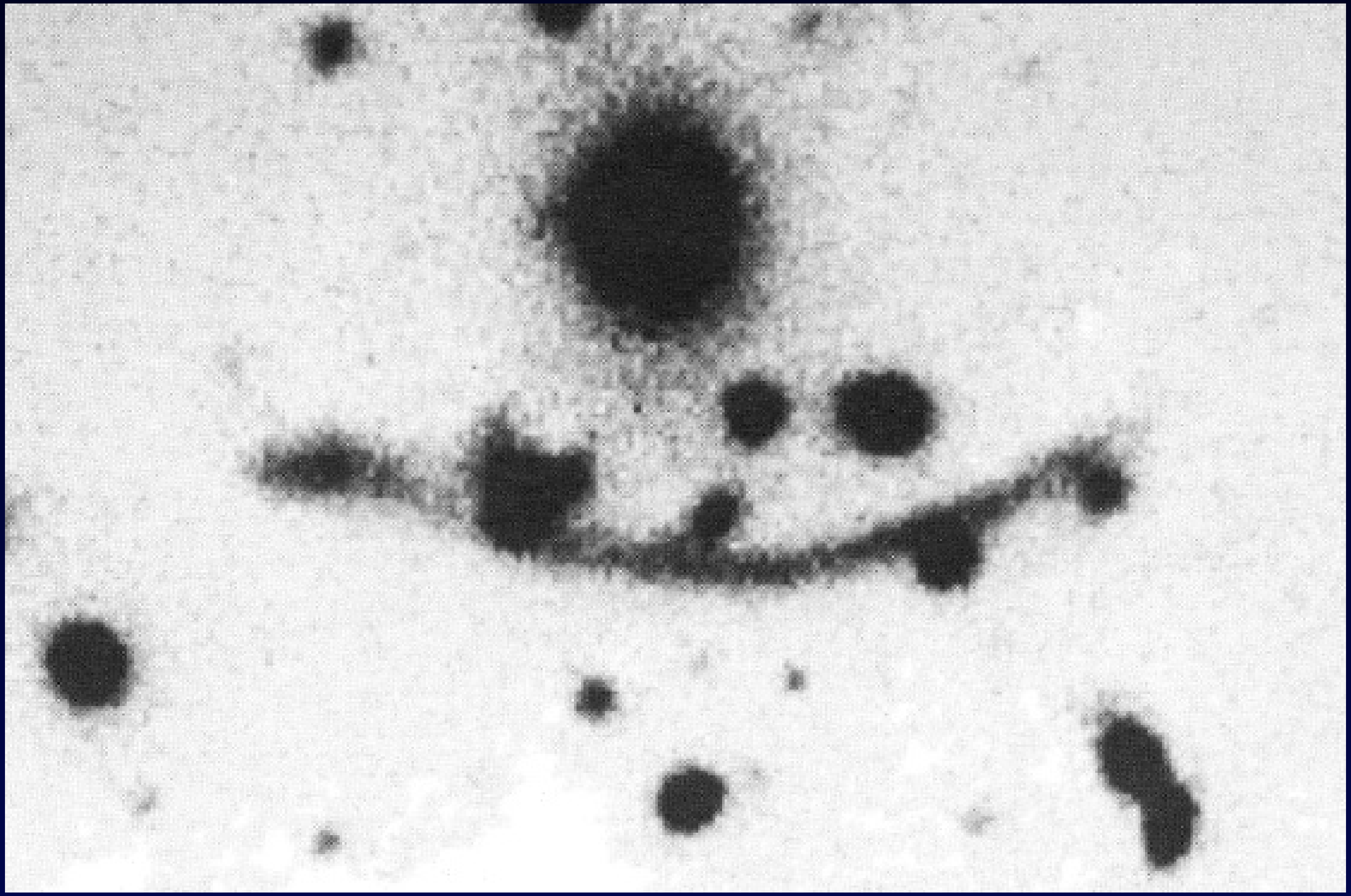

One of the first giant arc discovered, first spectroscopic measurement $z = 0.7$ (Soucail et al. 1988)

Original mass models based on ground-based data used a triple-image configuration.

# A370 Spiral

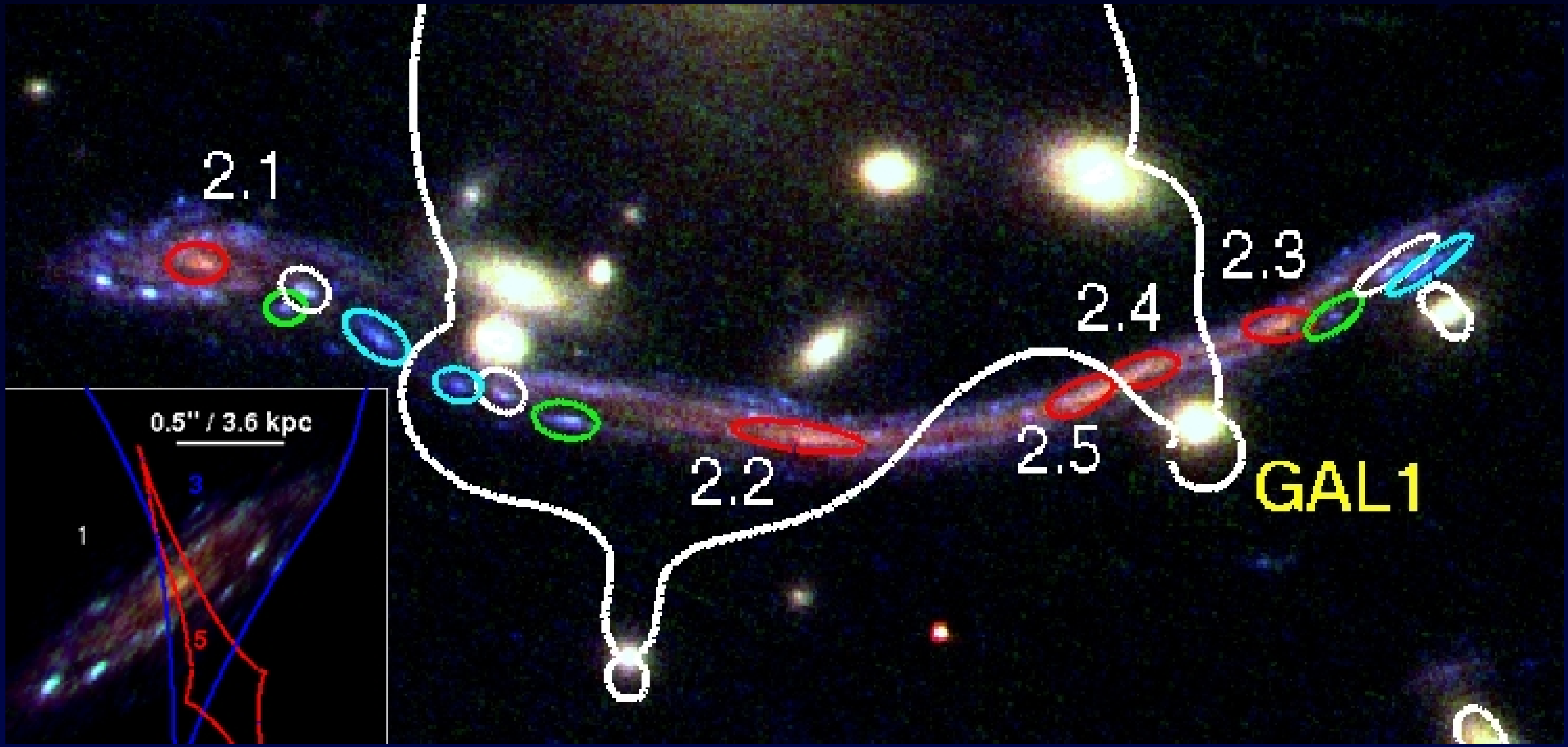


*Richard et al. 2010*

Refurbished Hubble ACS imaging: F475W, F625W and F814W

Improved resolution and color information show spiral galaxy crossing 2 caustics (regions with 1, 3 and 5 multiple images), with a red bulge and multiple blue star forming regions.

# Morphology at high redshift: star-forming regions

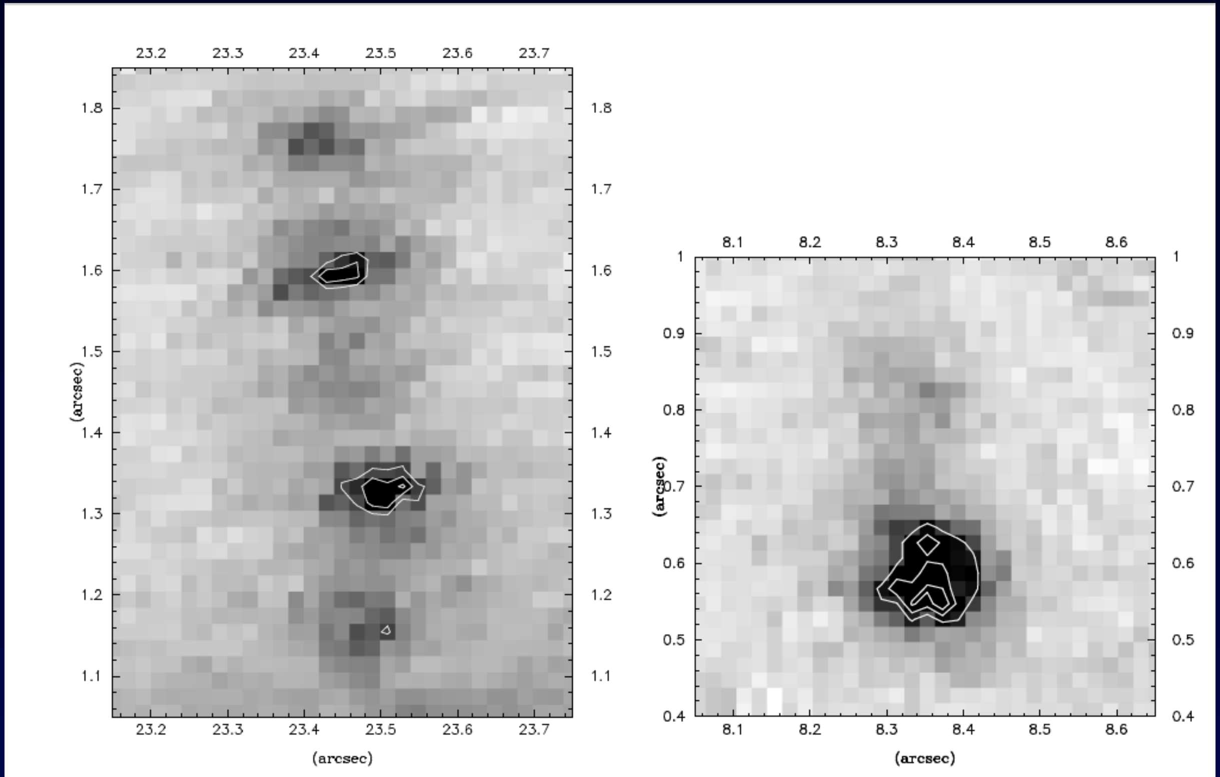


*Pello et al. 1999*

Reconstructed clumpy morphology: star-forming regions spaced by a few kpc.

Resolved Spectral Energy Distribution: comparison between Hubble and ground-based/near-infrared images (*Bunker et al. 1999*).

# Morphology at high redshift: resolved clumps at $z \sim 5$

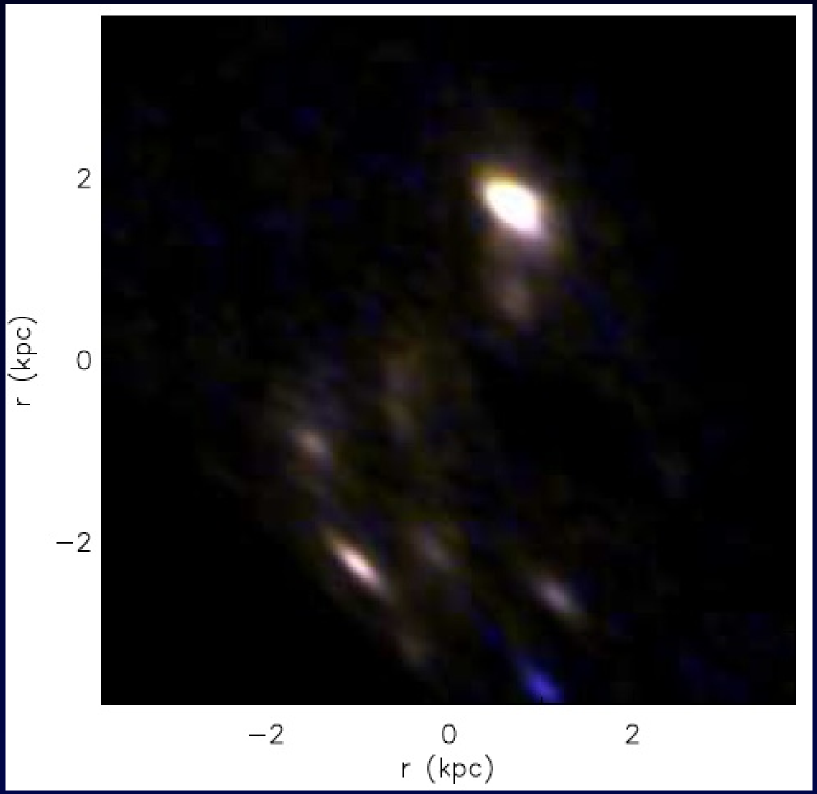


Swinbank et al. 2009


- Famous Franx et al. 1997 $z = 4.92$ galaxy
- 2 separate lens models and reconstructions agree on a very clump structure
- The brightest clumps are well-detected in $[OII]$ line

# Comparison with z=2-3

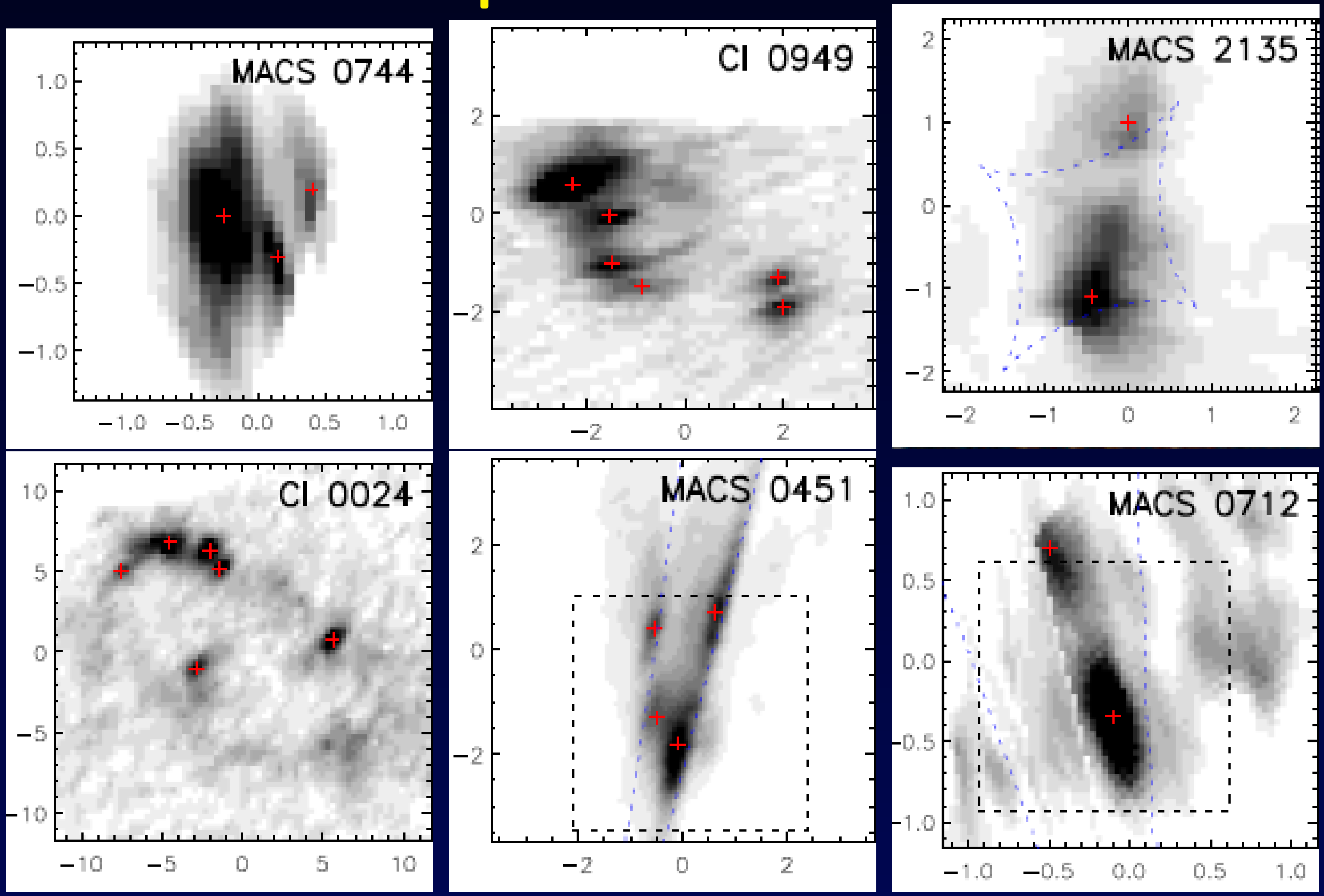


- Keck/OSIRIS observations of $z \sim 2-3$ sources (Jones et al. 2010)
- Combination of lensing + AO-IFU: $\sim$ 300 pc resolution: EELT science !

## How do we select clumps / star-forming regions ?

- Define a single isophote above a background (e.g. $3\sigma$) and find all local maxima (*Jones et al. 2010*)
- `daofind` IRAF task (*Förster Schreiber et al. 2011*): assumption on the size of the clumps to find (good for unresolved clumps with PSF size)
- `clumpfind` algorithm (*Williams et al. 1994*): use of multiple isophotes at different thresholds. No assumption on the clump shape or profile

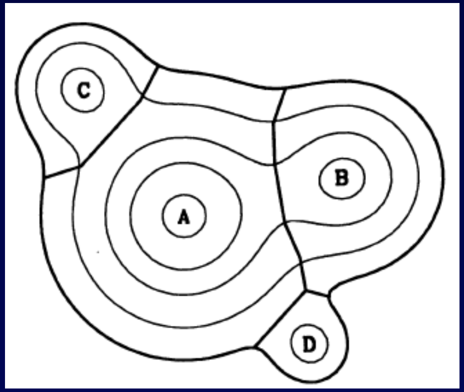

# Size-SFR diagram

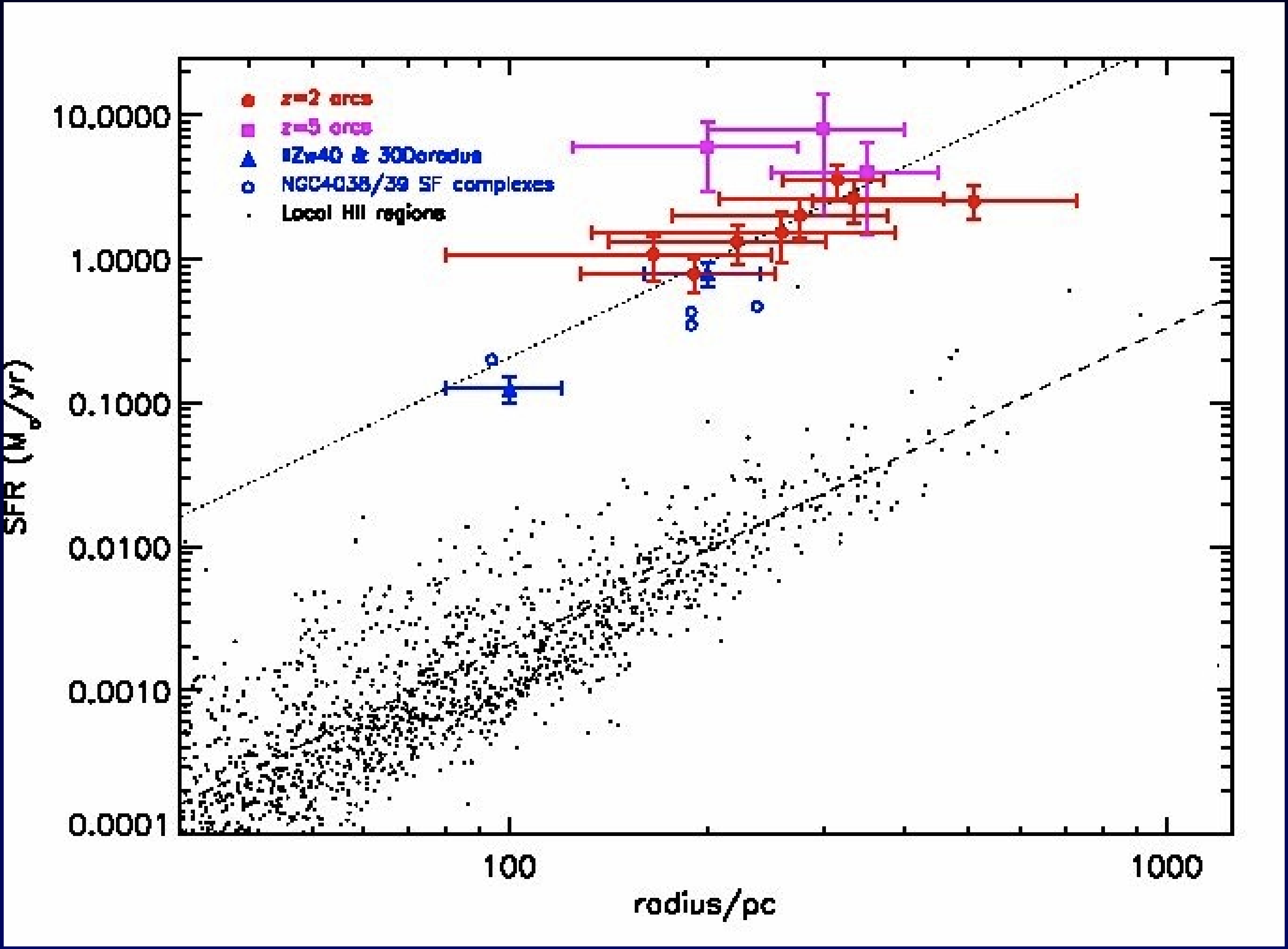

# Size-SFR diagram

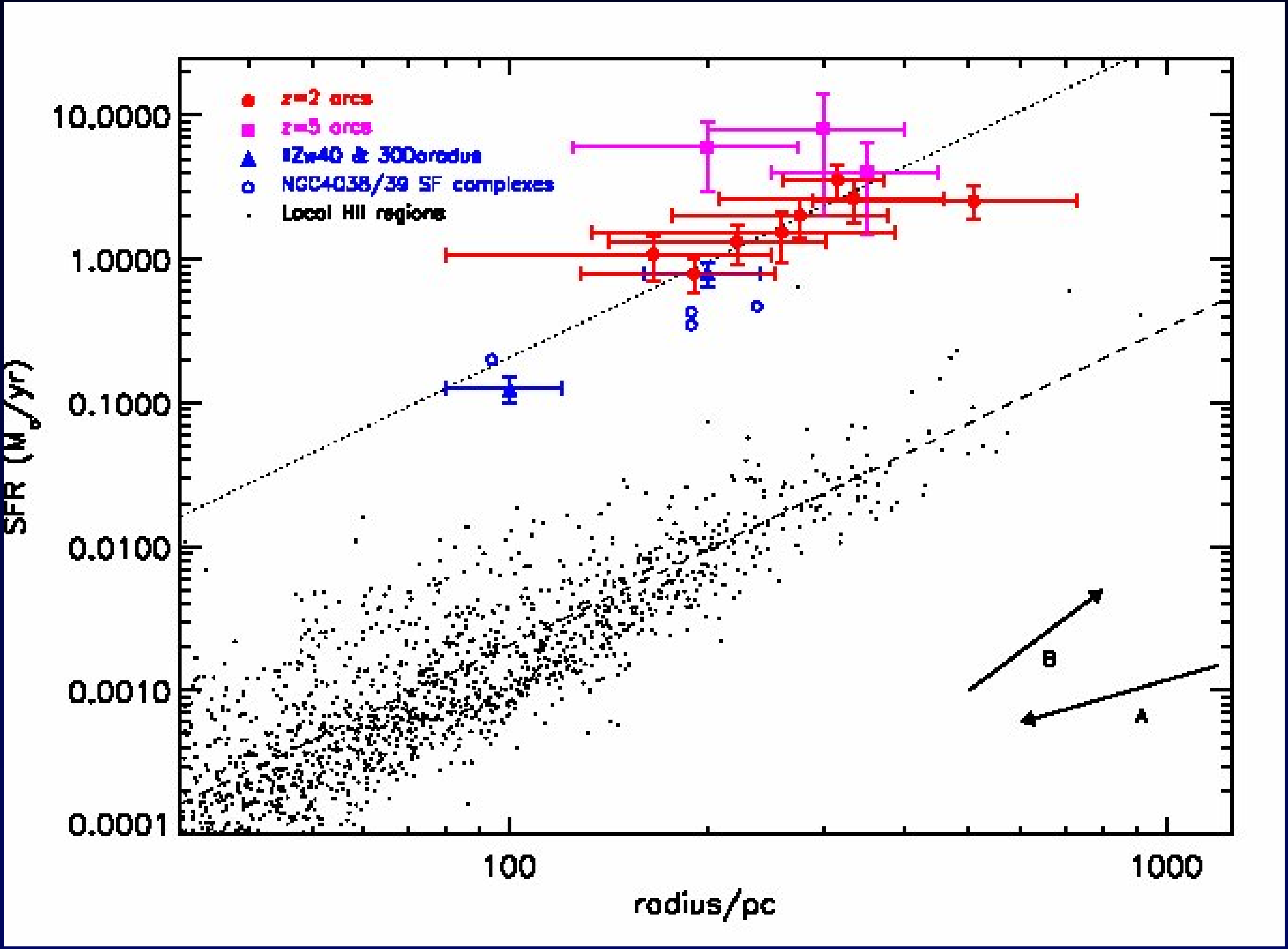

# Possible explanations, tests

Luminosities in the HII regions are ~50x larger than in local spirals, but diameters are consistent with the Jeans length for support by velocity dispersion.

On the size-SFR diagram, star-forming regions in lensed galaxies show star formation rate densities much higher than local spirals, comparable with the most vigorous local starbursts. This offset in $\Sigma_{\rm SFR}$ cannot be explained by

the different resolution or sensitivity of low and high-redshift observations.

Possible explanations:

1. There are two discrete star formation processes, one quiescent and the other activated in turbulent disks such as those generated in galaxy mergers or by cold flows
2. A continuous trend might exist with redshift, in which star formation always occurs in a range of sizes, but selection effects mean that only the most intense regions are visible at high-z.

# Narrow-band H$\alpha$ imaging program

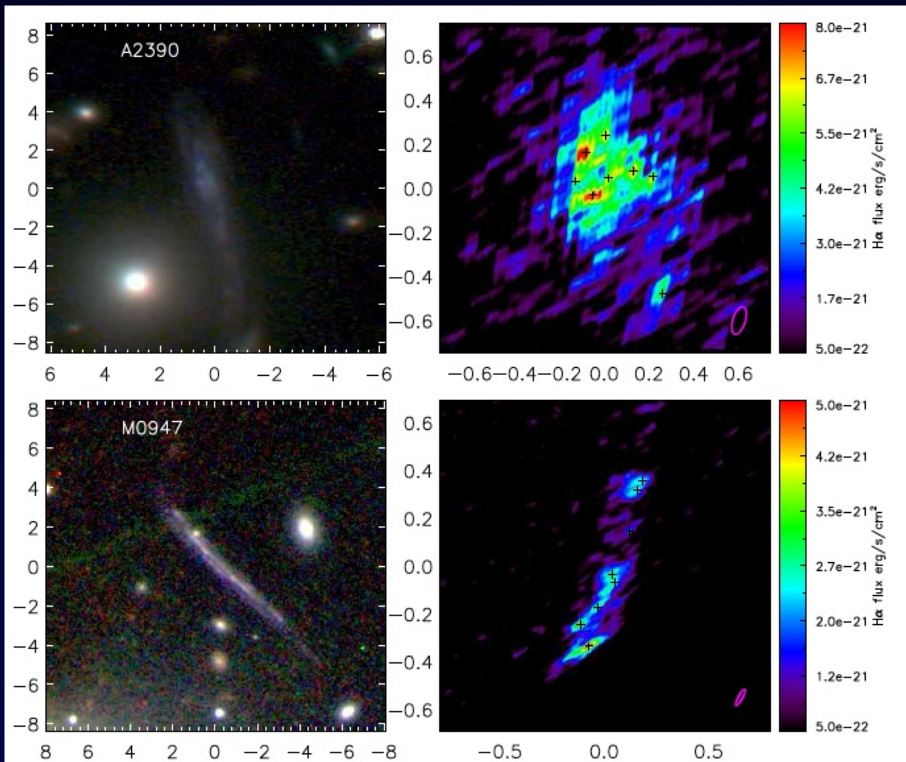


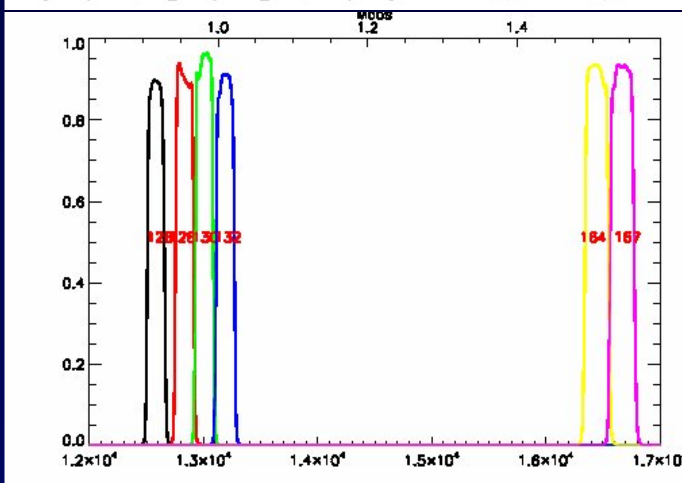

- Test *modes* of star formation at $z = 0 - 2$: continuous or bimodal ?
- WFC3 narrow band filters correspond to H$\alpha$ for $z \sim 1.0$ and $z \sim 1.5$
- Selection of 7 extended arcs with visible star-forming regions for H$\alpha$ (narrow-band excess) measurement
- Resolution: down to 50 pc and 0.02 M$\odot$/yr for a star-forming region

# size-SFR at z=1 (*Livermore et al. 2012*)

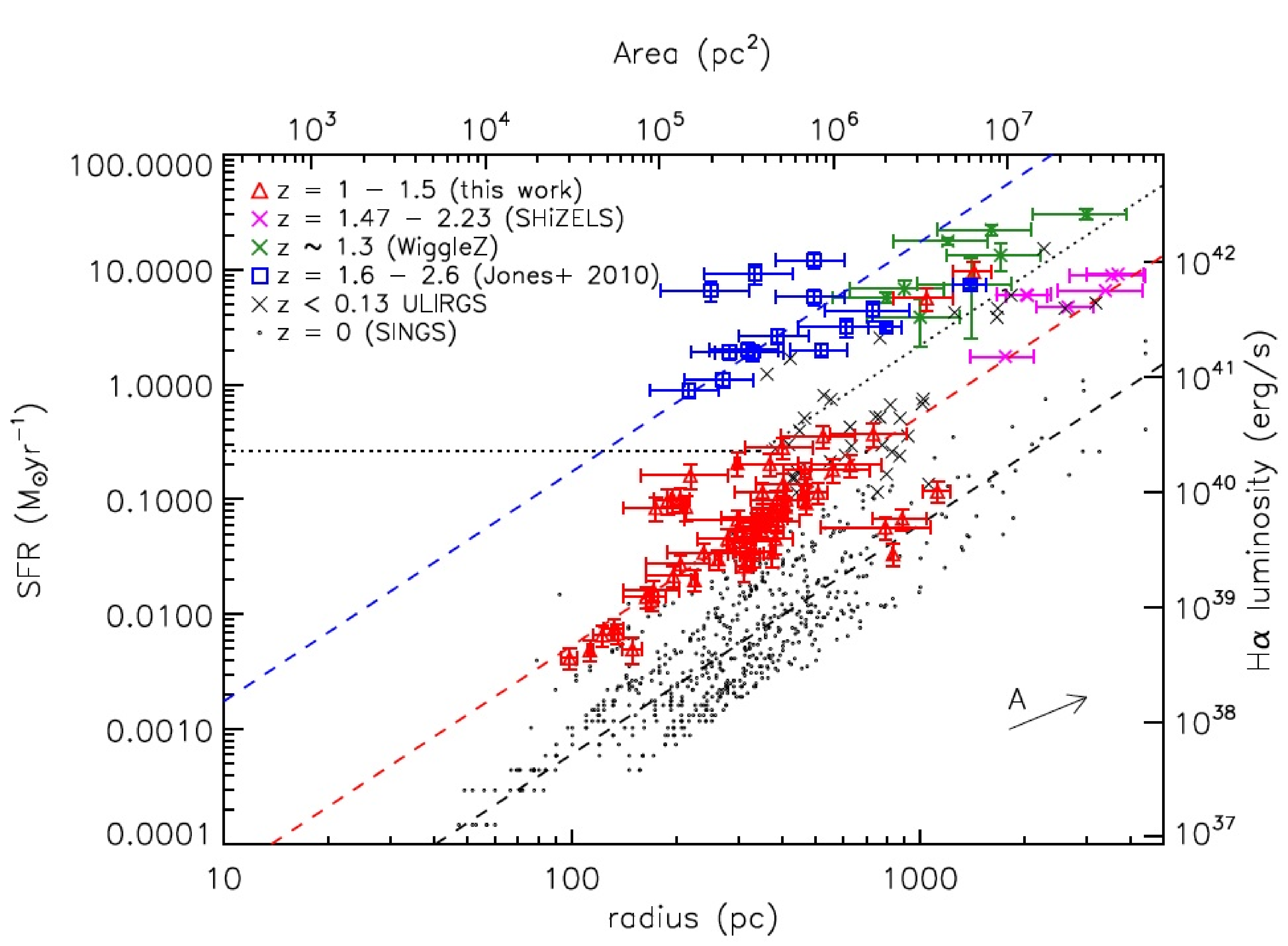

# HII region LF

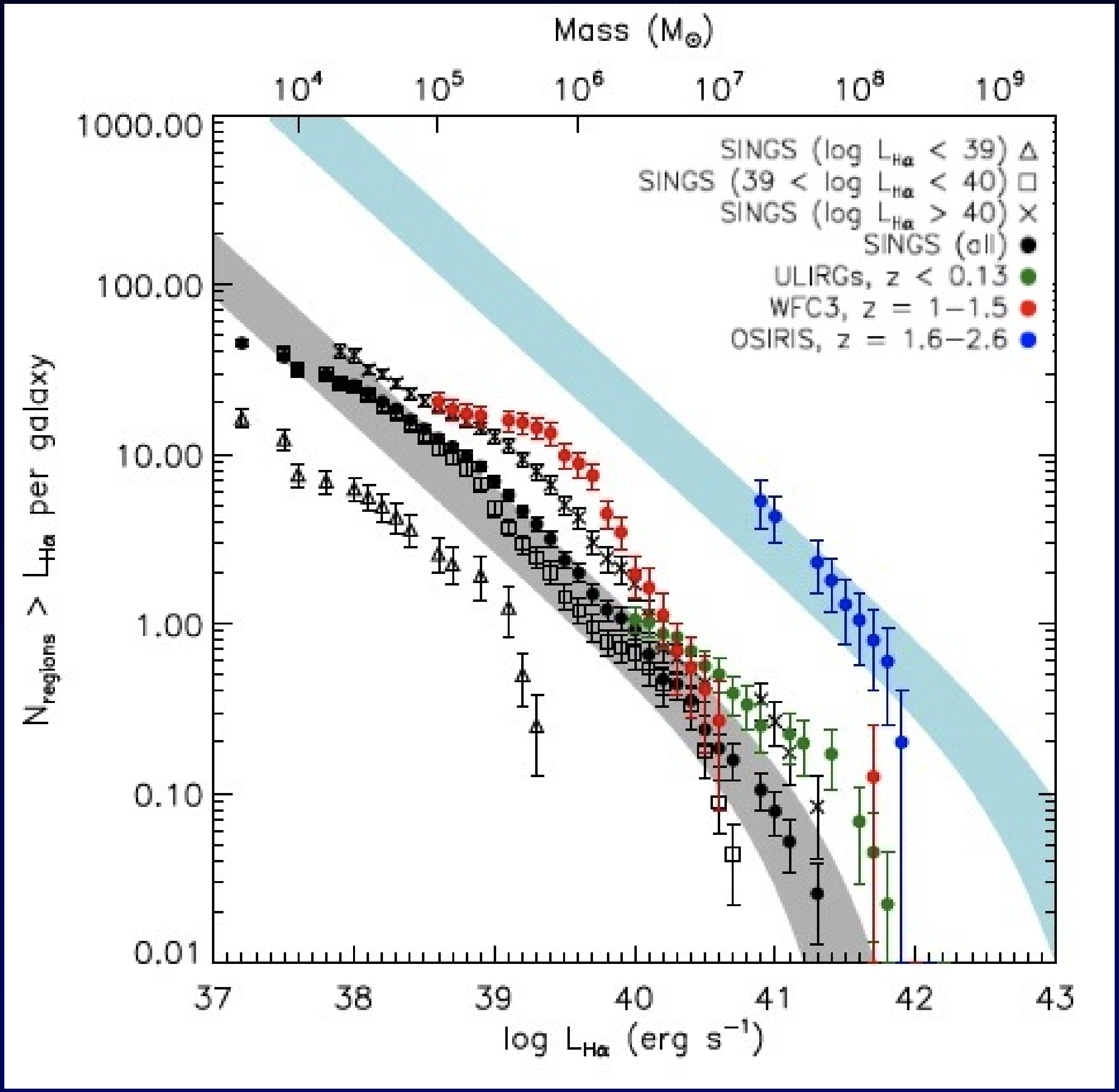


- Size-luminosity diagram: $z = 1 - 1.5$ galaxies are closer to local relation
- High-$z$ clumps similar to bright SF regions at $z = 0$ but more compact
- LF of HII regions compatible with predictions by *Hopkins et al. 2011*
- Evolution in luminosity and surface brightness are connected, due to the higher gas fractions and surface densities at high $z$

# High z morphology at z∼7

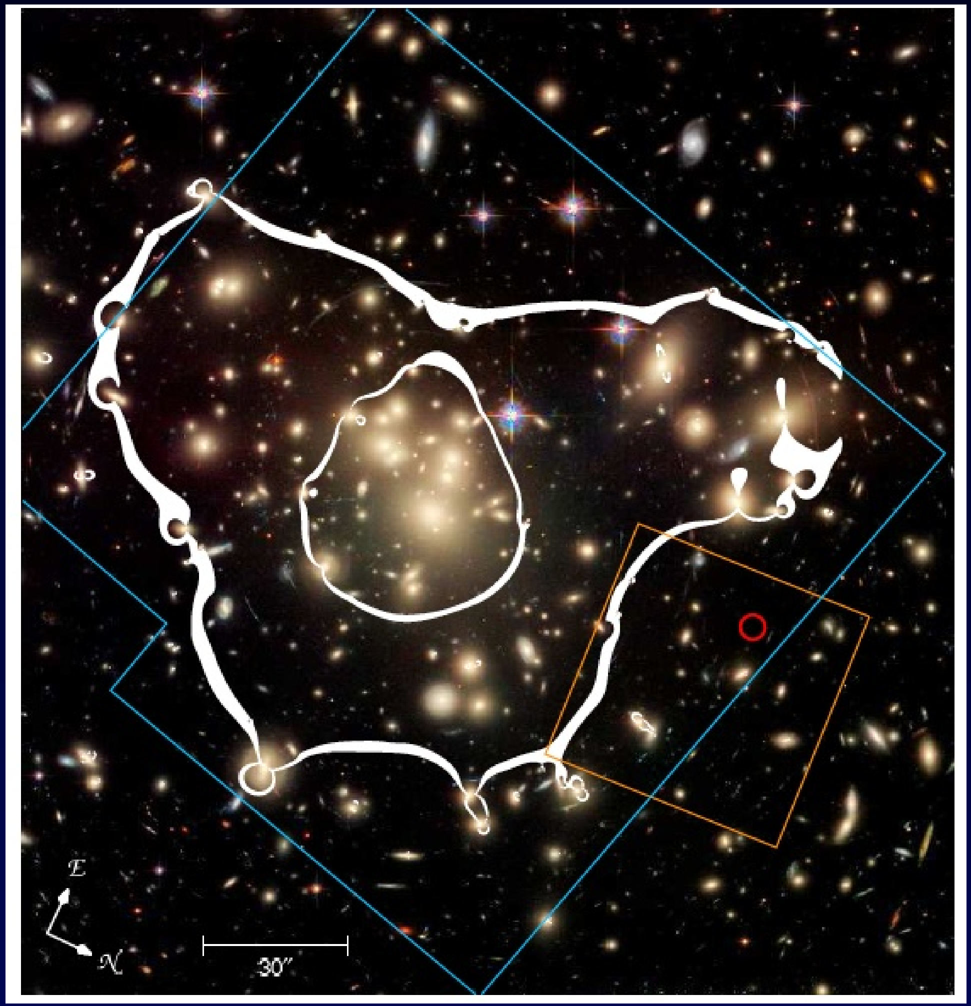


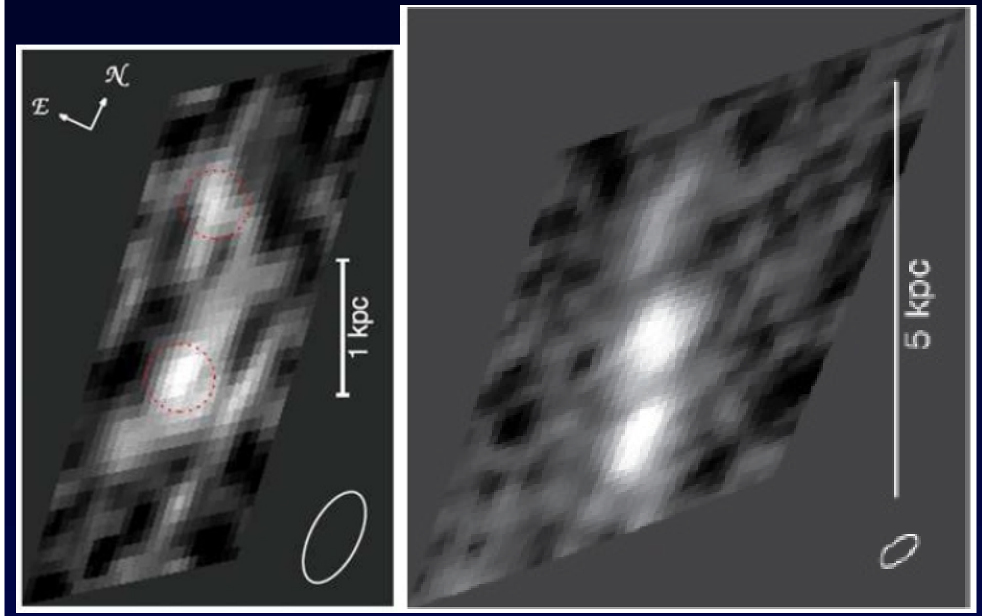


*Bradley et al. 2008, 2011*

Highest resolution achieved on $z > 6.5$ dropouts.

Clumpy morphology with clump sizes ∼500-1 kpc.

*Zheng et al. 2009*: Predominance of dual nuclei in very high-redshift galaxies ?

# Long wavelength observations and source reconstructions

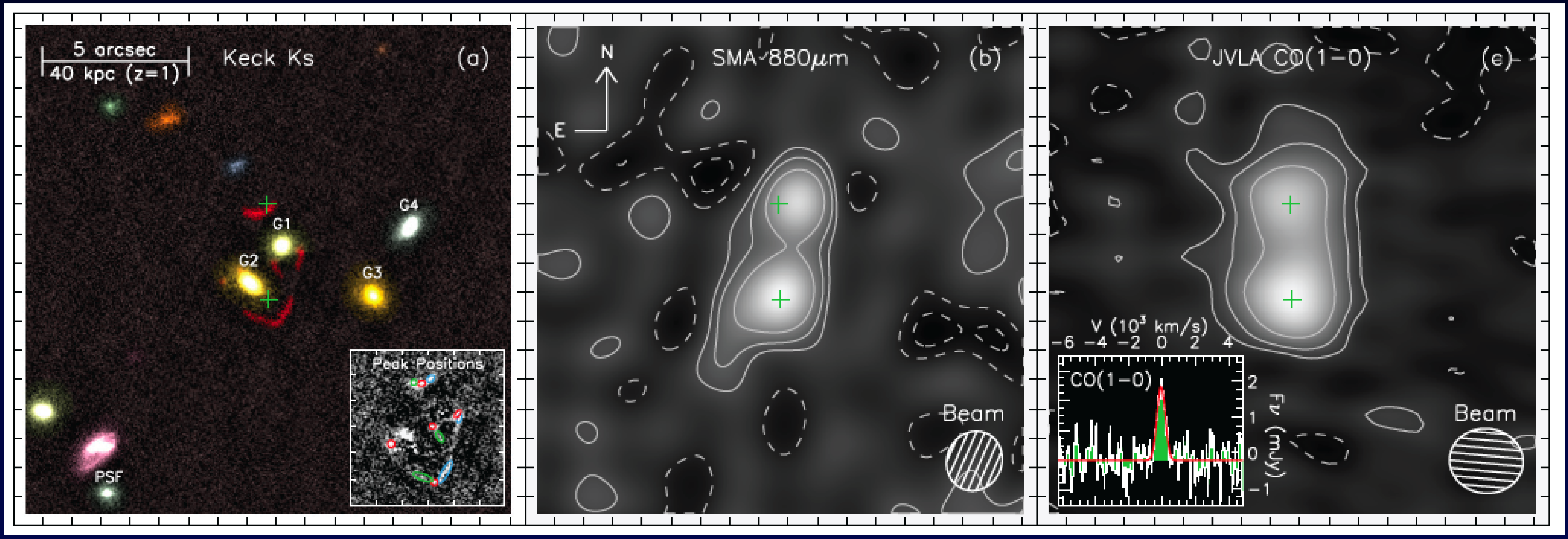


*Fu et al. 2012*: Herschel-ATLAS submm galaxy at $z = 3.256$

Discovered with Herschel (unresolved) at a bright source at 500 $\mu$m. Followed-up with Keck (adaptive optics), and at millimeter wavelength (SMA and JVLA)

# Long wavelength observations and source reconstructions

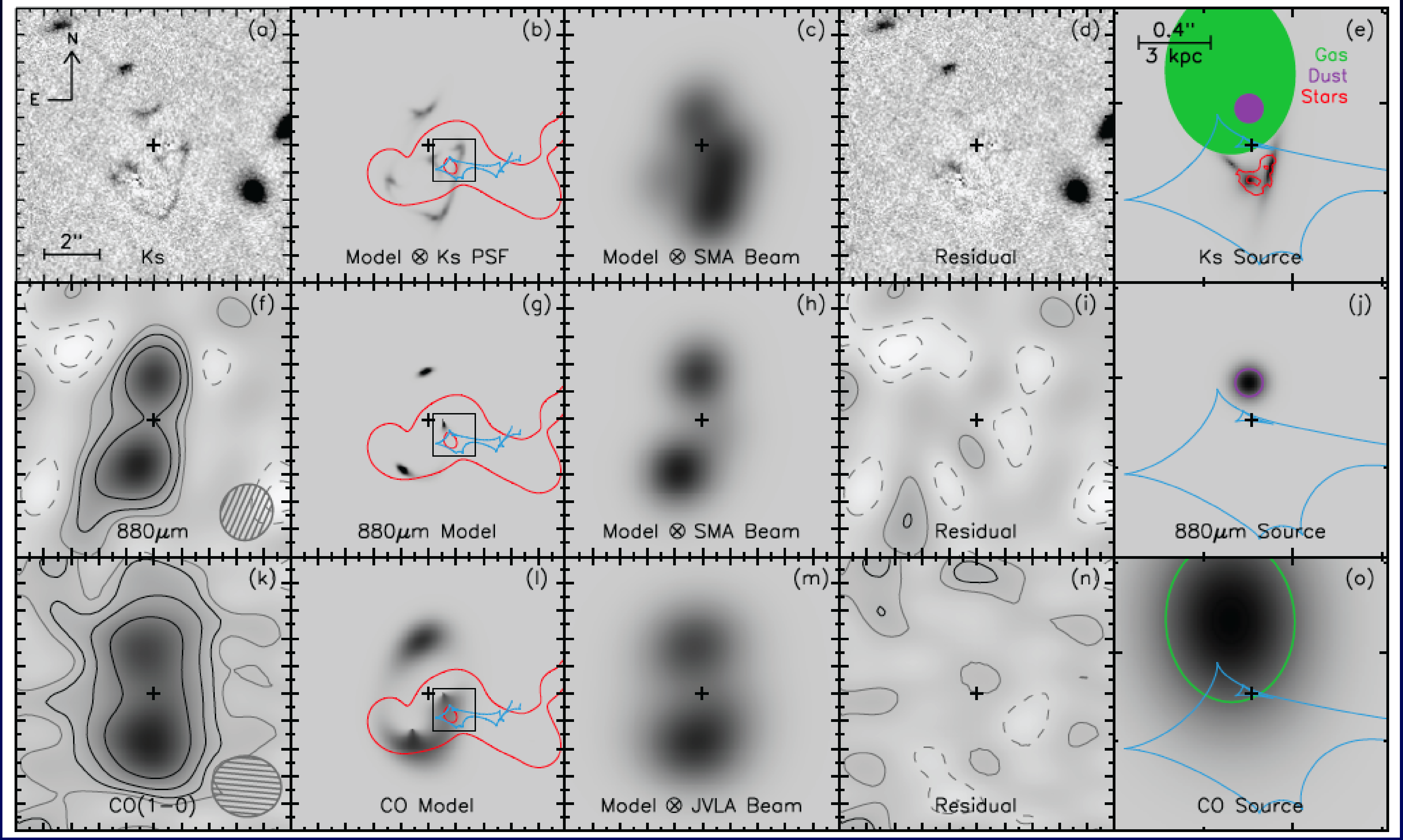

# Results

- Keck Adaptive Optics: quadruply imaged galaxy in the K band, emission from the stars
- Submillimeter Array: 880 $\mu$m continuum of dust emission, 2 images
- Jansky Very Large Array: CO (1-0) molecular gas, 2 images

Offsets and size differences measured in the reconstructed source between the 3 components.

The lensed source is warm ($T_{\rm dust}$ 40-65 K), hyperluminous ($L_{\rm IR} \sim 1.7 \times 10^{13}$ $L_\odot$), starburst (2000 $M_\odot$/yr), similar intrinsically to unlensed $z > 2$ SMGs.

# Morphology of lensed submm sources: the Eyelash

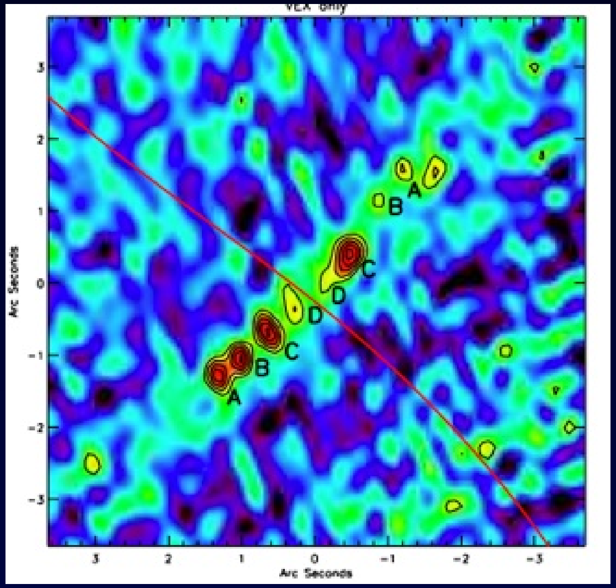


Very bright 870 $\mu$m source at $z = 2.3$ lensed by the cluster MACSJ2135 (Swinbank et al. 2010), $\mu = 30$

EVLA and PdBI high resolution observations show a clumpy morphology with 4 unresolved regions (folded along the critical curve) in dust continuum and molecular gas.

These regions (on scales of L$_J$ ~400 pc, are 10$\times$ denser than in local galaxies: hint for a highly turbulent ISM (Swinbank et al. 2011).

# Radio Interferometry source reconstructions

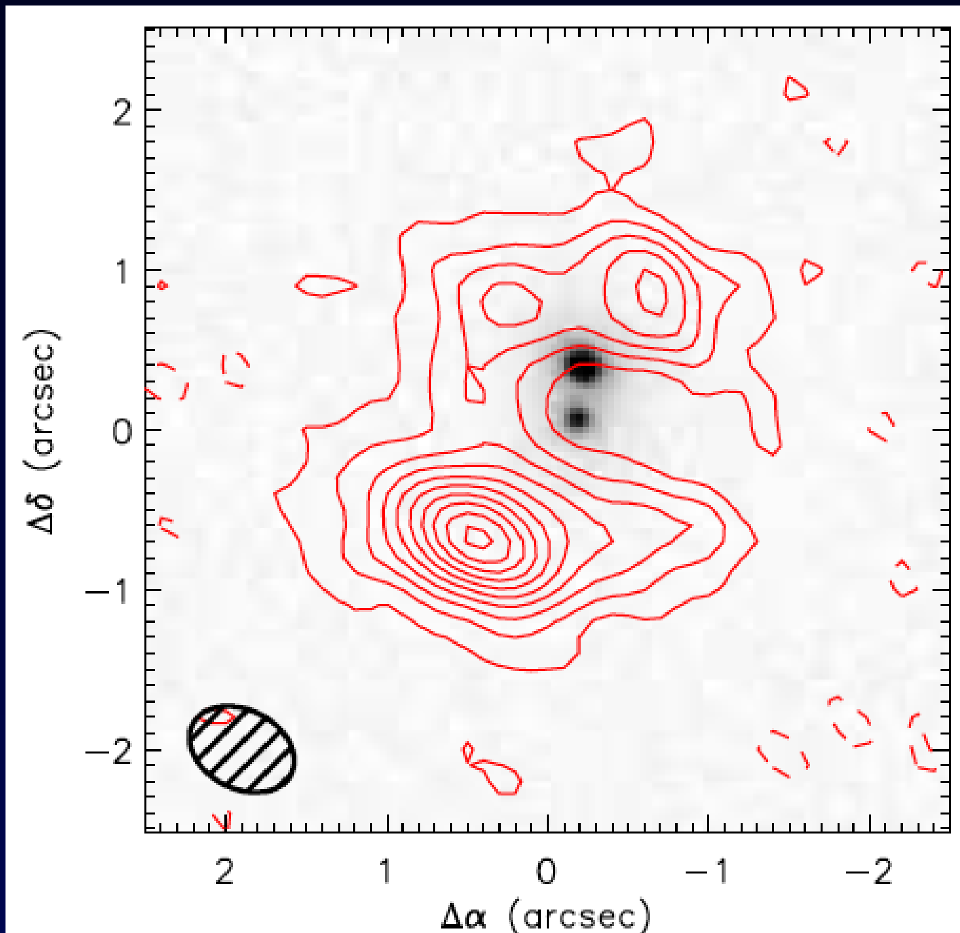


$$\chi^2 = \sum_{u,v}^{N} \frac{(V_{\mathrm{SMA}}(u,v) - V_{\mathrm{model}}(u,v))^2}{\sigma(u,v)^2}$$

*Bussmann et al. 2012*
$z = 4.243$ H-ATLAS submm source, 2 lensing galaxies.

Parametric source reconstruction in the visibility plane of the SMA data (0.6" resolution) to prevent correlated noise in the 'cleaned' image.
Especially important for large beams and limited coverage in the uv-plane.

# Conclusions

Gravitational lensing is currently the only way to resolve physical scales of $100 - 500$ pc in distant $(z > 1)$ galaxies.

This technique can be used in morphological studies to:

- Measure the profile, shape, and resolve the SED of intrinsic sources, down to very low masses ($10^{7-9}$ $M_\odot$)
- Measure the physical properties of compact regions within these galaxies: star-forming regions and the formation of bulges
- Measure the offsets in multiwavelength studies between the stellar, dust and cold gas components

High redshift star-forming galaxies show a very clumpy morphology, with star-forming regions being even more concentrated in the past than local galaxies: this is certainly due to the higher gas fractions leading to higher star formation surface brightnesses.

Drawback: currently only small samples of extended arcs at $z > 2$ to study morphological trends against, e.g. stellar mass or gas fraction.

# Integral Field Spectroscopy

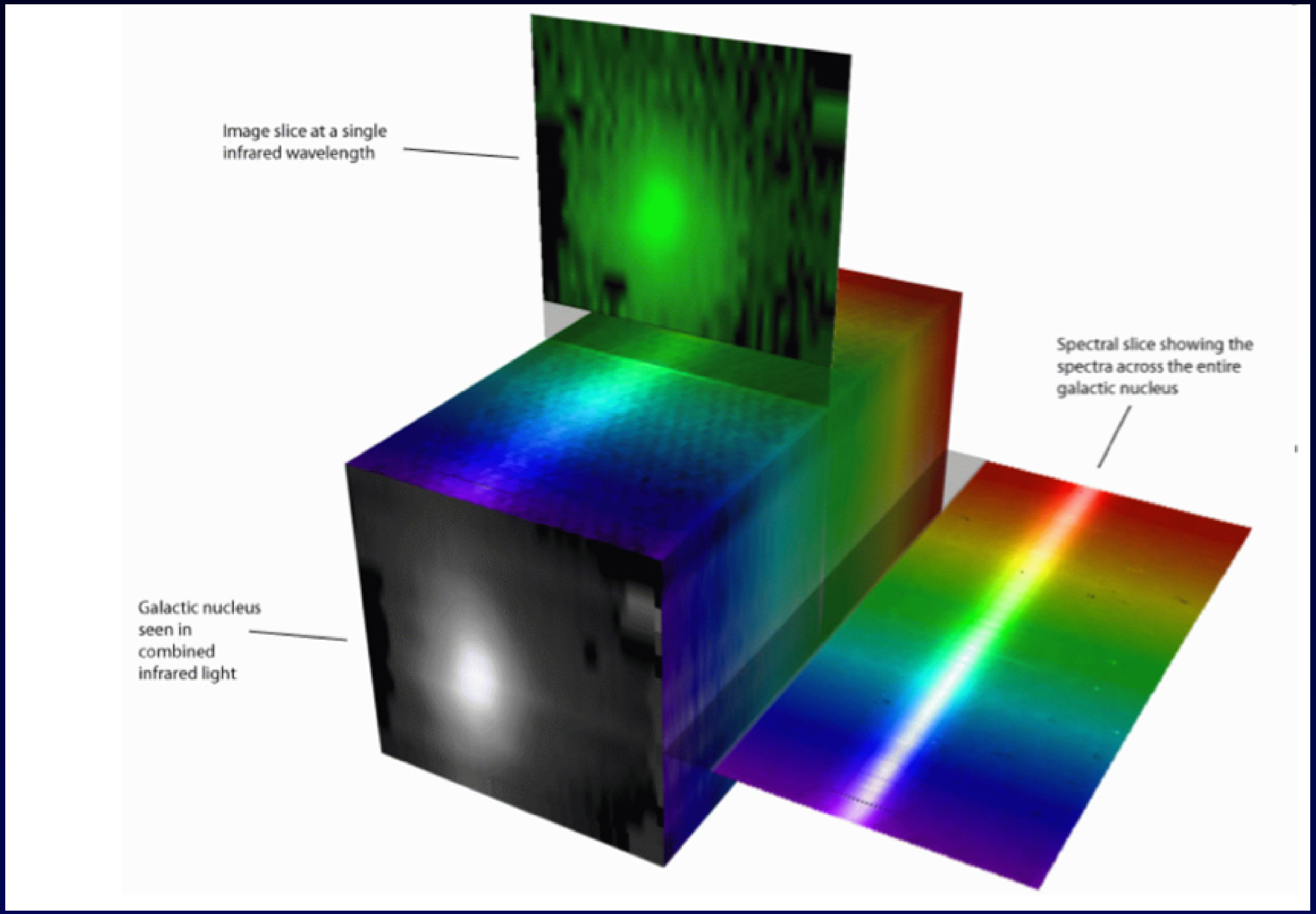


- At each wavelength you get an image
- At each position you get a spectrum

# Different IFU concepts

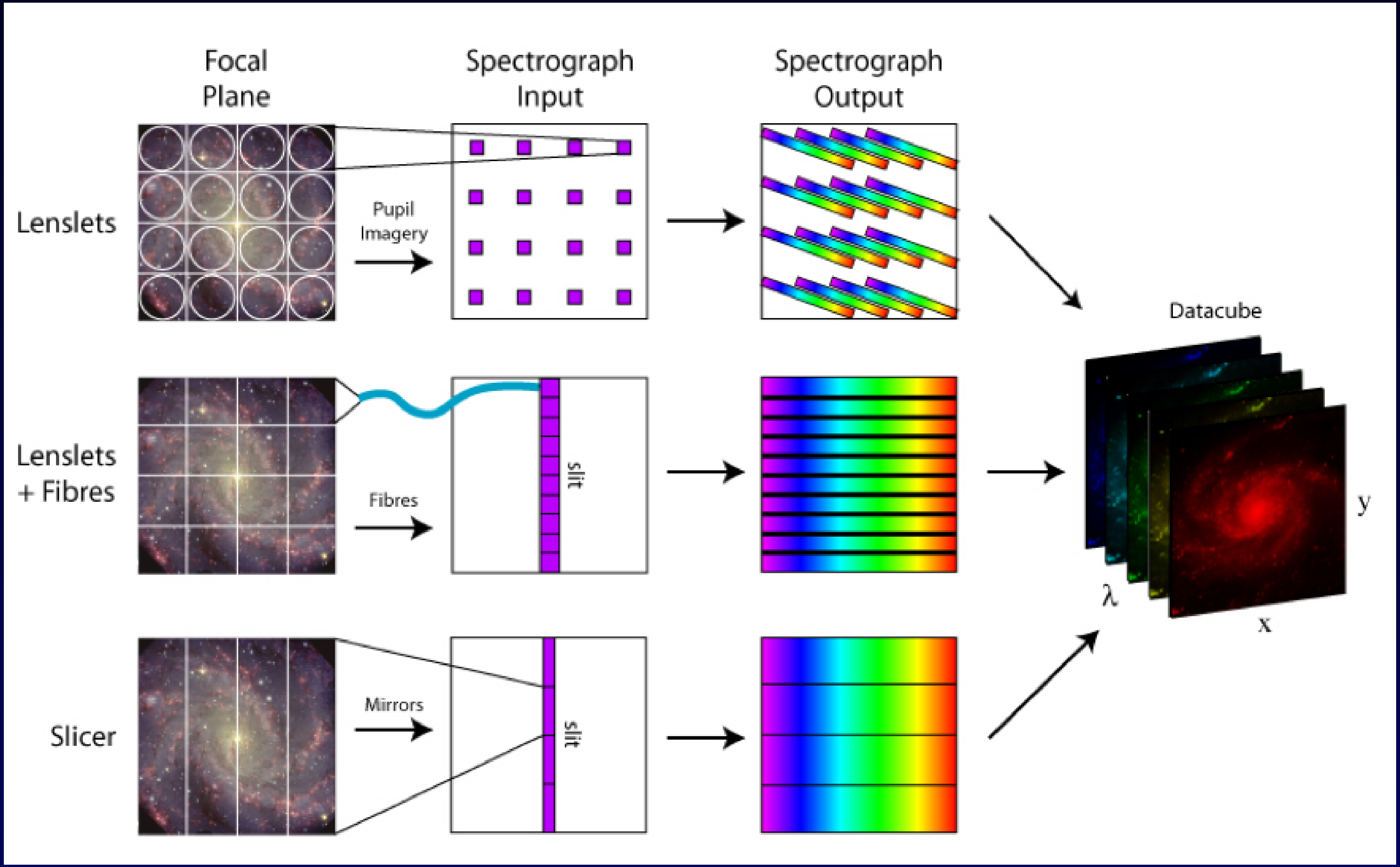

# Resolved kinematics

# Resolved kinematics: motivation

Study **galaxy assembling** at $z > 2$: test early stellar formation of massive galaxies observed at $z = 1 - 2$

**Internal properties** of early galaxies, such as their dynamical state, chemical properties and the distribution of their star-forming regions, provide key tests of galaxy formation models.

**Analysing the dynamics** of high redshift galaxies enables to distinguish chaotic or well-ordered velocity fields, depending on the maturity of the systems.

**Integral Field Spectrographs** with Adaptive Optics (SINFONI, OSIRIS, NIFS) are currently the best instruments for these studies.

*Genzel et al.*
*Forster-Schreiber et al.*

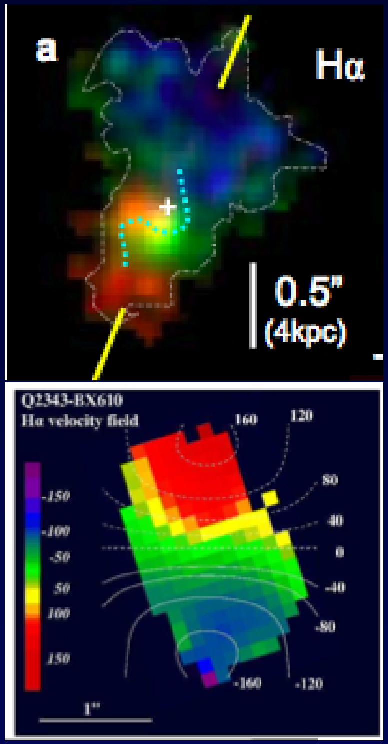


*Law et al.*

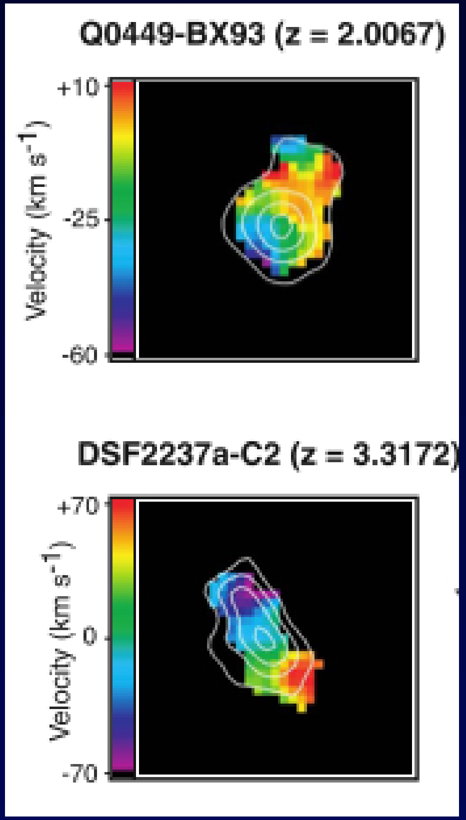

# IFU+AO observing procedure for $z > 1$ galaxies

Target selection:

- Known spectroscopic redshift, avoid contaminating OH lines and near-infrared gaps
- Estimation (or measurement) of total emission line flux
- Size of the IFU adapted to source size for sky subtraction
- Presence of a Tip-Tilt star for optimal AO (ex: $R < 18$ within 30" for SINFONI)

Data analysis: spectral line fitting: $\lambda_0(x, y)$ (velocity field) and $\sigma(x, y)$ (velocity dispersion field)

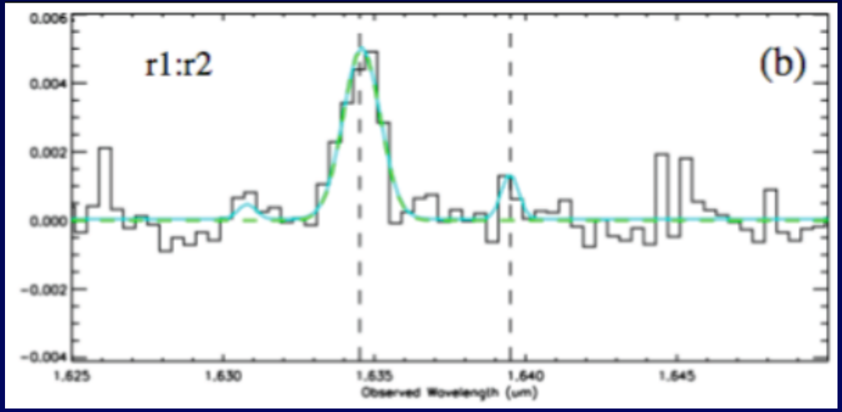

# A few kinematical models

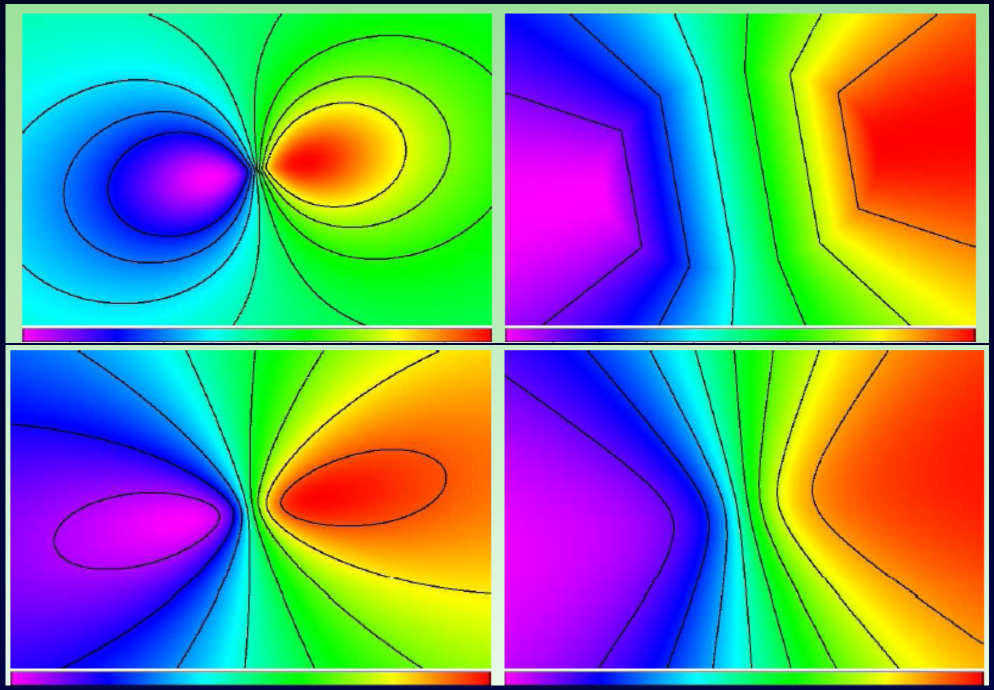

*(based on Epinat et al. 2009)*

Projection effect: inclination $i$ and position angle $\theta$.

Exponential model:

$$V(r) = \frac{r}{r_0}\sqrt{\pi G \Sigma_0 r_0 \left(I_0 K_0 - I_1 K_1\right)}$$

Plateau model:

$$V(r) = V_t \frac{r}{r_t}, \text{for } r < r_t,$$
$$V(r) = V_t, \text{for } r \geq r_t.$$

Isothermal model:

$$V(r) = \sqrt{4\pi G \rho_0 r_c^2 \left[\frac{r_c}{r} \ln\left(\frac{r}{r_c} + \sqrt{1 + \frac{r^2}{r_c^2}}\right) - \frac{1}{\sqrt{1 + \frac{r^2}{r_c^2}}}\right]}$$

'Arctan' model:

$$V(r) = V_t \frac{2}{\pi} \arctan \frac{2r}{r_t}$$

# Beam smearing effect

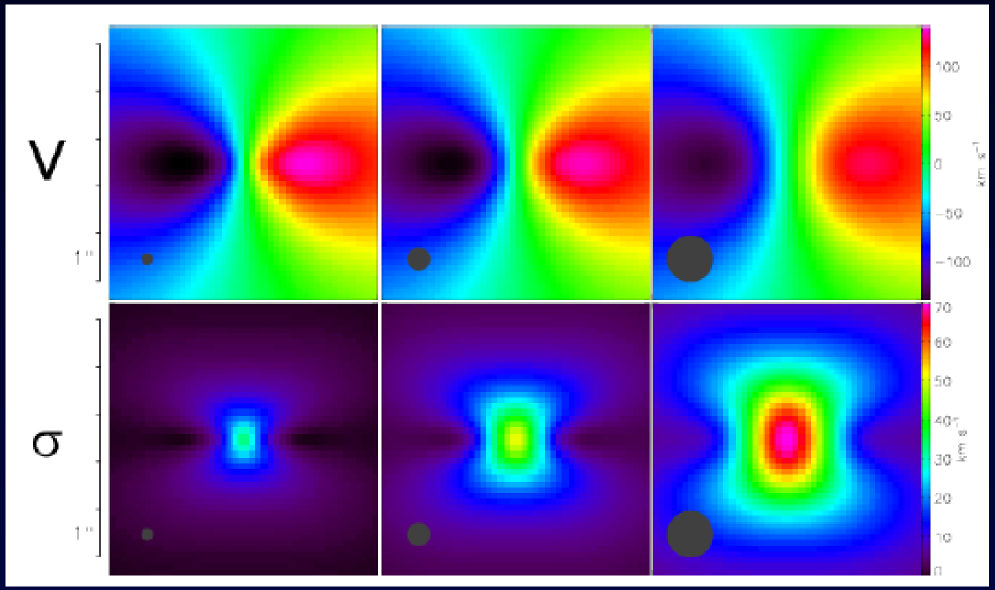


*Epinat et al. 2010*

Smearing effects due to the Point Spread Function (PSF), the Line Spread Function (LSF) and the discrete pixels.

- Seeing increasing from 0.125 to 0.5
- Null local velocity dispersion
- Decrease of the observed velocity gradient
- Central peak appearing in apparent velocity dispersion

# Observational results: $z \sim 1.2$

50 galaxies of the MASSIV sample (*Contini et al. 2012*)

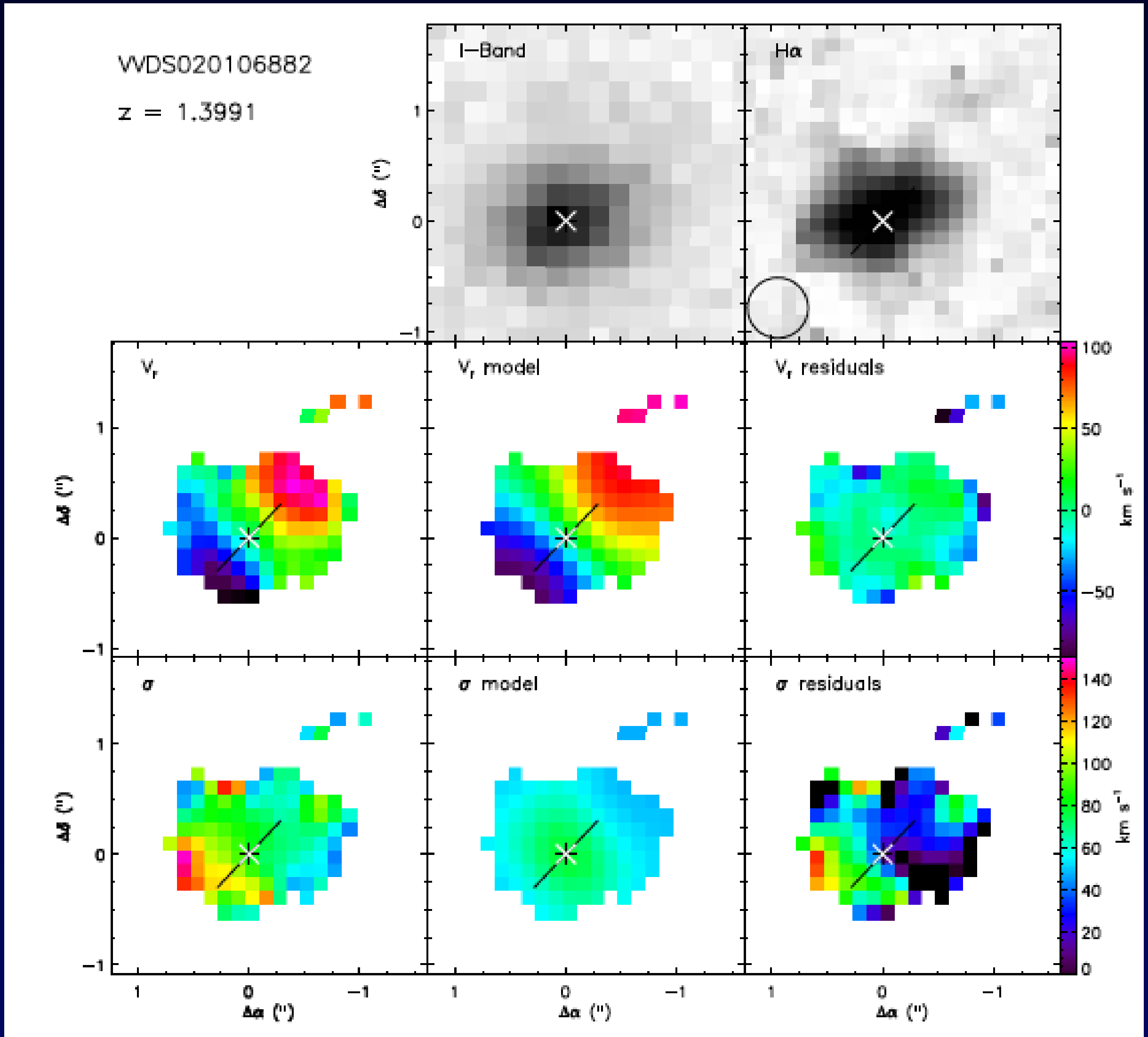

# Observational results: $z \sim 2$

*Forster-Schreiber et al. 2009*

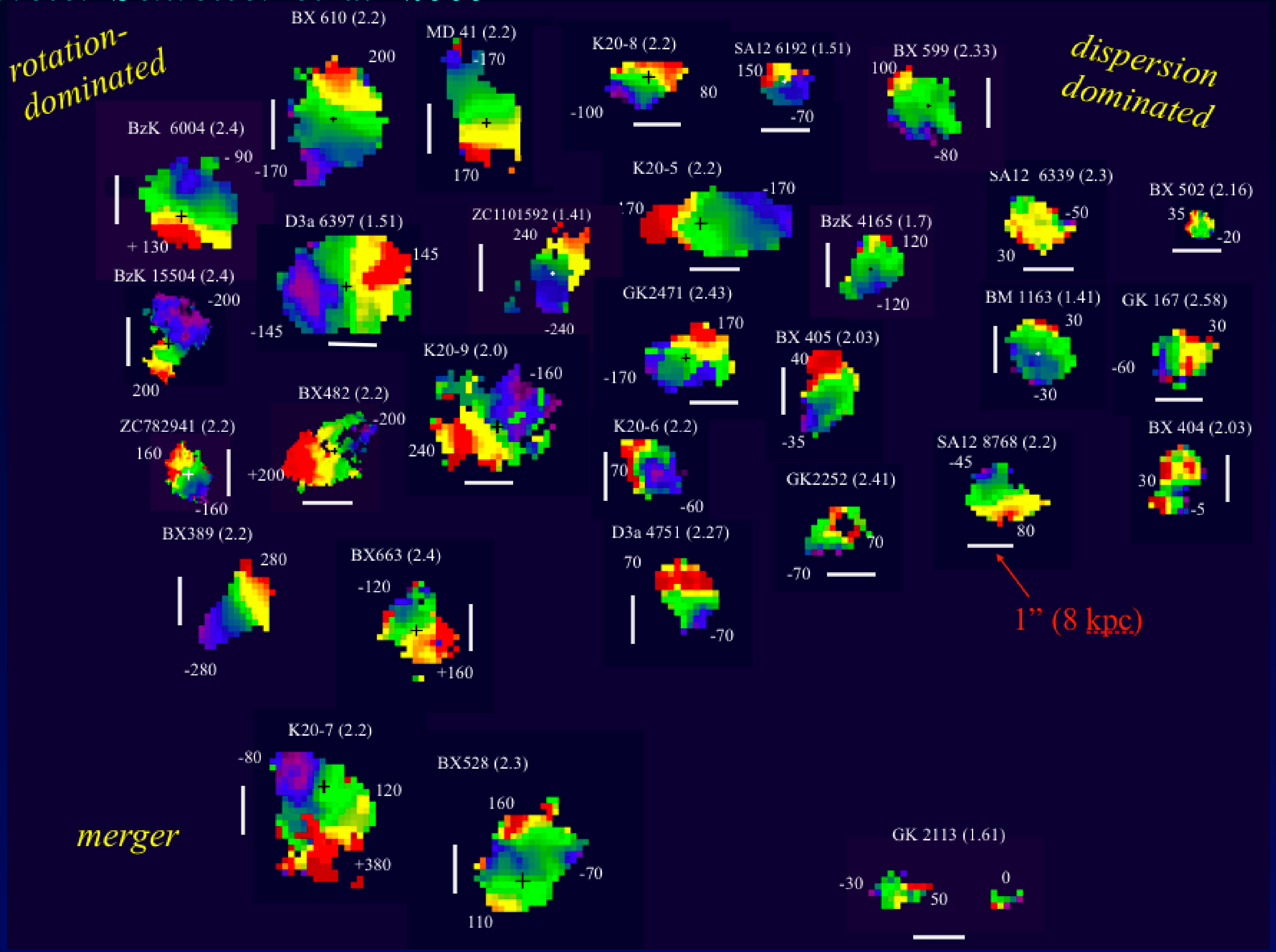

## Observational results

- $z \sim 1.3$ MASSIV (Epinat et al., 2012) : 50% of the galaxies show rotation, 35% are dispersion dominated. Ionized gas turbulence $\sigma \sim 60$ km/s.

- SINS (Forster-Schreiber et al., 2009) : ~60% of the galaxies show rotation, 25-30% are dispersion dominated. Non-rotating objects support cold gas accretion

A consensus is not reached on the interpretation of the kinematics.

One clear evidence : high redshift galaxies have higher velocity dispersion on average:

- $\sigma \sim 60$ km/s for MASSIV at $z \sim 1.2$

- $\sigma \sim 60 - 90$ km/s for SINS at $z \sim 2.2$ and LSD/AMAZE at $z \sim 3.3$

- Lower $z$ galaxies have $\sigma \sim 20 - 40$ km/s.

However, at $z > 2$, current samples contain only very massive and high-SFR galaxies: how about more typical high $z$ galaxies ?

# Where gravitational lensing kicks in....

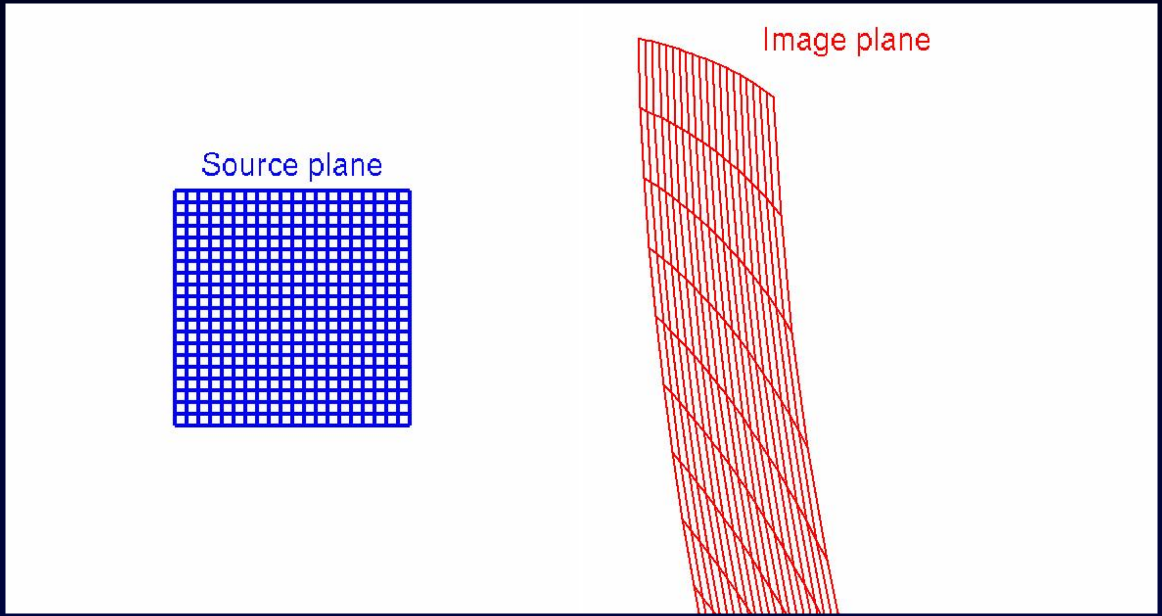


- For a given source redshift, lensing does not depend on $\lambda$
- Plane-by-plane source reconstruction of the IFU datacube $F(x, y, \lambda)$
- But: PSF and LSF effects

$$\sigma^2_{\rm measured} = [\sigma_{\rm intrinsic}\ (1+z)]^2 + \sigma^2_{\rm LSF} + \sigma^2_{\rm smearing}$$

# Velocity field as additional parameters

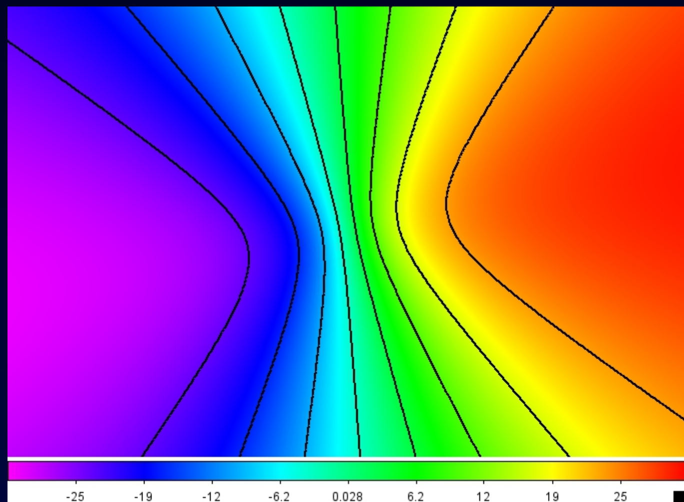


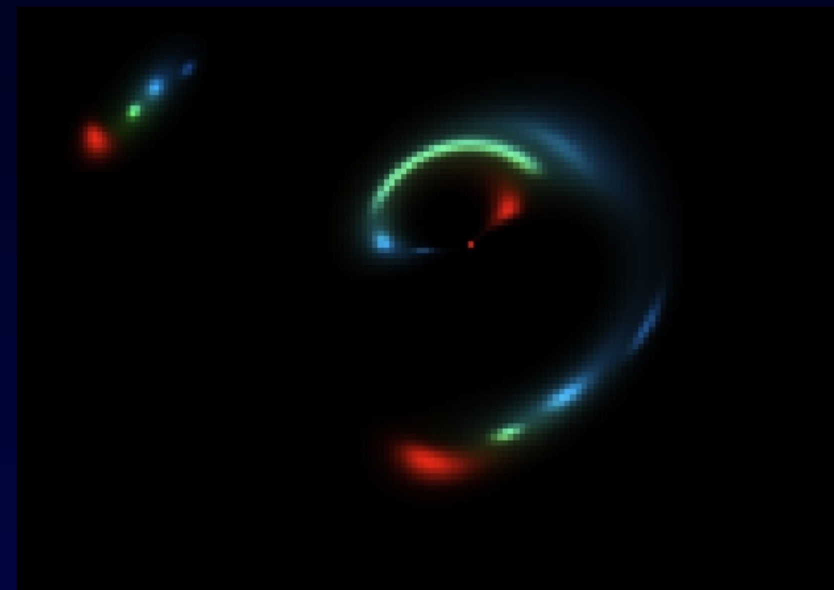

Reconstruction of a lensed datacube: include velocity fields in the Bayesian optimisation, assuming all regions of the lensed galaxy share 1 velocity field.

2 steps optimisation:

1. optimise location, shape and total line flux of each clump from the collapsed cube and/or high-resolution image (HST) including PSF

2. optimise velocity field parameters ($\lambda_c$, $x_c$, $y_c$, $i$ or $e$, $\theta$, $r_t$, $v_t$, $\sigma_0$) including LSF+PSF and pixelisation from the full cube and its variance

# Early IFU lensed studies

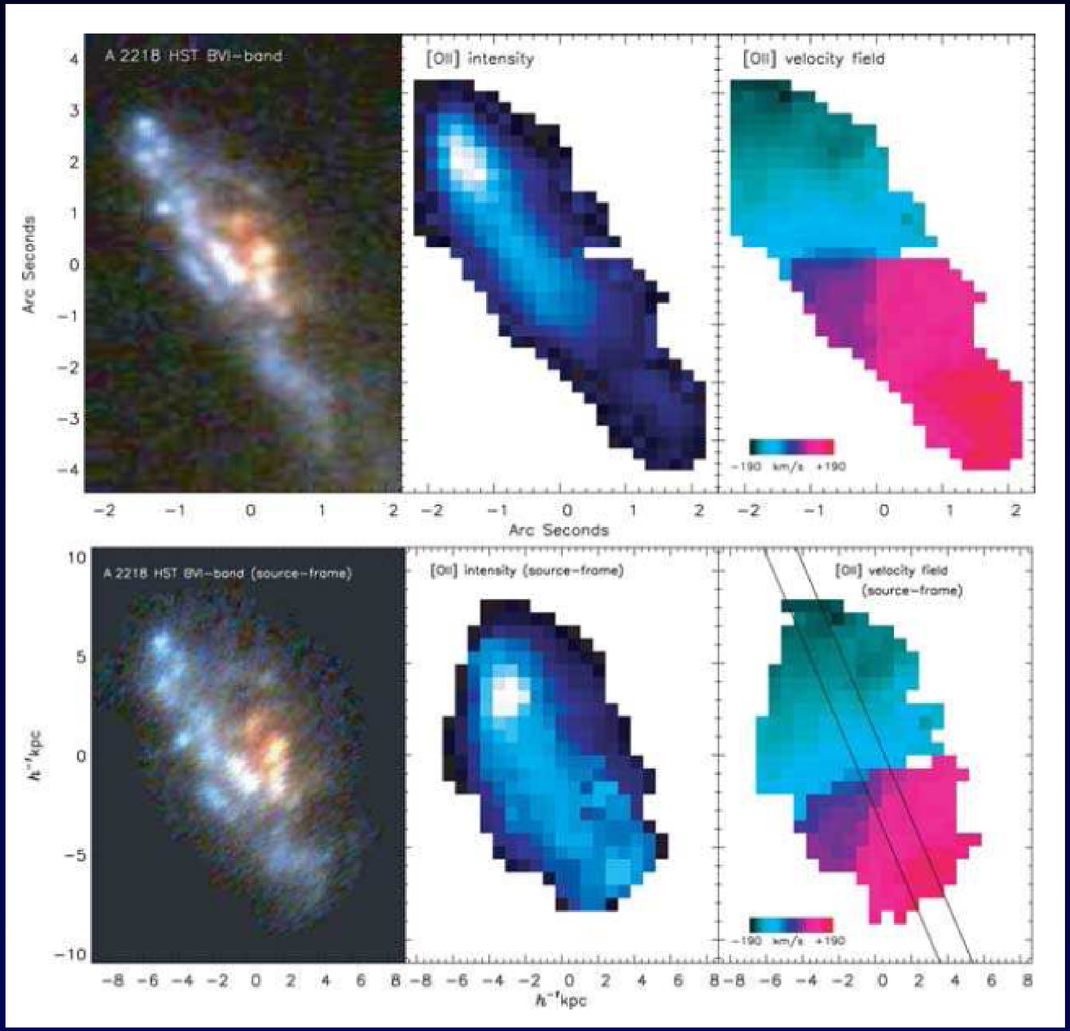


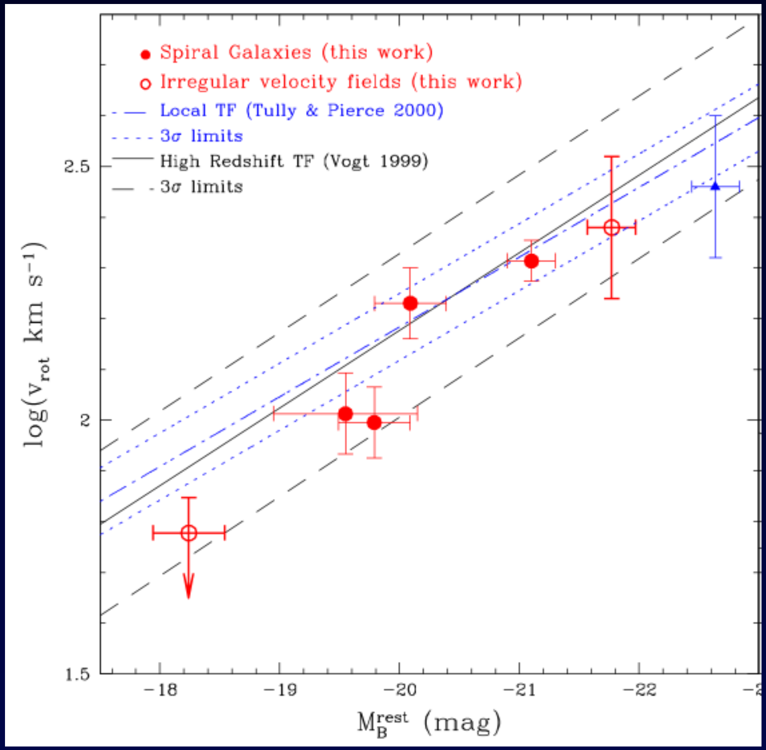


Sample of $z \sim 1$ lensed galaxies: evolution of the Tully-Fisher relation.

*Swinbank et al. 2006*

# Cosmic Eye

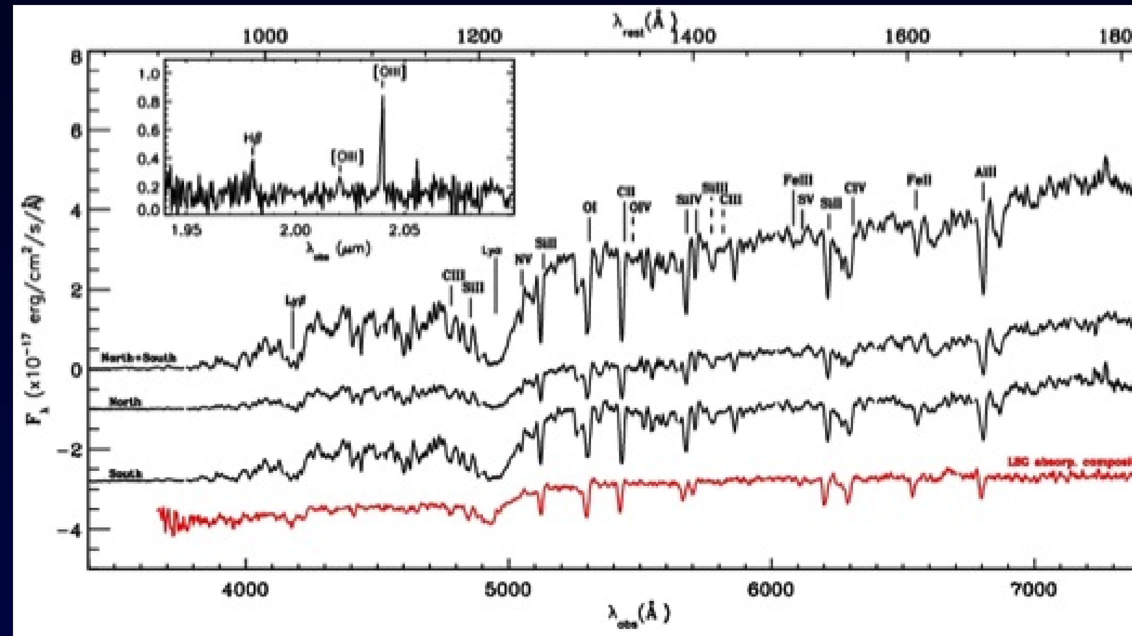


- Found in MACS2135 HST snapshot, z=3.07 (Keck) *Smail et al. 2007*
- Lyman-Break Galaxy, brighter than CB58, strong emission lines in rest-frame optical
- Further follow-up: HST (PI: Richard), CO (*Coppin et al. 2007*), lens model (*Dye et al 2008*), Spitzer/IRAC-MIPS-IRS (*Siana et al. 2009*)
- Simultaneous discovery of other lensed LBGs in SDSS: the 8 o'clock arc, the "cosmic horseshoe", the clone, etc...

Stark et al. 2008

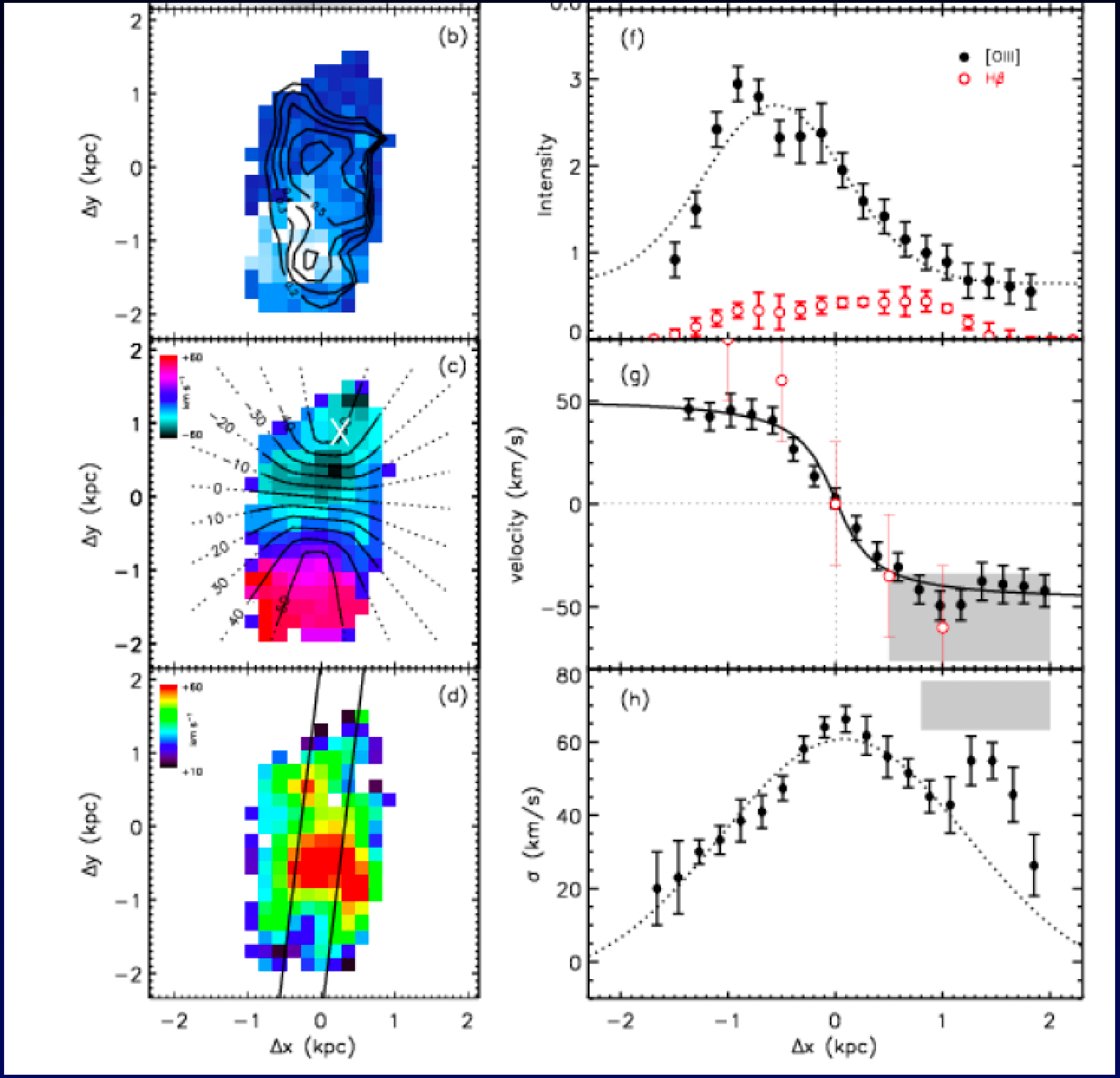

# Cosmic Eye interpretation

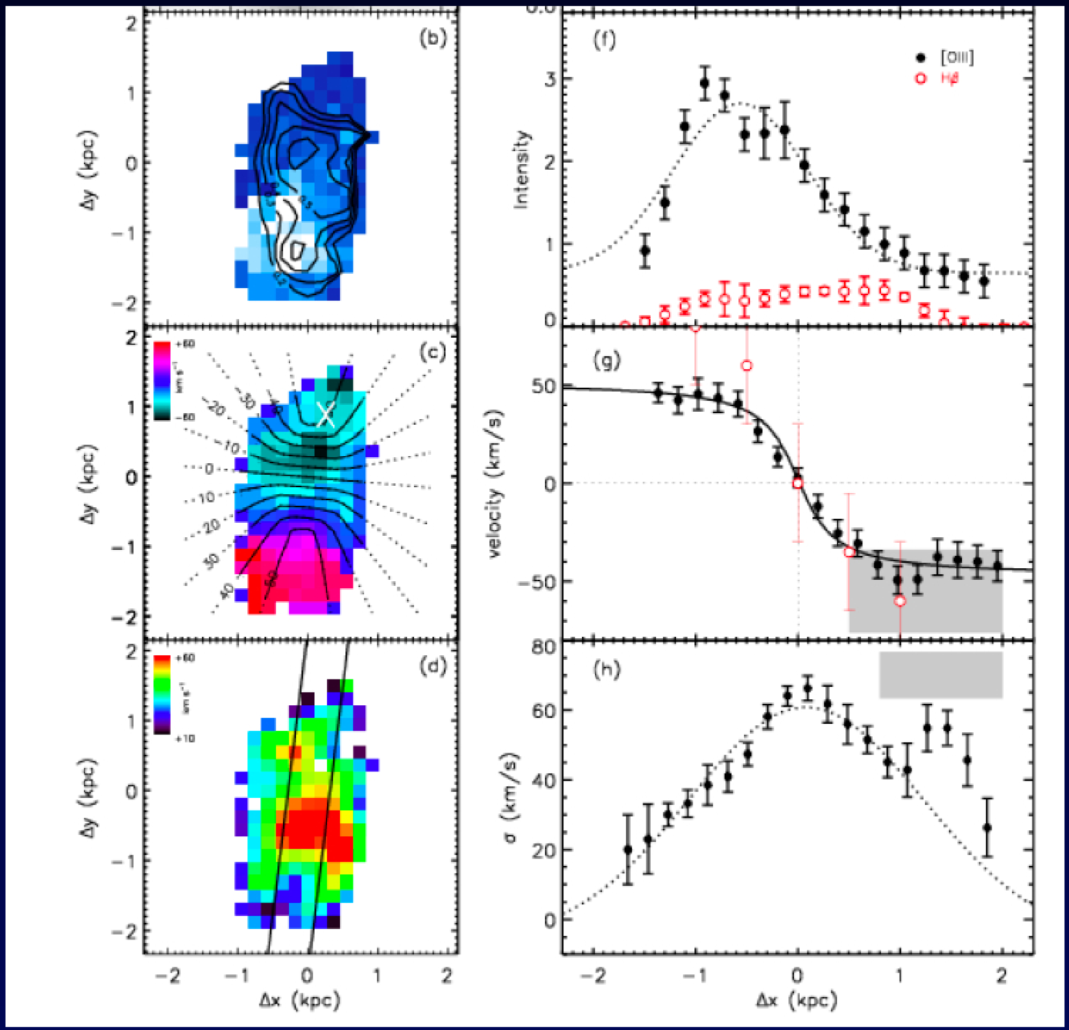


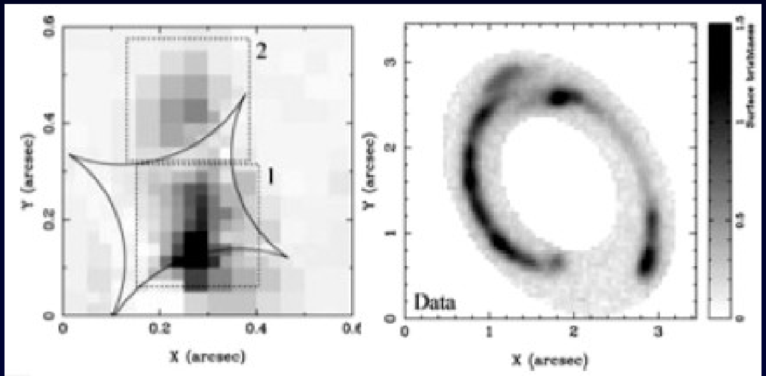


- Strong $[OII]$, H$\beta$, $[OIII]$ detected, with biconic velocity field and FWHM peak at the centre, suggesting rotation
- v$_c$=54±7 km/s, Mdyn=5 $10^9$ M$_\odot$ (<1.8 kpc)
- Nature: rather than a major merger, 2 clumps formed by fragmentation. Random velocities are significant

# Resolved kinematics: a small sample

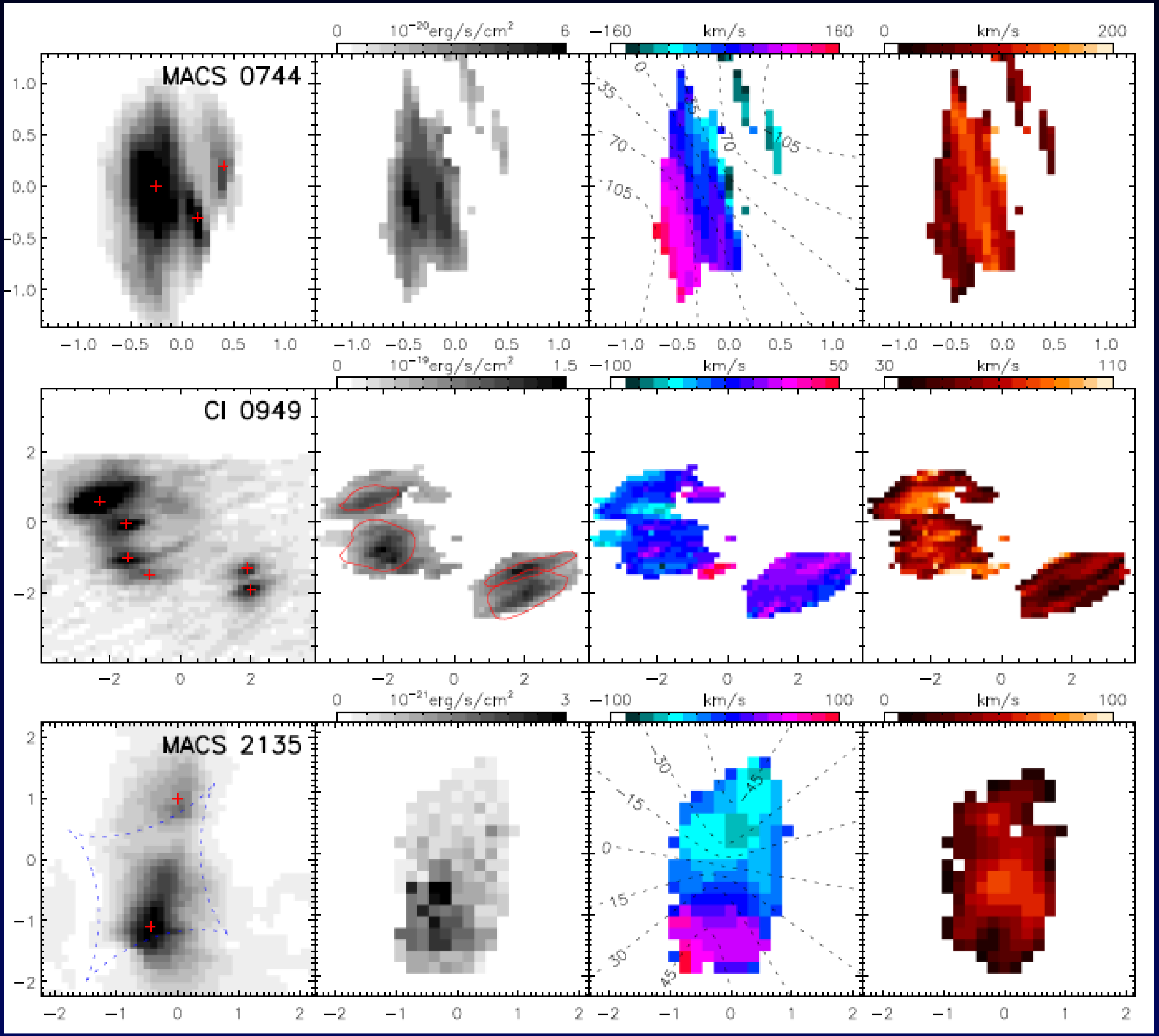


Jones et al. 2010: OSIRIS+AO observations of 6 lensed galaxies

# Resolved kinematics: extracted velocity field

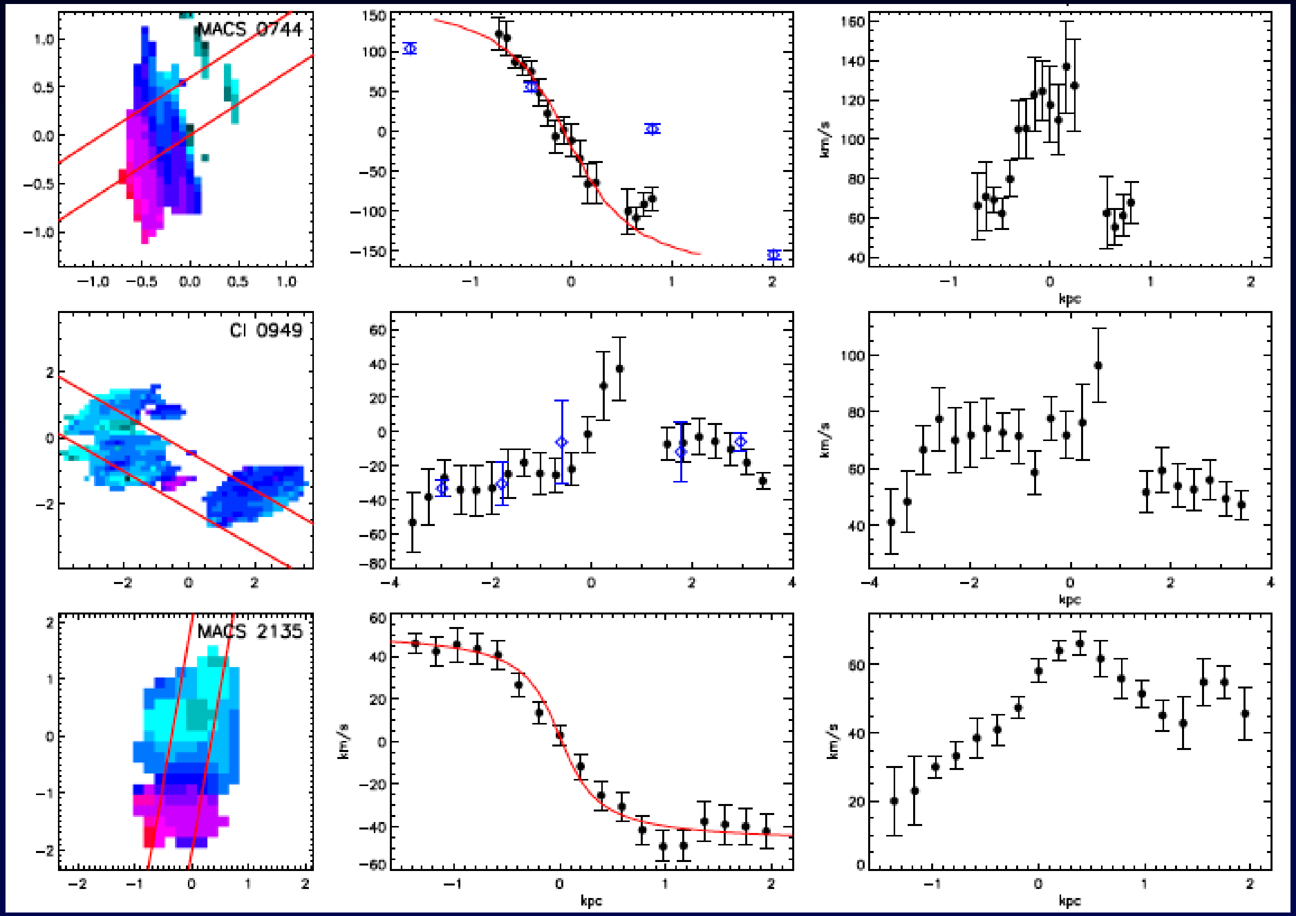


Extraction of velocity field and velocity dispersion profiles along the kinematical gradient. 5 / 6 galaxies are isolated and the velocity fields are well-fitted by a rotation curve, 1 galaxy shows signs of a merger.

(almost) impossible to distinguish the resolved kinematics here without lensing!

# RCS0224 high z kinematics

Swinbank et al. 2007

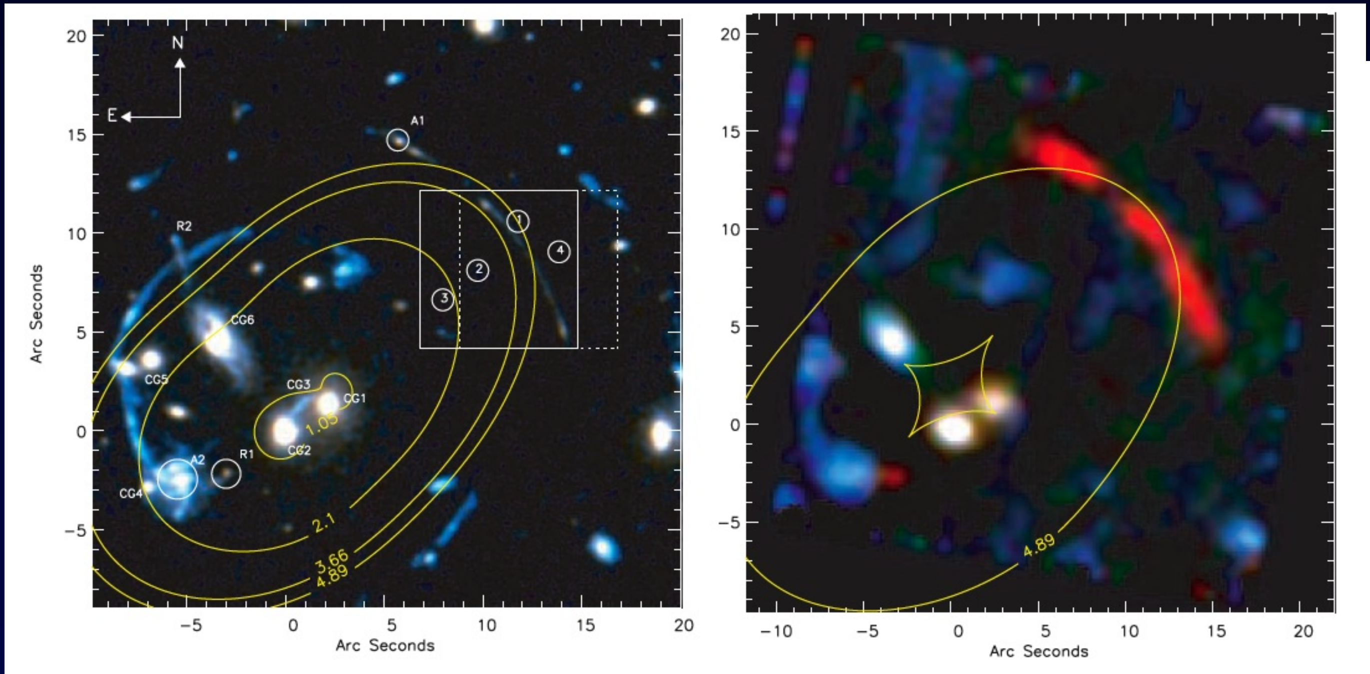


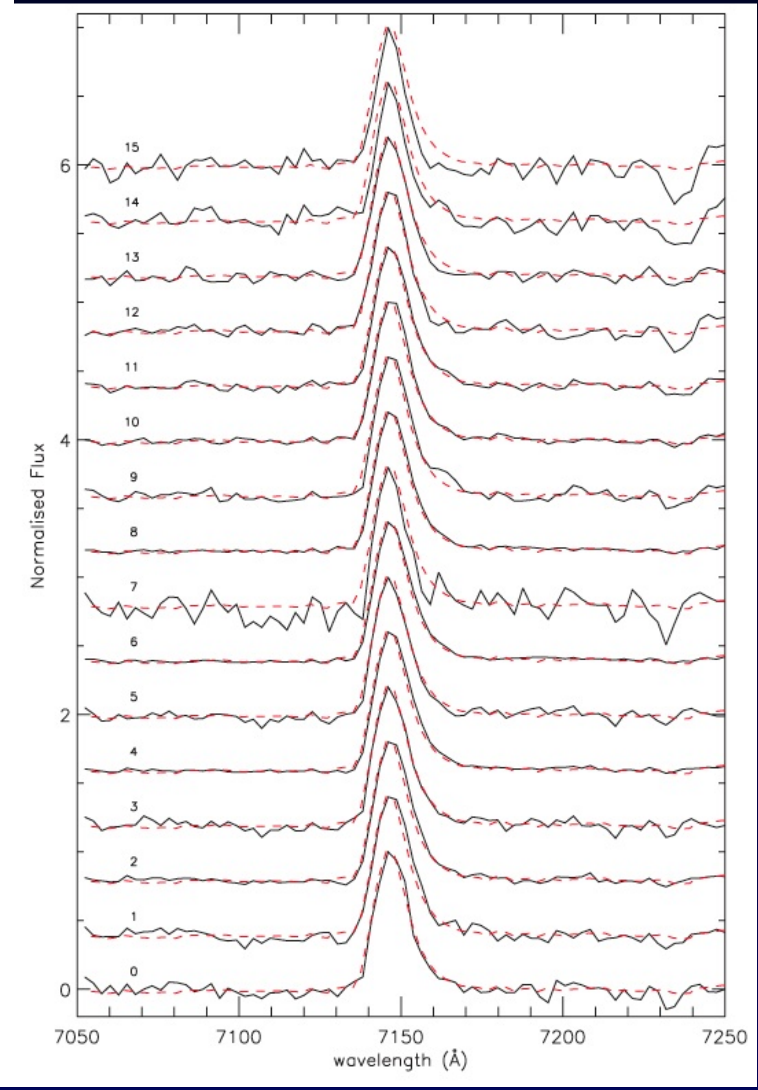


- z=4.88, magnification ×16 (∼3 magnitudes), spreads over 15 arcsecs
- Kinematics from VIMOS (Ly$\alpha$, SiII) and SINFONI ($[OII]$)
- No adaptive optics. Seeing VIMOS: 0.8". Seeing SINFONI: 0.6"

# RCS0224 interpretation

- Ly$\alpha$ more extended and shifted in velocity by $+200 \pm 40$ km s$^{-1}$ from the ionized gas ($[OII]$ emission)
- UV absorption lines offsetted by -400±100 km s$^{-1}$
- Suggests the presence of superwinds linked with star formation

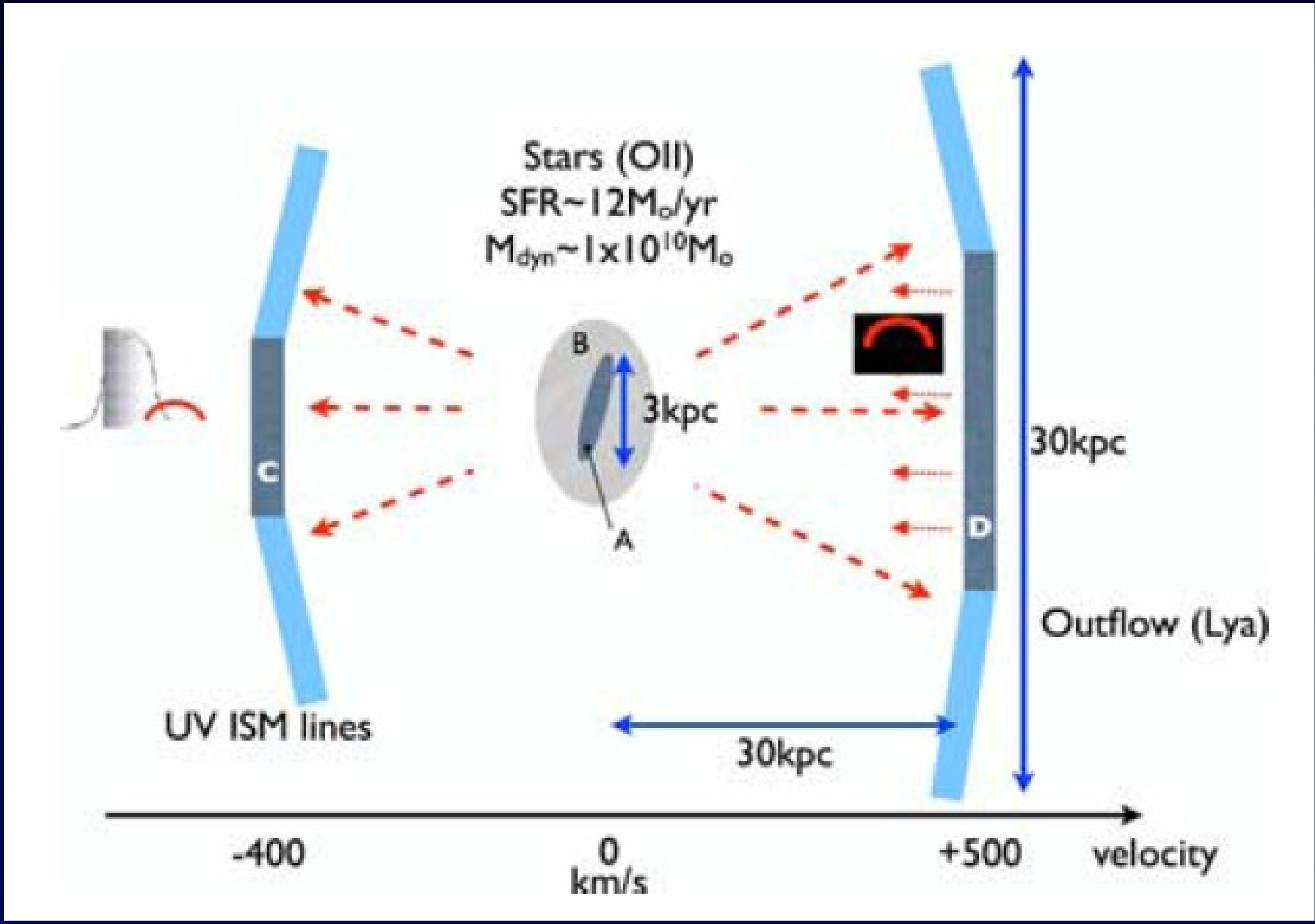

# MS1358 high z kinematics

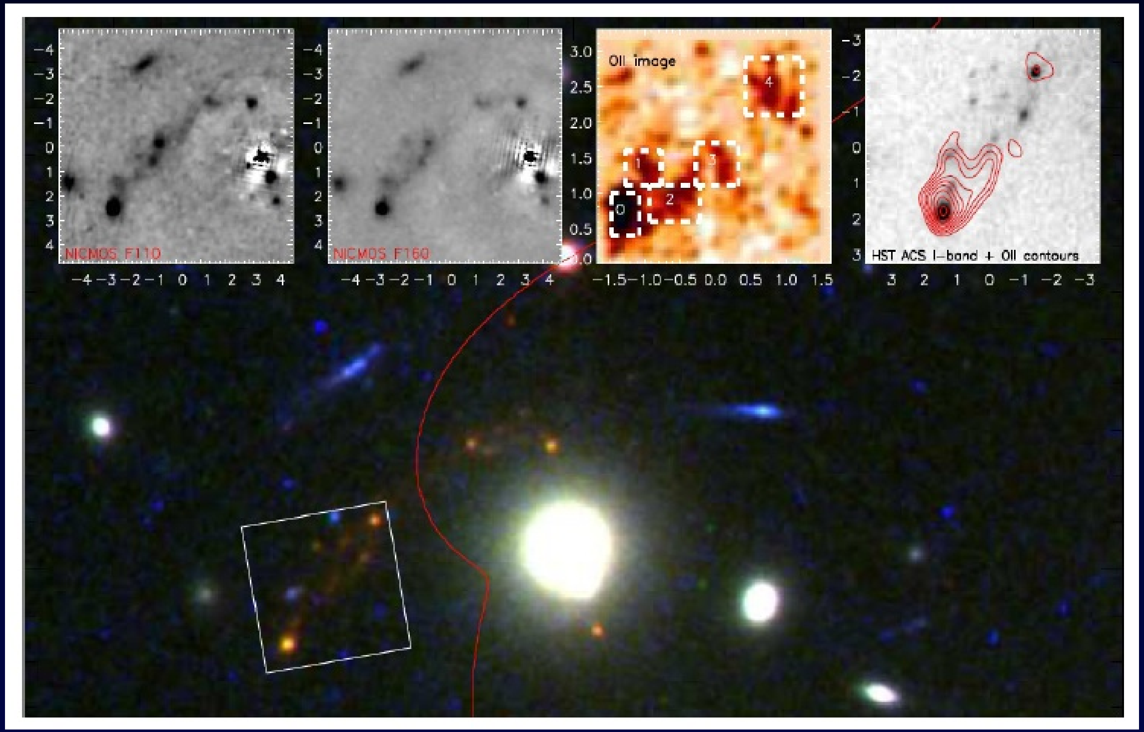


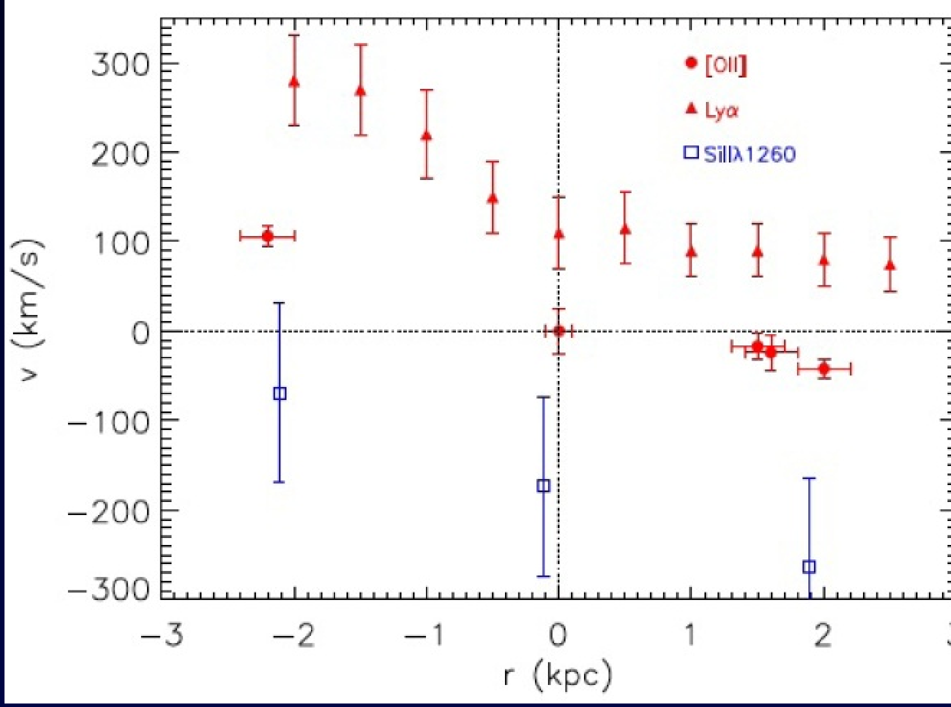


*Swinbank, Webb, Richard et al. 2009*

- Famous $z = 4.92$ arc from Franx et al. (1997)
- L* LBG, amplified by $\mu \sim 25$, SFR~40 $M_\odot$/yr
- NIFS-IFU: [OII] line emission + long slit optical spectroscopy.
- Kinematics results show a similar result to RCS0224

# Eyelash: resolving a bright submm galaxy


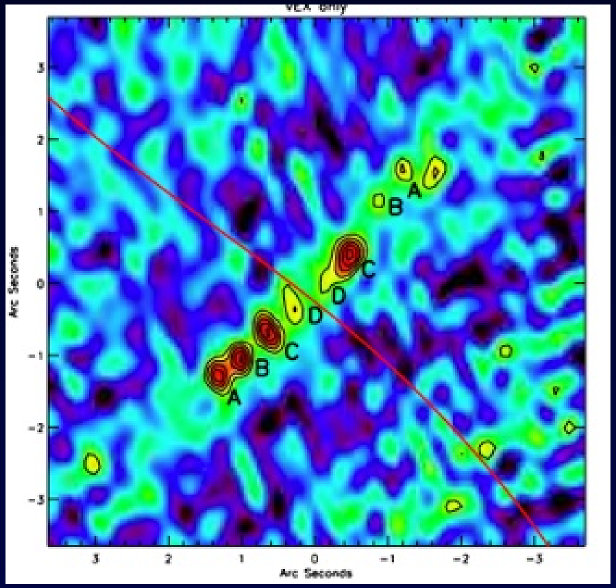


- Found with APEX/LABOCA when following-up the "cosmic eye"
- Not detected with HST, brightest far-infrared / submm galaxy (800 mJy at 300$\mu$m)
- $z = 2.3$ confirmed with CO, now 11 CO transitions covered and some resolved (*Danielson et al. 2010*)

# Radio datacube

Eyelash

Detailed observations with PdBI (CO 6-5) and EVLA (CO 1-0) at 100 pc resolution.

# Velocity field and 'Butterfly diagram'

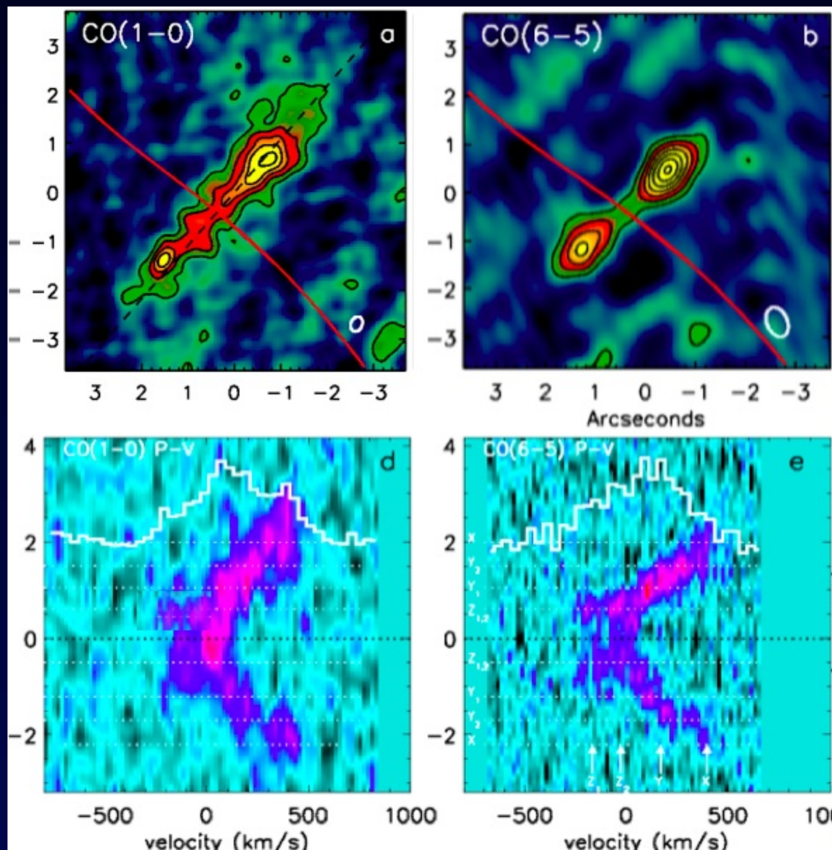


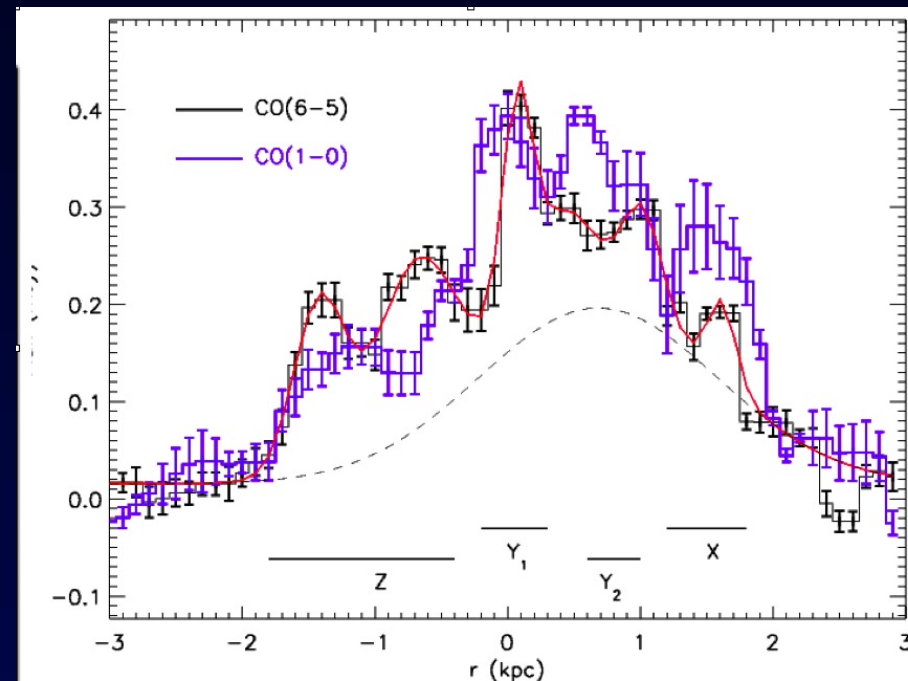


- Detailed observations with PdBI (CO 6-5) and EVLA (CO 1-0) at 100 pc resolution
- 'Butterfly' shaped position-velocity diagram showing symmetry
- Observed CO structures coincide with continuum-detected clumps from SMA

# Resolved abundances

# Resolved abundances and metallicity gradients

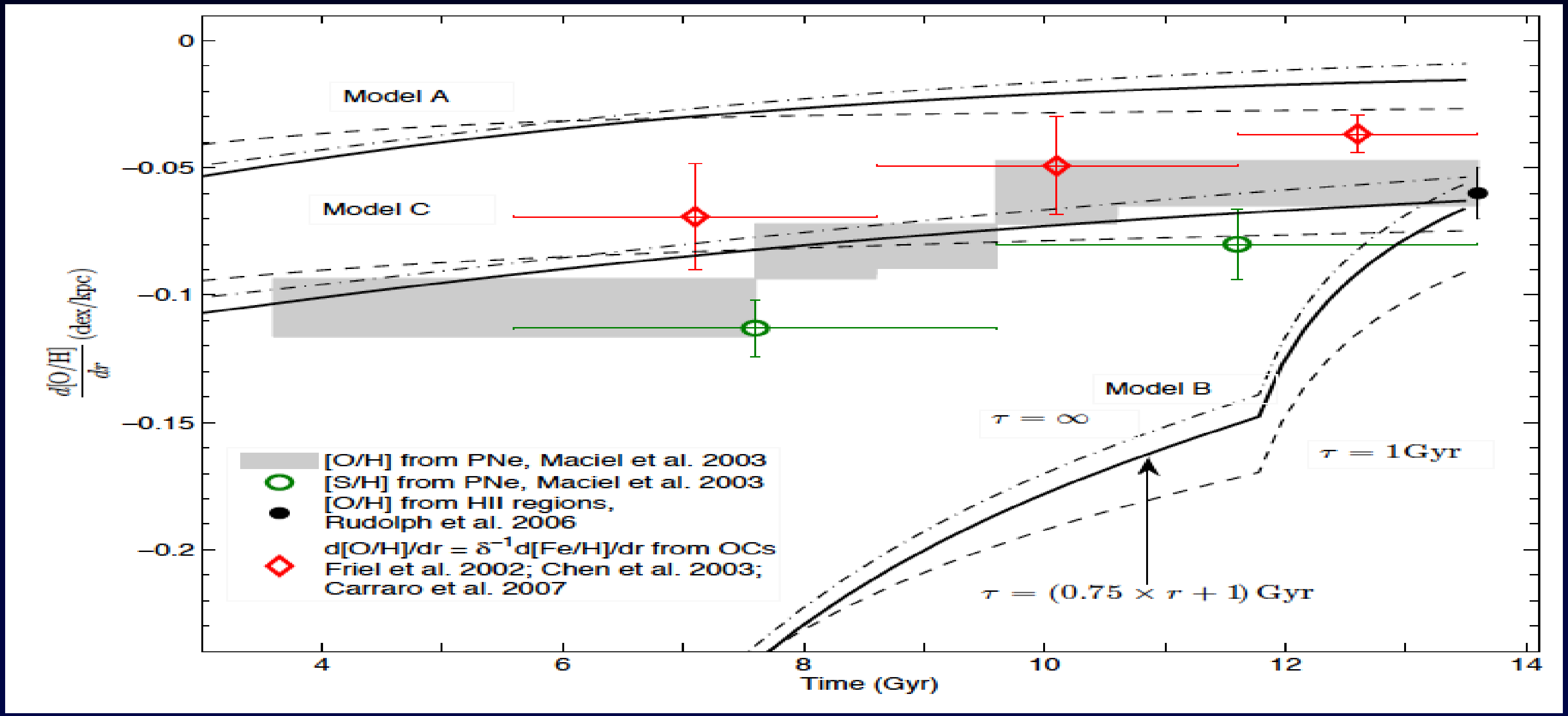


*Fu et al. 2012*: model of gradient evolution for the Milky Way.

Variation of radial abundance gradients (metallicity gradients) with time is sensitive to galaxy formation history.

# Metallicity gradients at high redshift

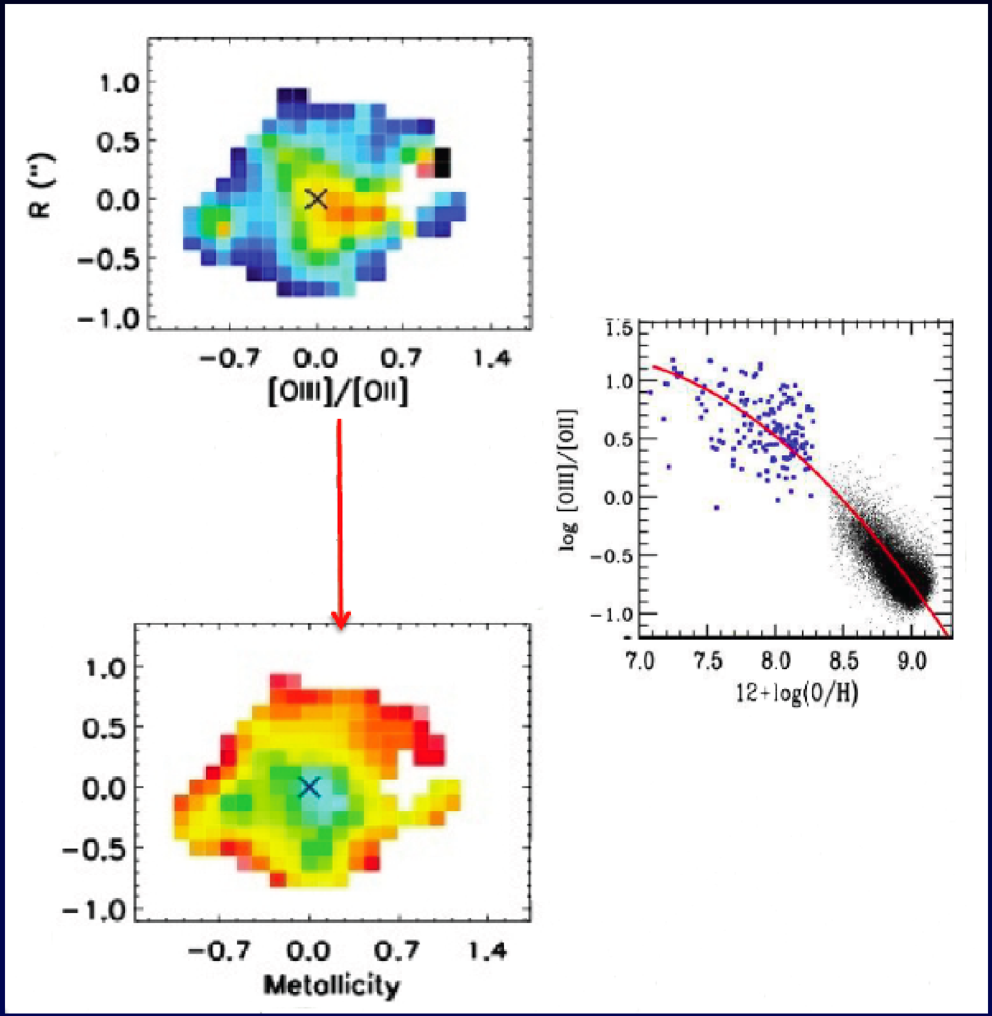


Measurements are challenging!

- Obtaining sufficient spatial resolution is difficult
- Must rely on strongline metallicity estimates
- HII regions blended with AGN and shock emission

Typical nebular line ratios diagnostics for abundances:

$[OIII]/[OII]$, $[NII]/H_\alpha$, R23 ([OII], [OIII], H$\beta$)

# AGN contamination

AGN activity can mimic a strong metallicity gradient.

But we can identify AGN from the BPT diagram (*Wright et al. 2010*)

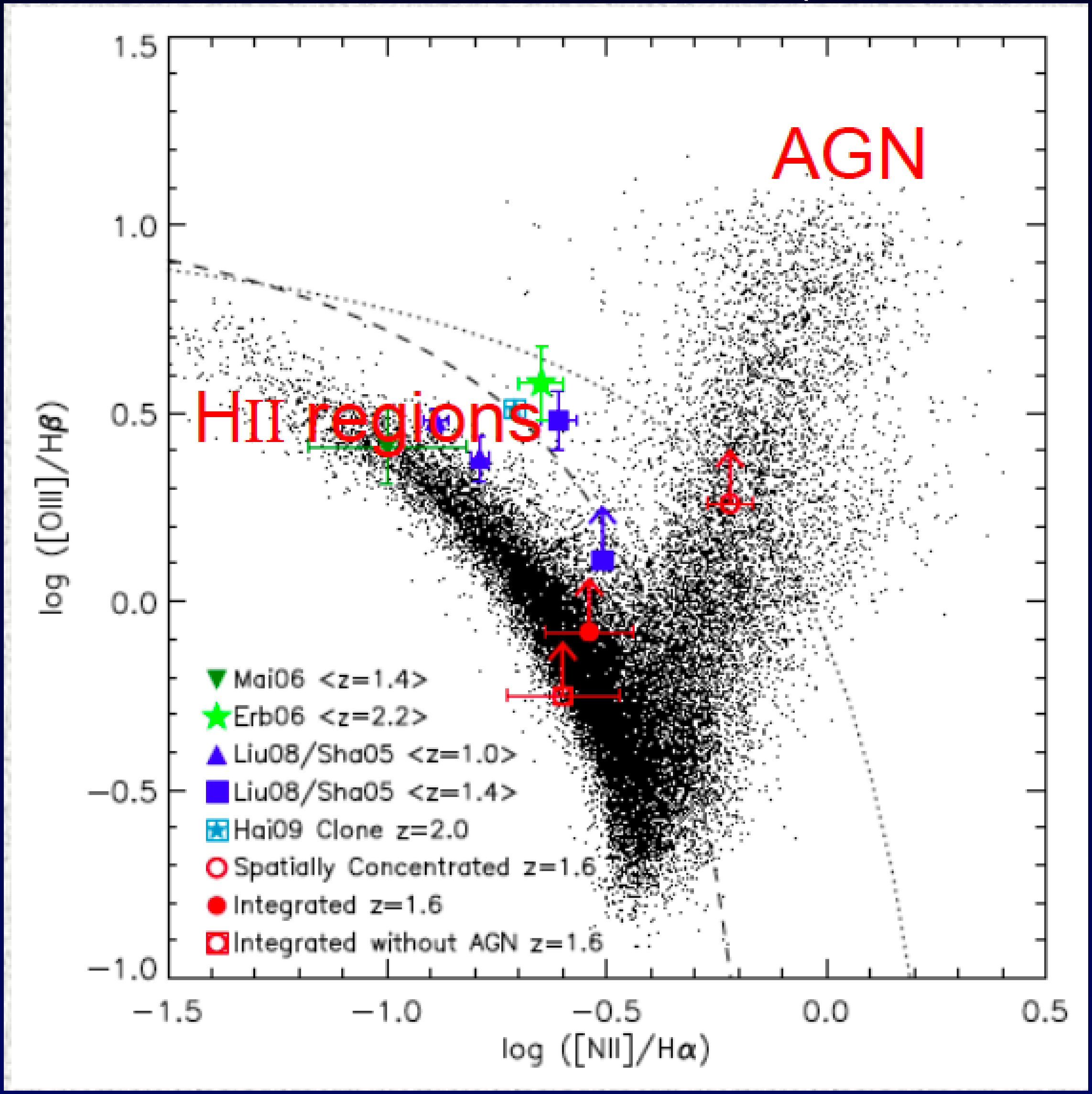

# Shocks contamination

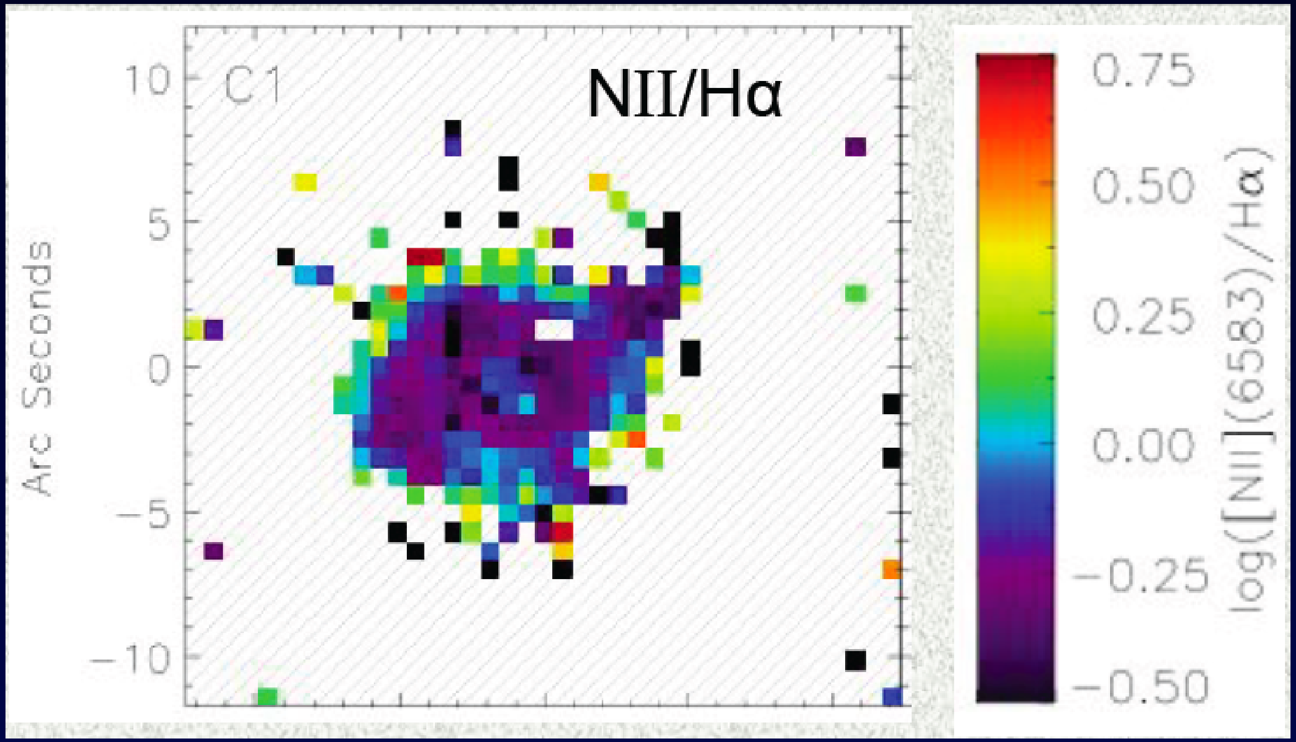


Shocks dominate at large radii and can mimic a metallicity gradient

# Metallicity gradients at $z \sim 1.2$

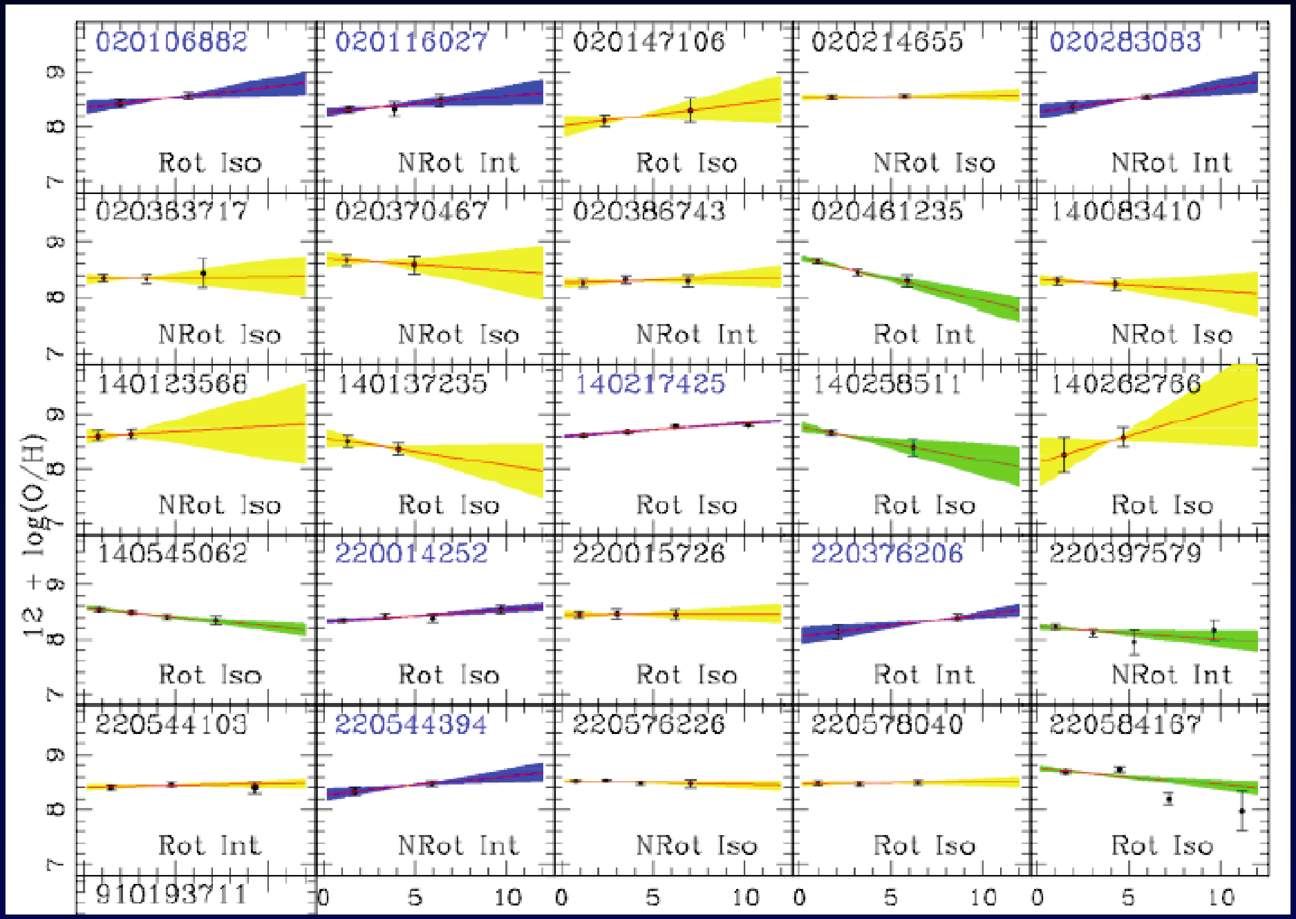


Queyrel et al. 2011

Metallicity gradients in the MASSIV survey ($z \sim 1.2$): dominated by flat or increasing radial gradients.

# Gradients at $z = 3$

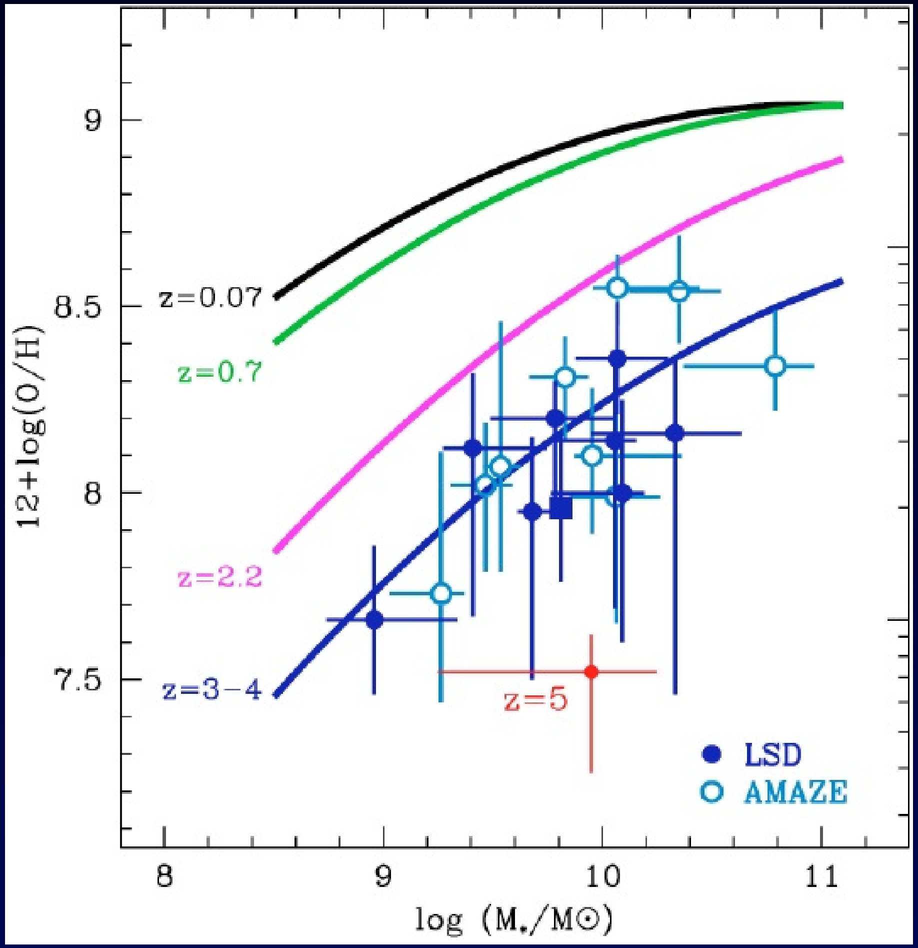


LSD and AMAZE samples: 'evolution' of mass-metallicity at high $z$

*Maiolino et al. (2009), Mannucci et al. (2009)*

Metallicity gradients

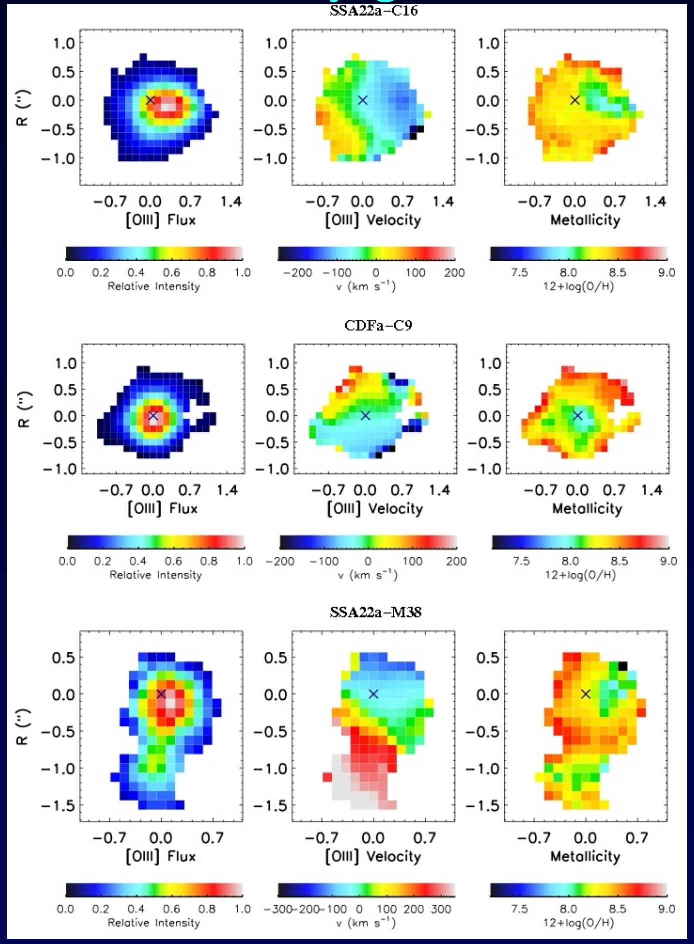


*Cresci et al. (2010)* measured positive metallicity gradients in large massive $z \sim 3$ galaxies using H$\beta$ and $[OIII]$

# First lensed metallicity gradient measurement

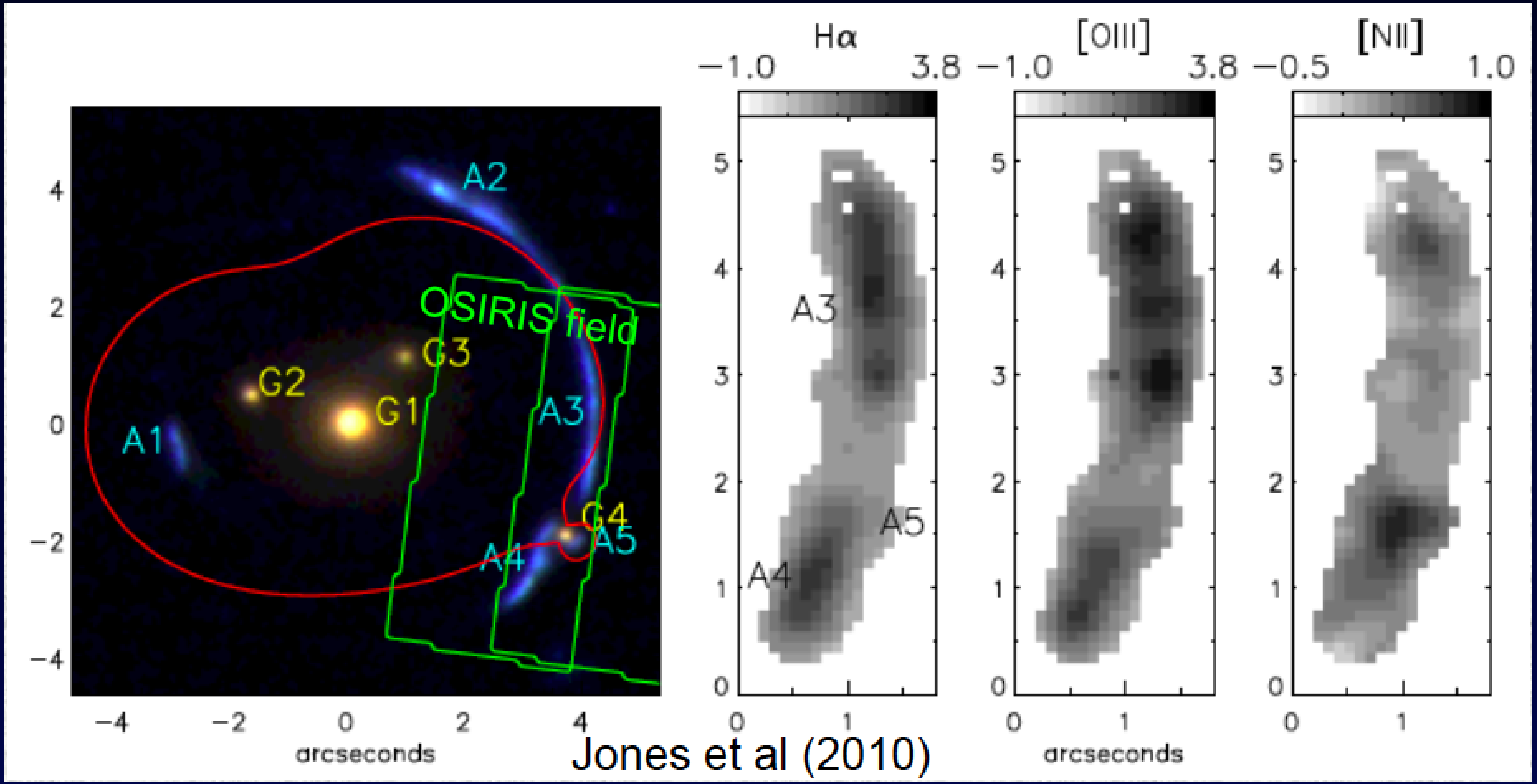


*Jones et al. 2010b*

OSIRIS + AO observations of the 'clone' arc (*Lin et al. 2009*) at $z = 2$.

# Clone results

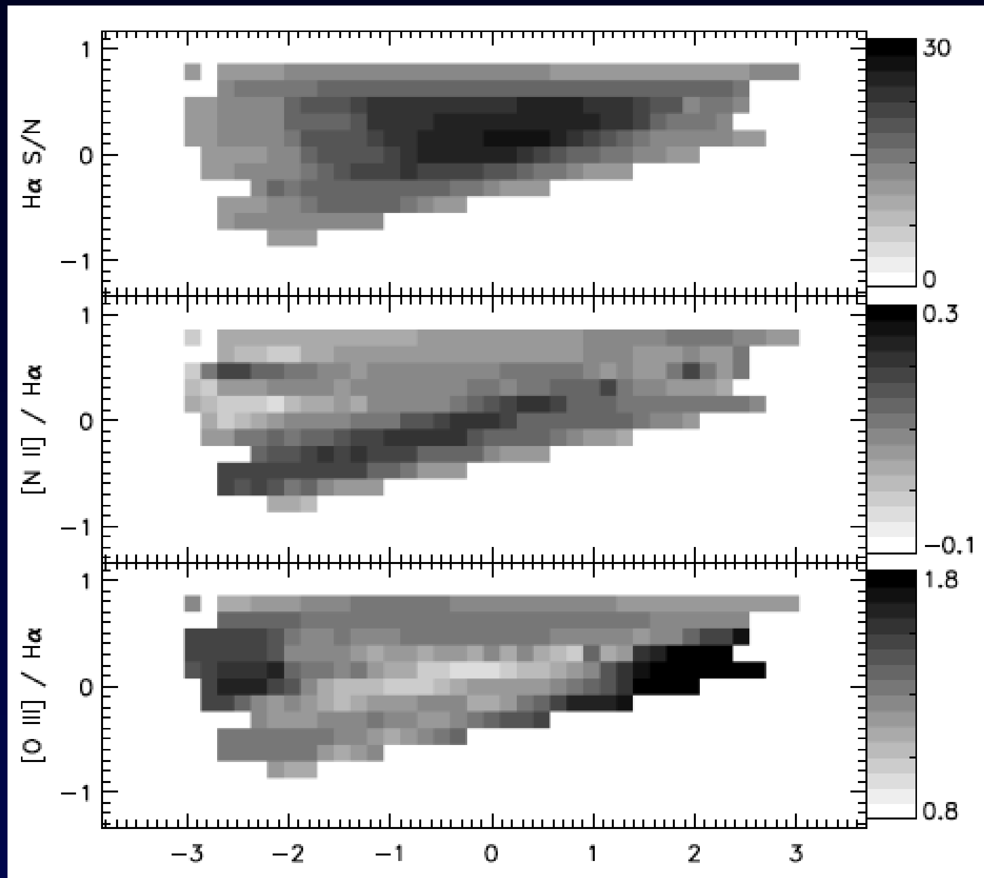


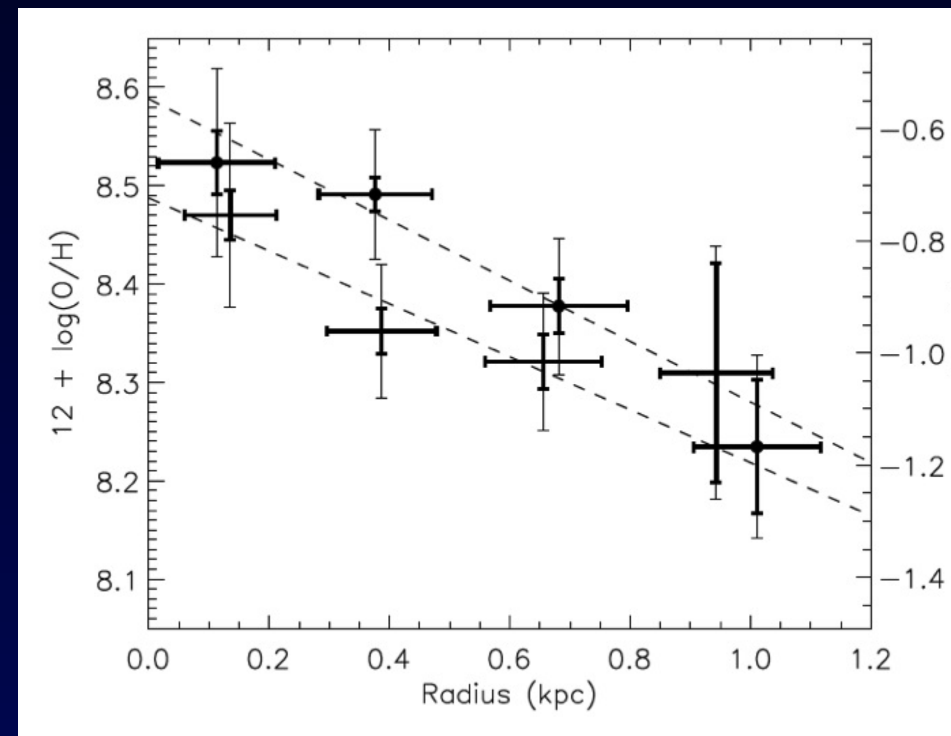


Gradient of decreasing metallicity seen from $[NII]/H\alpha$ and $[OIII]/H\alpha$

Supports a scenario of inside-out galaxy formation.

# A grand-design spiral at $z = 1.5$

*Yuan et al. 2011*

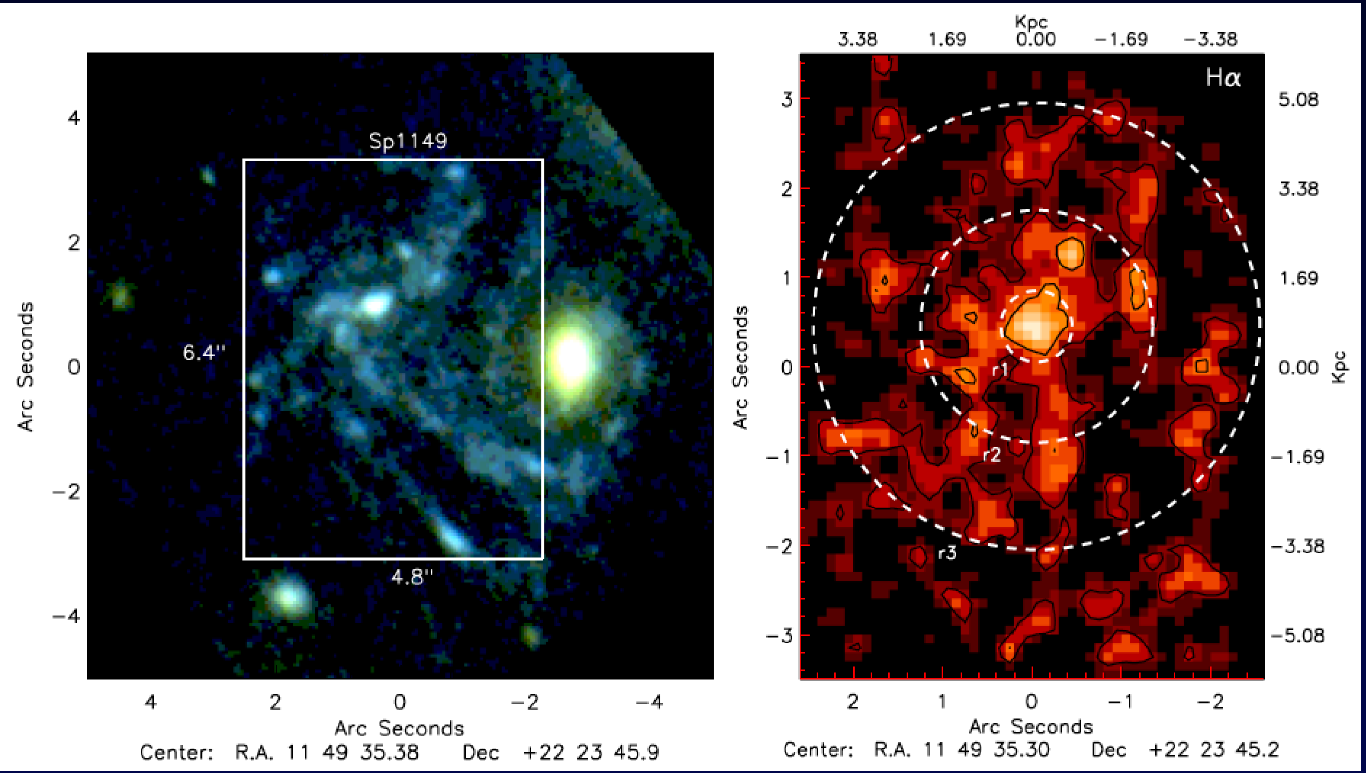


- Lensed face-on spiral galaxy at $z = 1.5$ (*Smith et al. 2009*)
- Magnification $\sim 22 - 25$, relatively isotropic
- Keck/OSIRIS measurements of H$\alpha$ and $[NII]$ line emission

# A grand-design spiral at $z = 1.5$

*Yuan et al. 2011*

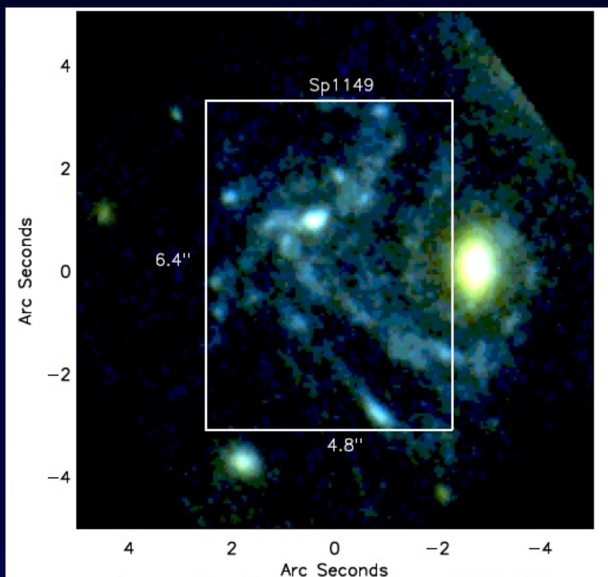


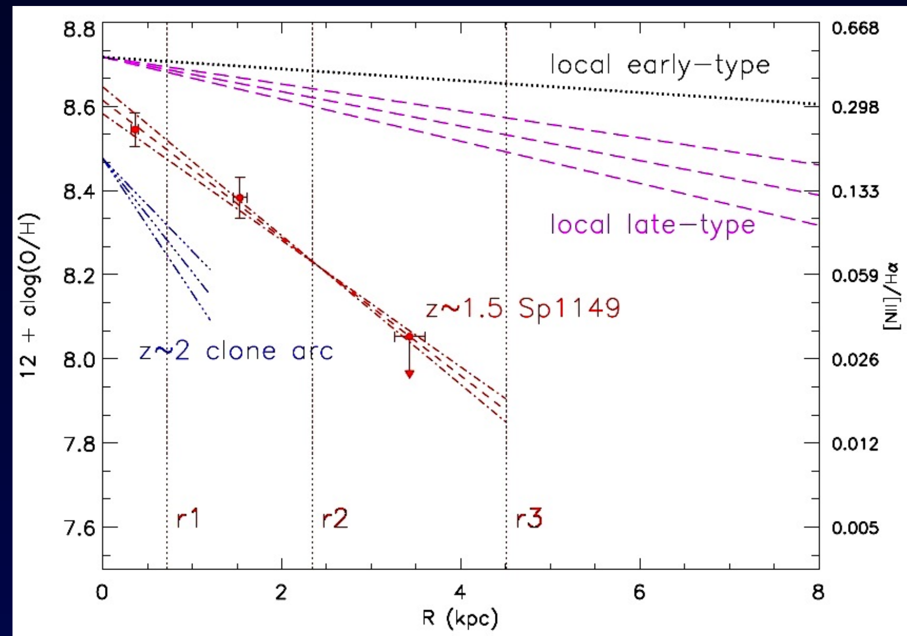


- Observations of H$\alpha$ and $[NII]$ in MACS1149 $z = 1.5$
- Measurement of a gradient of decreasing metallicity from the center, less steep than the 'clone'
- Results in apparent contradiction with Cresci et al. 2010, but lower mass / SFR and more robust emission lines

# More gradients

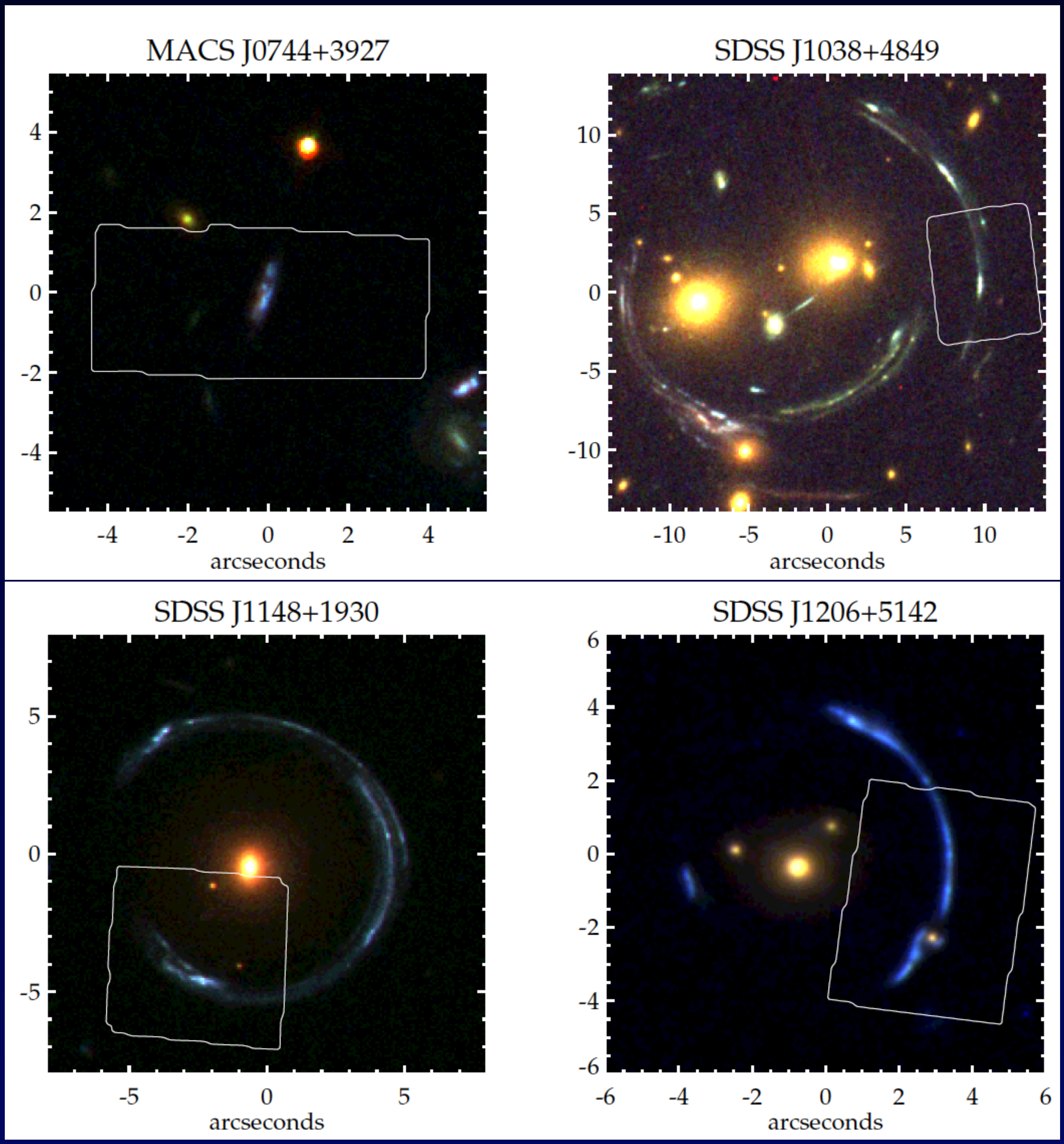


*Jones et al. 2012*

4 lensed galaxies, observed with Keck/OSIRIS + AO

$z = 2.0 - 2.4$

$0.5 - 4$ hours in H$\alpha$, $[NII]$, $[OIII]$, H$\beta$

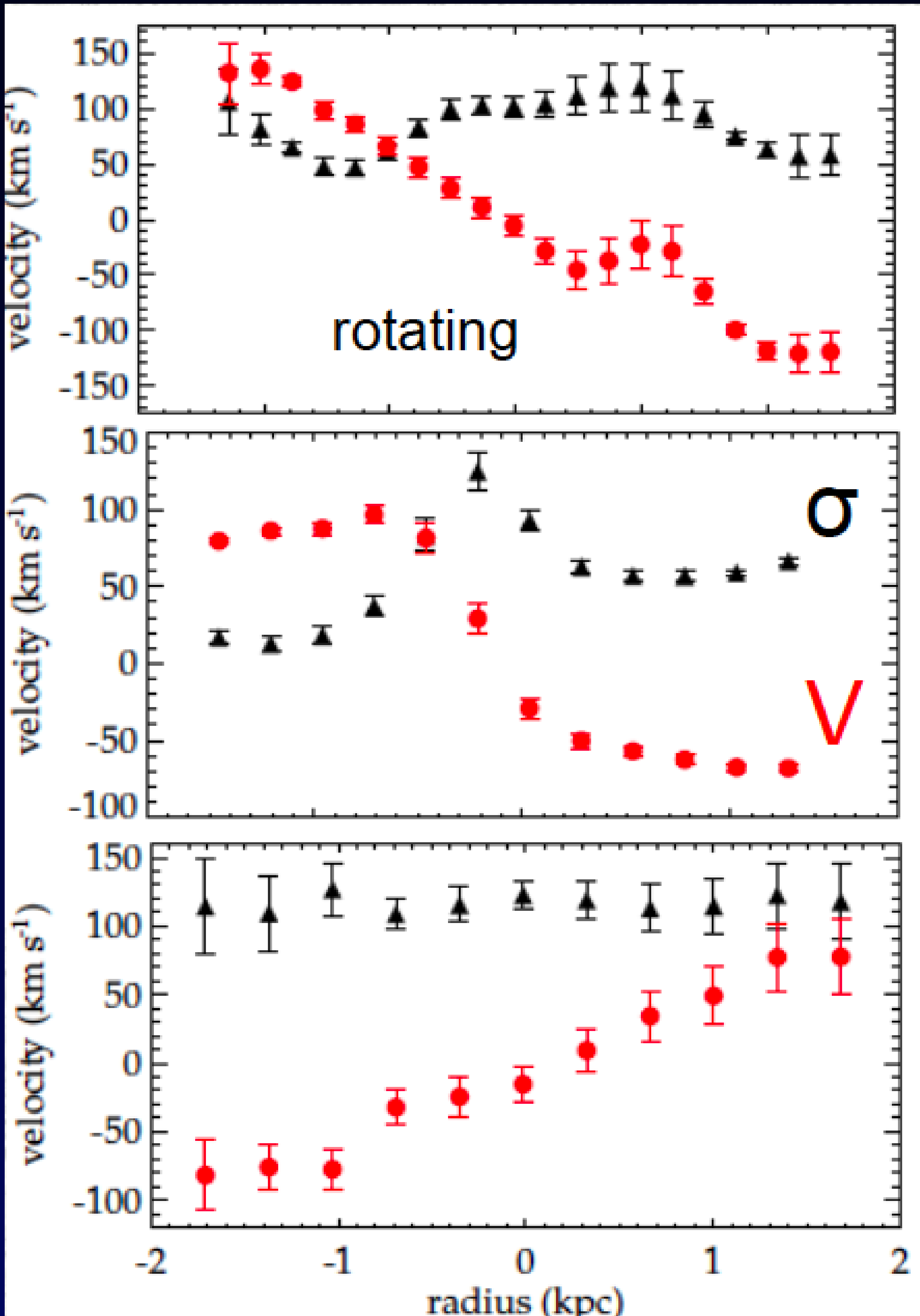


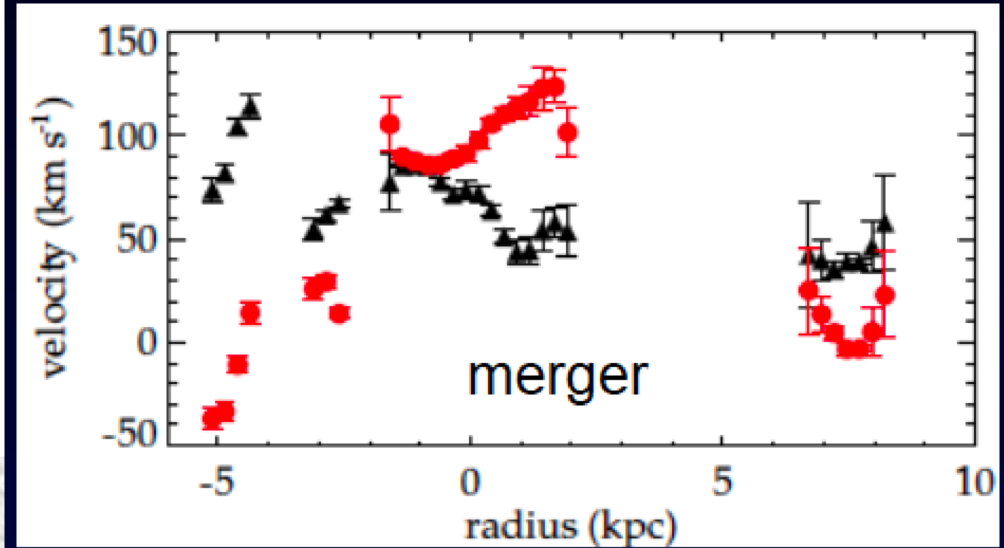


- 3 galaxies isolated and rotating; 1 merger
- High velocity dispersion:

  $V/\sigma$ = 0.8-1.4
- Gravitationally unstable.

  Toomre parameter Q$\simeq$0.6

# BPT diagram

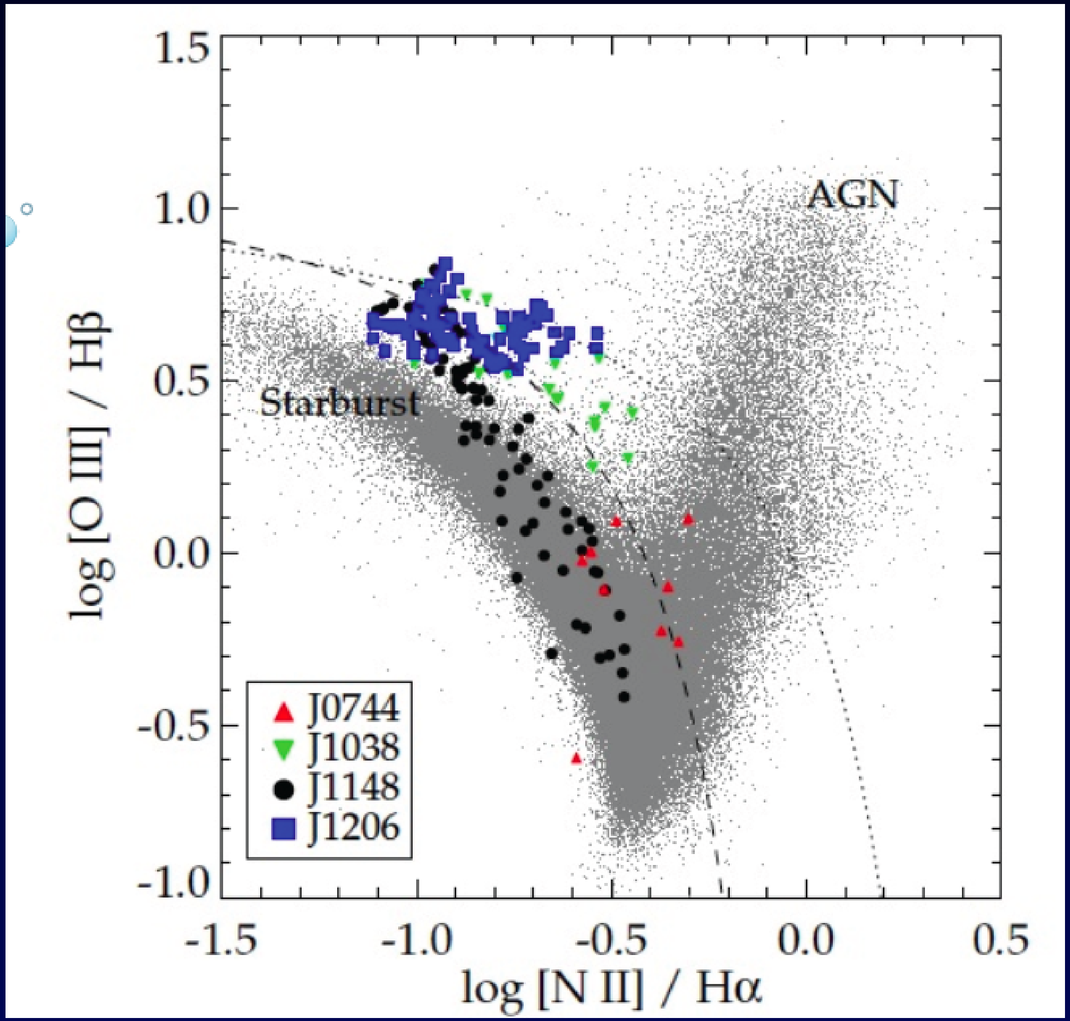


Each point is an individual OSIRIS pixel.
All regions are consistent with photoionization by massive stars.
No strong shocks or AGN detected.

# Interpretation

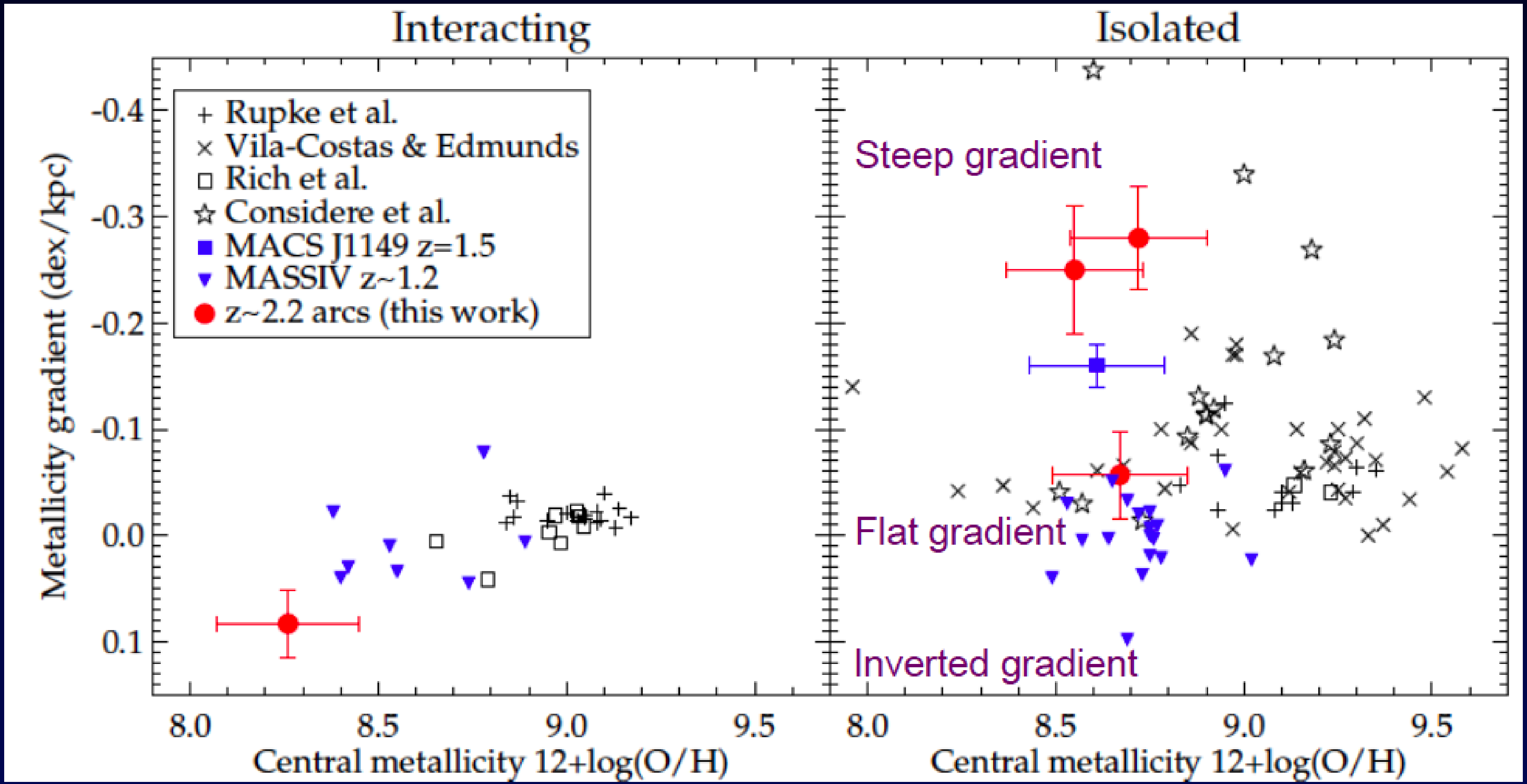

# Interpretation

- Need to compare appropriate galaxies at different redshifts.
- Determine host halo mass, and compare the same halos at different cosmic times. (Statistical description of gradient evolution)
- Halo mass estimated from stellar mass: M*/Mhalo relation (e.g. Moster et al)
- Halo growth known from merger trees in Millennium simulations

# Interpretation

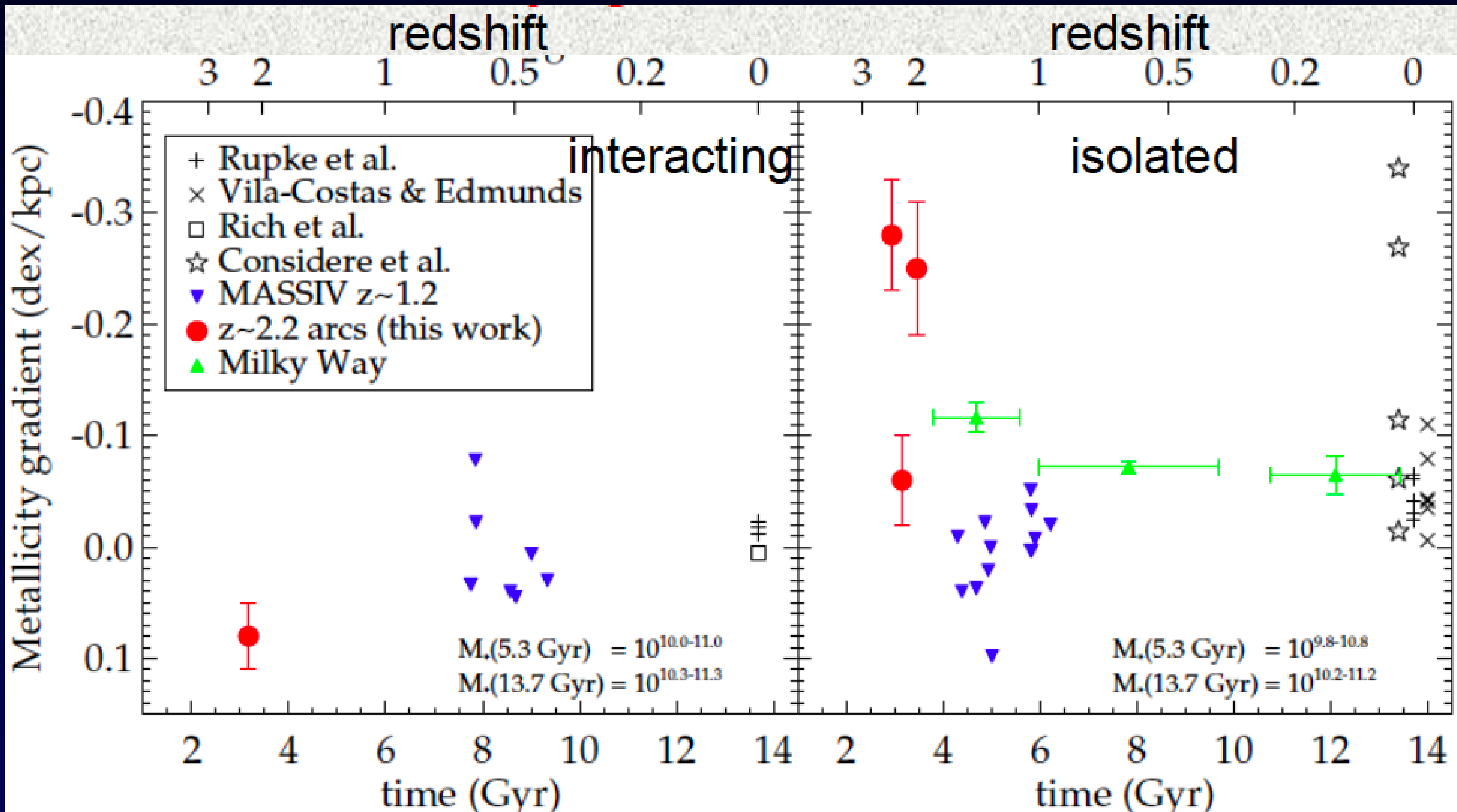


Evolution of average metallicity gradients is consistent with expected radial growth: $R \propto (1+z)^{-1.27}$ (*van Dokkum et al. 2010*)

# A2667 triply-imaged arc

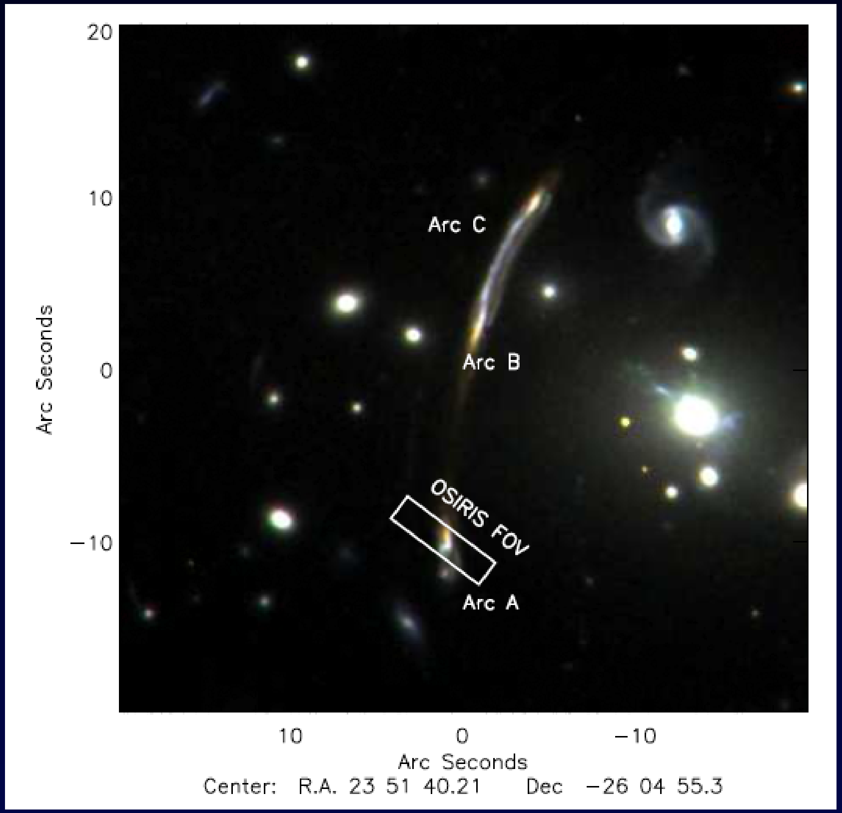


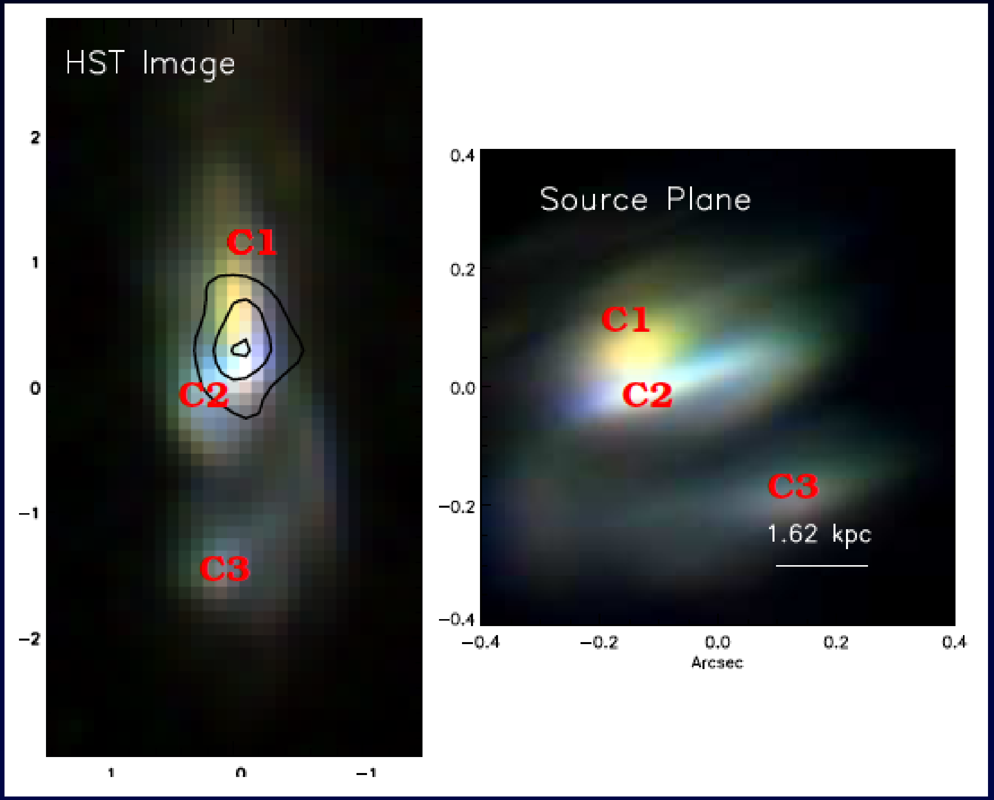


*Yuan et al. 2012*

- $z = 1.03$ giant arc in the lensing cluster Abell 2667 *Covone et al. 2007*
- Reconstructed morphology show clumpy morphology with color differences
- Face-on clumpy disk or merger ?

# A2667 triply-imaged arc: presence of shocks

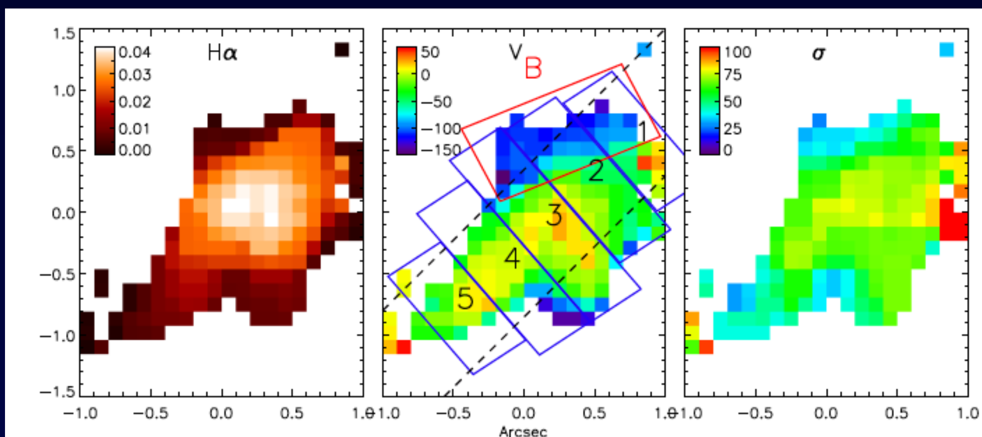


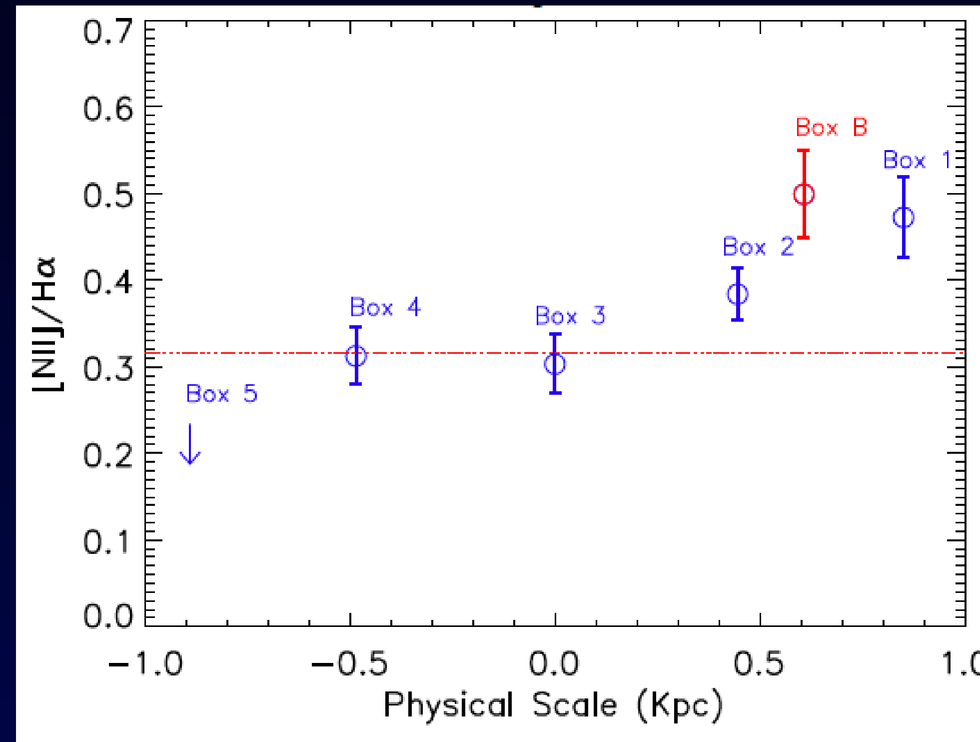


- $[NII]/H\alpha$ measured in different parts of the source
- Enhanced $[NII]/H\alpha$ in the outskirts (B)
- Compatible with a shock model. Galactic winds ?

## Conclusions

- Integral-field studies of distant galaxies are now providing key diagnostics of dynamical states of galaxies, such as $v/\sigma$, distribution of star-formation, role of mergers

- Coupling with gravitational lensing, source-plane studies can reach $\sim 100$ pc resolution and resolve the kinematics and abundance gradients in less massive galaxies

- Coupling nebular lines with UV ISM lines (and Ly$\alpha$) also allows spatially resolved studies of feedback in young galaxies: measuring the energetics of the winds.

- A high fraction of isolated galaxies at $z = 2$ have steep and negative metal gradients

- Gradients decrease by a factor 2.6±0.9 between $z = 2.2$ and $z = 0$ Consistent with radial size growth

# Perspectives: MUSE+lensing

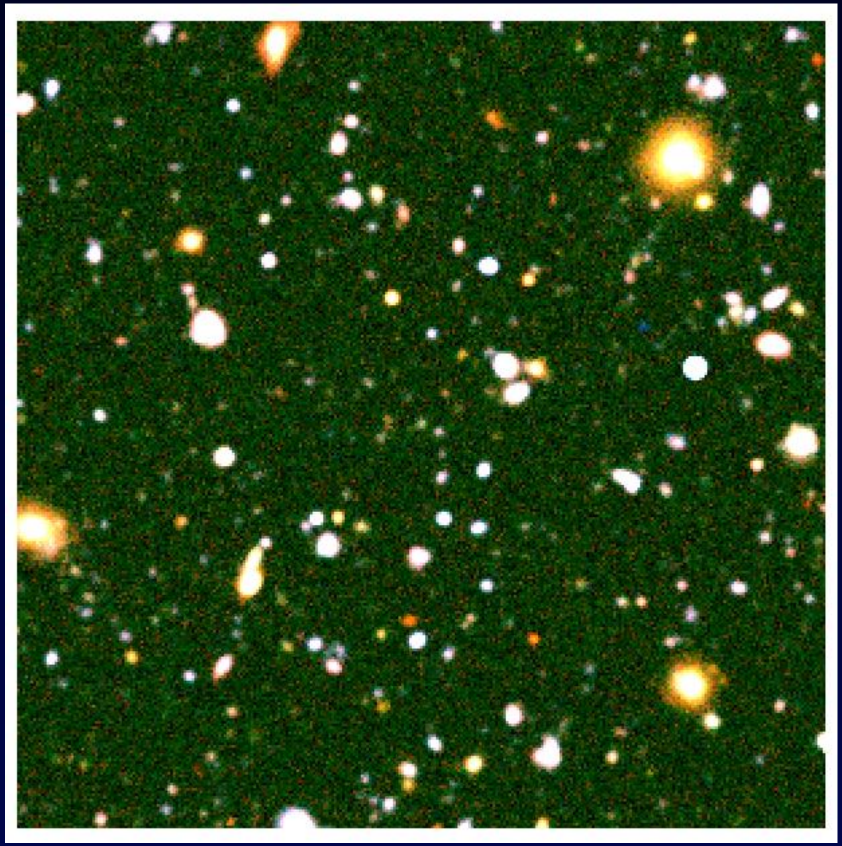

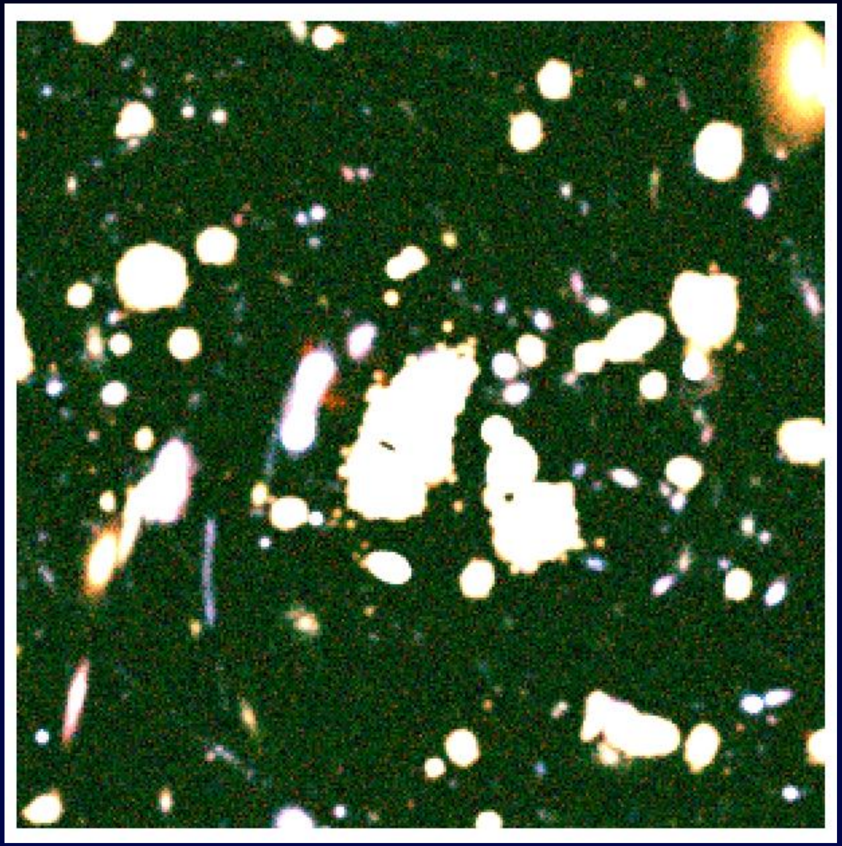

1x1 arcmin$^2$ IFU 4600-9600 Å: well adapted to cluster cores!

# Perspectives: KMOS+lensing

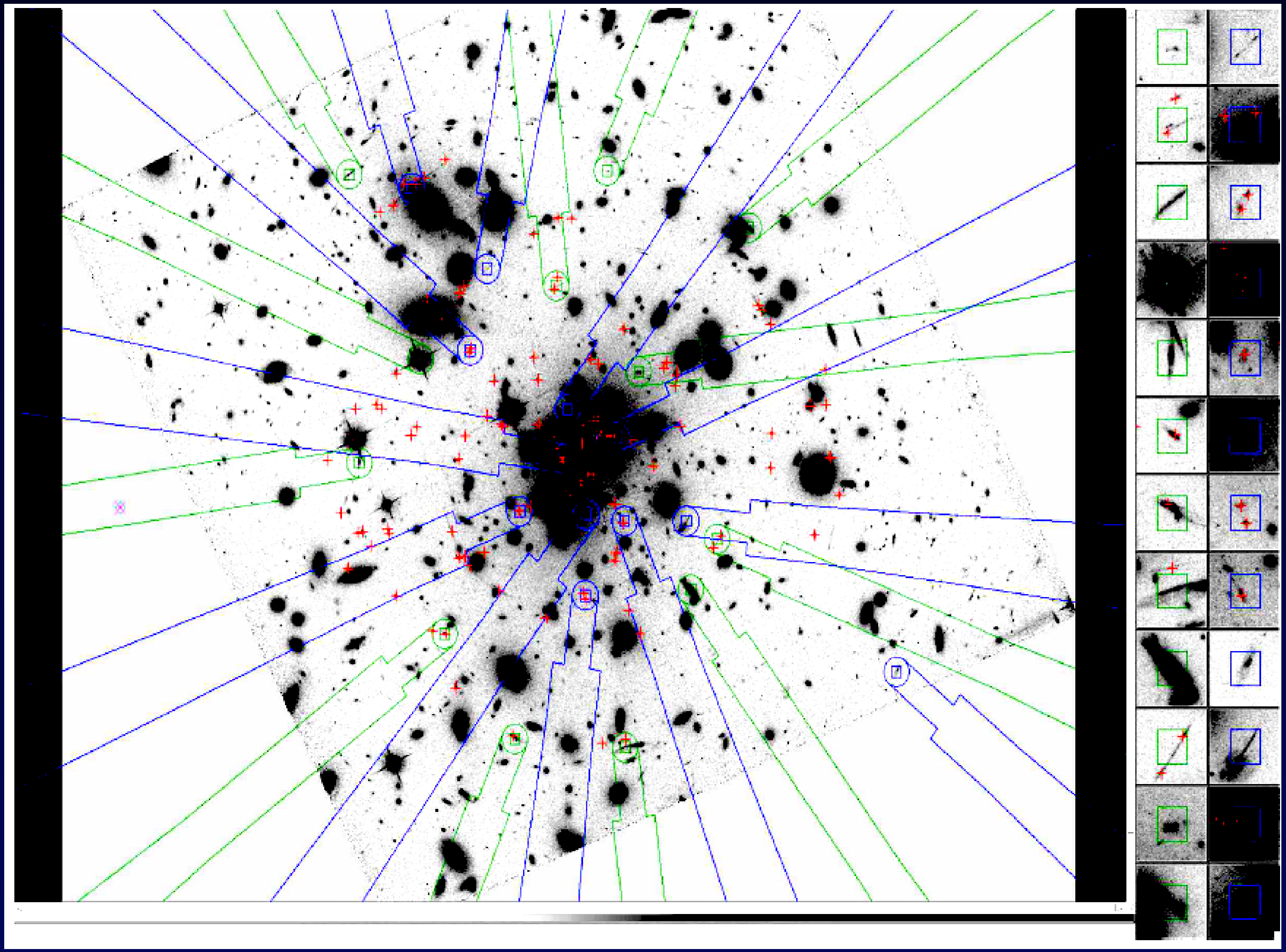

1 Outline
2 Advantages of magnification
3 Strong lensing and magnification effect
4 Strong lensing and magnification effect
5 Example of resolutions achieved
6 Historically: first source interpretation of a giant arc
7 Strong Lensing models: constraints from multiple images
8 Strong Lensing models: constraints from multiple images
9 Strong Lensing models: constraints from multiple images
10 Multiple images and resolution
11 Multiple images and caustic crossing
12 Direct reconstruction
13 Direct reconstruction
14 Parametric source reconstructions
15 Non-Parametric reconstructions: Adaptive grid
16 Adaptive grid: application
17 Morphology
18 Resolved morphology
19 Non-lensed examples: observations
20 Non-lensed examples:SINS
21 Non-lensed examples: observations
22 Non-lensed examples: size evolution
23 Resolution limit

24 Spectacular source reconstructions: RCSGA032727-132609
25
26
27 Spectacular source reconstructions:RCSGA032727-132609
28 A370 giant arc
29 A370 Spiral
30 Morphology at high redshift: star-forming regions
31 Morphology at high redshift: resolved clumps at $z \sim 5$
32 Comparison with z=2-3
33 How do we select clumps / star-forming regions ?
34 Size-SFR diagram
35 Size-SFR diagram
36 Possible explanations, tests
37 Narrow-band H$\alpha$ imaging program
38 size-SFR at z=1 (*Livermore et al. 2012*)
39 HII region LF
40 High z morphology at z∼7
41 Low masses: extending the size-mass relation
42 Long wavelength observations and source reconstructions
43 Long wavelength observations and source reconstructions
44 Results
45 Herschel Lensing Survey: source reconstructions
46 Morphology of lensed submm sources: the Eyelash
47 Radio Interferometry source reconstructions

48 Conclusions
49 Integral Field Spectroscopy
50 Different IFU concepts
51 Kinematics
52 Resolved kinematics: motivation
53 IFU+AO observing procedure for $z > 1$ galaxies
54 A few kinematical models
55 Beam smearing effect
56 Observational results: $z \sim 1.2$
57 Observational results: $z \sim 2$
58 Observational results
59 Where gravitational lensing kicks in....
60 Velocity field as additional parameters
61 Early IFU lensed studies
62 Cosmic Eye
63
64 Cosmic Eye interpretation
65 Resolved kinematics: a small sample
66 Resolved kinematics: extracted velocity field
67 RCS0224 high z kinematics
68 RCS0224 interpretation
69 MS1358 high z kinematics
70 Eyelash: resolving a bright submm galaxy
71 Radio datacube

72 Velocity field and 'Butterfly diagram'
73 Abundances
74 Resolved abundances and metallicity gradients
75 Metallicity gradients at high redshift
76 AGN contamination
77 Shocks contamination
78 Metallicity gradients at $z \sim 1.2$
79 Gradients at $z = 3$
80 First lensed metallicity gradient measurement
81 Clone results
82 A grand-design spiral at $z = 1.5$
83 A grand-design spiral at $z = 1.5$
84 More gradients
85
86 BPT diagram
87 Interpretation
88 Interpretation
89 Interpretation
90 A2667 triply-imaged arc
91 A2667 triply-imaged arc: presence of shocks
92 Conclusions
93 Perspectives: MUSE+lensing
94 Perspectives: KMOS+lensing
95 Table of Contents